

Fall 2010

An improved layer-by-layer self-assembly technique to generate biointerfaces for platelet adhesion studies: Dynamic LbL

Juan Manuel Lopez
Louisiana Tech University

Follow this and additional works at: <https://digitalcommons.latech.edu/dissertations>



Part of the [Nanoscience and Nanotechnology Commons](#)

Recommended Citation

Lopez, Juan Manuel, "" (2010). *Dissertation*. 402.
<https://digitalcommons.latech.edu/dissertations/402>

This Dissertation is brought to you for free and open access by the Graduate School at Louisiana Tech Digital Commons. It has been accepted for inclusion in Doctoral Dissertations by an authorized administrator of Louisiana Tech Digital Commons. For more information, please contact digitalcommons@latech.edu.

AN IMPROVED LAYER-BY-LAYER SELF-ASSEMBLY TECHNIQUE
TO GENERATE BIOINTERFACES FOR PLATELET ADHESION
STUDIES: DYNAMIC LbL

by

Juan Manuel Lopez, B.S., M.S.E.

A Dissertation Presented in Partial Fulfillment
of the Requirements for the Degree
Doctor of Philosophy

COLLEGE OF ENGINEERING AND SCIENCE
LOUISIANA TECH UNIVERSITY

November 2010

UMI Number: 3438519

All rights reserved

INFORMATION TO ALL USERS

The quality of this reproduction is dependent upon the quality of the copy submitted.

In the unlikely event that the author did not send a complete manuscript and there are missing pages, these will be noted. Also, if material had to be removed, a note will indicate the deletion.



UMI 3438519

Copyright 2011 by ProQuest LLC.

All rights reserved. This edition of the work is protected against unauthorized copying under Title 17, United States Code.



ProQuest LLC
789 East Eisenhower Parkway
P.O. Box 1346
Ann Arbor, MI 48106-1346

LOUISIANA TECH UNIVERSITY

THE GRADUATE SCHOOL

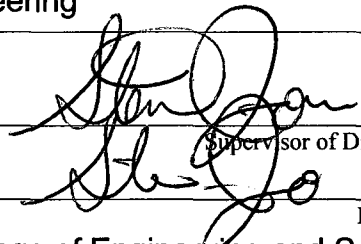
9/3/2010

Date

We hereby recommend that the dissertation prepared under our supervision by Juan Manuel Lopez

entitled AN IMPROVED LAYER-BY-LAYER SELF-ASSEMBLY TECHNIQUE TO GENERATE BIOINTERFACES FOR PLATELET ADHESION STUDIES: DYNAMIC LbL

be accepted in partial fulfillment of the requirements for the Degree of Doctor of Philosophy, Biomedical Engineering



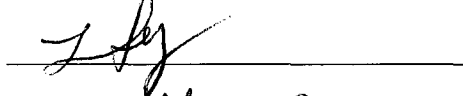
Supervisor of Dissertation Research

Head of Department

College of Engineering and Science, BIEN

Department

Recommendation concurred in:



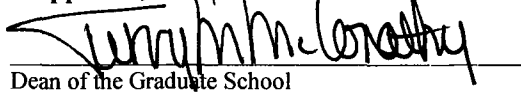
Advisory Committee

Approved:



Director of Graduate Studies

Approved:



Dean of the Graduate School



Dean of the College

ABSTRACT

Layer-by-layer self-assembly (LbL) is a technique that generates engineered nano-scale films, coatings, and particles. These nanoscale films have recently been used in multiple biomedical applications. Concurrently, microfabrication methods and advances in microfluidics are being developed and combined to create “Lab-on-a-Chip” technologies. The potential to perform complex biological assays *in vitro* as a first-line screening technique before moving on to animal models has made the concept of lab on a chip a valuable research tool.

Prior studies in the Biofluids Laboratory at Louisiana Tech have used layer-by-layer and *in vitro* biological assays to study thrombogenesis in a controlled, repeatable, engineered environment. The reliability of these previously established techniques was unsatisfactory for more complex cases such as chemical and shear stress interactions.

The work presented in this dissertation was performed to test the principal assumptions behind the established laboratory methodologies, suggest improvements where needed, and test the impact of these improvements on accuracy and repeatability.

The assumptions to be tested were: 1) The fluorescence microscopy (FM) images of acridine orange-tagged platelets accurately provide a measure of percent area of surface covered by platelets; 2) fibrinogen coatings can be accurately controlled, interact with platelets, and do not interfere with the ability to quantify platelet adhesion; and 3) the dependence of platelet adhesion on chemical agents, as measured with the modified

methods, generally agrees with results obtained from our previous methods and with known responses of platelets that have been documented in the literature.

The distribution of fibrinogen on the final LbL surface generated with the standard, static process (s-LbL) was imaged by tagging the fibrinogen with an anti-fibrinogen antibody bound to fluorescein isothiocyanate (FITC). FITC FM images and acridine orange FM images were taken sequentially at selected surface locations to generate a composite overlap of presumed platelet adhesion as a function of fibrinogen distribution. The method was unable to distinguish the surface from the adhered cells. The surface inhomogeneity and porosity retained a large amount of acridine orange stain, even in the absence of platelets, and components in the platelet-rich plasma (PRP) were found to fix acridine orange in a mode that fluoresced in the FITC imaging FM. Both of these problems obfuscated the platelet adhesion FM results when using s-LbL surfaces and acridine orange staining of platelets.

A dynamic process (d-LbL) was developed in which a solution of the molecule to be layered was constantly washed over the surface, and was constantly mixed to maintain a more homogeneous distribution of solute relative to the surface during the layering process. The d-LbL surfaces were tested as described above, and found to reduce the size and number of regions of anomalous acridine orange pooling trapped by the surface, providing a greater consistency and reliability in identifying platelets.

The improved surface was then used in a series of platelet adhesion experiments under static and dynamic flow conditions, and with and without the chemical additive L-arginine. The complex microchannel system used in prior studies was replaced with a simpler system involving fewer nuisance variables for these tests.

The tests were performed on both collagen and fibrinogen surfaces. Collagen has been used as a thrombogenic surface in multiple studies in the literature, but produces additional variables in thrombogenesis control that are avoided when fibrinogen is used. In these tests, fibrinogen was found to be as thrombogenic as collagen, and platelet coverage of both biointerfaces was reduced by L-arginine in a manner similar to previously reported work.

The simpler system differed from the previous microchannel system in important factors: 1) It exposed the platelets to much lower shear stresses; 2) It introduced an oscillatory flow, which introduced a higher degree of variability in the adhesion than previously reported; 3) the previous work had not removed the acridine orange surface problems. Therefore, a direct comparison between results was not possible.

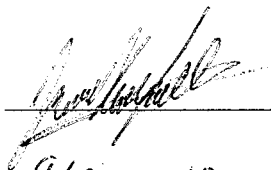
The new d-LbL surface process was successful in testing the basic assumptions. Testing showed that the new process eliminated the anomalous acridine orange retention problem during fluorescence imaging. This improvement in fluorescence response meant that the FM results matched the platelet adhesion on plain glass slides and adhesion reported by others in microfluidic flows. The chemical additive responses behaved as expected, with an increase in L-arginine contributing to a decrease in thrombogenesis under dynamic conditions, but not under static conditions.

APPROVAL FOR SCHOLARLY DISSEMINATION

The author grants to the Prescott Memorial Library of Louisiana Tech University the right to reproduce, by appropriate methods, upon request, any or all portions of this Dissertation. It is understood that "proper request" consists of the agreement, on the part of the requesting party, that said reproduction is for his personal use and that subsequent reproduction will not occur without written approval of the author of this Dissertation. Further, any portions of the Dissertation used in books, papers, and other works must be appropriately referenced to this Dissertation.

Finally, the author of this Dissertation reserves the right to publish freely, in the literature, at any time, any or all portions of this Dissertation.

Author



Date

9/3/2010

DEDICATION

This dissertation is dedicated to my family. Without all of you, I would never have accomplished any of the things that have mattered in my life. To Manuel and Ruth Lopez, my loving parents: I have always known that in you, I had my biggest source of support, and that has mattered more to me than I will ever be able to repay. To Joanna and Josh, my siblings: thank you for always challenging me to be the best person I can be. To my grandparents: Ed and Lois Oglesby, you provided an environment where inquisitiveness and inventiveness were cultivated, and were always willing to help me improve myself. To my abuelo, Manuel Lopez: I miss you, and I thank you for giving me the family that I have loved and enjoyed and some of my earliest experiences with science.

TABLE OF CONTENTS

ABSTRACT.....	iii
DEDICATION.....	vii
LIST OF FIGURES	xiv
LIST OF TABLES.....	xx
ACKNOWLEDGMENTS	xxi
CHAPTER 1 INTRODUCTION	1
1.1 Hemostasis and Cardiovascular Disease.....	1
1.2 Platelet Adhesion	1
1.3 Nanotechnology Biointerfaces/Lab-on-a-Chip.....	2
1.4 Limitations of Prior Approaches.....	3
1.5 Current Work	5
1.5.1 Hypothesis 1.....	6
1.5.2 Hypothesis 2.....	7
1.5.3 Hypothesis 3.....	7
1.5.4 Hypothesis 4.....	8
CHAPTER 2 BACKGROUND	9
2.1 Thrombi	9
2.1.1 Coagulation Overview	9
2.1.2 Nitric Oxide and L-Arginine.....	12
2.1.3 Fibrinogen.....	13
2.2 Layer-by-Layer Self-Assembly (LbL) in Biomedical Applications.....	14

2.3	Lab-on-a-Chip (LoC).....	17
2.4	Previous Studies from our Laboratory.....	18
2.4.1	Collagen/Static Studies – Frilot.....	18
2.4.2	Fibrinogen/Dynamic Studies – Eshaq.....	18
CHAPTER 3 METHODS.....		20
3.1	Experimental Workflow for Hypotheses Tests.....	20
3.1.1	Hypothesis 1.....	20
3.1.2	Hypothesis 2.....	22
3.1.3	Hypothesis 3.....	22
3.1.4	Hypothesis 4.....	23
3.2	s-LbL and d-LbL Biointerfaces for Platelet Adhesion Studies.....	23
3.2.1	Overview.....	23
3.2.2	Process Summary.....	23
3.2.3	Solution Preparations.....	24
3.2.4	Surface Preparation.....	29
3.3	Platelet Adhesion Tests.....	37
3.3.1	Overview.....	37
3.3.2	Pre-Experiment Preparation.....	38
3.3.3	Blood Collection and Processing.....	44
3.3.4	Use of d-PRP in Platelet Adhesion Tests.....	51
3.4	Post-Experiment Processing.....	56
3.4.1	Overview.....	56
3.4.2	Equipment List.....	57
3.4.3	Preparing Samples for Imaging.....	58
3.4.4	Microscopy.....	60

3.4.5	Image and Data Processing.....	65
3.5	d-LBL Biointerfaces for Platelet Adhesion Studies	70
3.5.1	Overview.....	70
3.5.2	Equipment and Reagents List	71
3.5.3	Solutions Preparations	72
3.5.4	Surface Preparation.....	73
3.5.5	Storage	76
3.5.6	Platelet Adhesion Studies with d-LbL	76
3.6	Bioanalyzer Flow Cytometry.....	76
3.6.1	Overview.....	76
3.6.2	Equipment and Reagents List	77
3.6.3	Sample Preparation	78
3.6.4	Chip Preparation	78
3.6.5	Sample Loading	79
3.6.6	Agilent Software	80
3.7	SEM Imaging of Surfaces.....	81
3.7.1	Overview.....	81
3.7.2	Equipment List.....	81
3.7.3	SEM Imaging Process.....	81
3.8	Particle Tracking.....	82
3.8.1	Experimental Setup.....	83
3.8.2	Equipment and Software List.....	83
3.8.3	Data Processing.....	86
3.8.4	Transport Model.....	88

3.9	Statistical Analysis.....	92
3.9.1	Overview.....	92
3.9.2	Hypothesis 1.....	93
3.9.3	Hypothesis 2.....	95
3.9.4	Hypothesis 3.....	96
3.9.5	Hypothesis 4.....	96
CHAPTER 4 RESULTS		98
4.1	Overview.....	98
4.2	Particle Tracking.....	99
4.2.1	Overview.....	99
4.2.2	Images Containing the Particles.....	100
4.3	Flow Cytometry	110
4.3.1	Overview.....	110
4.3.2	Histograms of Platelet Count vs. Fluorescent Intensity	113
4.4	s-LbL Results.....	116
4.4.1	Static and Dynamic Flow Conditions	118
4.4.2	s-LbL Percent Surface Area Coverage Summary	120
4.4.3	Red-Green Comparisons.....	121
4.5	d-LbL Results	131
4.5.1	PRP Exposure to d-LbL Fibrinogen	132
4.5.2	PRP Exposure to d-LbL Collagen.....	134
4.5.3	d-LbL Percent Surface Area Coverage	135
4.6	s-LbL and d-LbL: Comparisons and Statistics	137
4.6.1	FE-SEM Surface Comparisons	137
4.6.2	s-LbL to d-LbL Comparison.....	139

4.6.3	Statistics	140
CHAPTER 5 DISCUSSION		146
5.1	Particle Tracking	146
5.1.1	Overview	146
5.1.2	Comparison of Flow Field to Other Sources	147
5.1.3	Limitations and Sources of Error	147
5.1.4	New Questions Raised	148
5.2	Flow Cytometry	149
5.2.1	Overview	149
5.2.2	Comparison of Platelet Counts to the Literature	150
5.2.3	Limitations and Sources of Error for Platelet Counts	150
5.2.4	New Questions Raised	150
5.3	s-LbL Results	151
5.3.1	Overview	151
5.3.2	Comparison of Results to Frilot, Eshaq, and the Literature	153
5.3.3	Limitations and Sources of Error	154
5.3.4	New Questions Raised and Unresolved Questions	155
5.4	d-LbL Results	157
5.4.1	Overview	157
5.4.2	Comparison of Results to s-LbL and Previous Studies	159
5.4.3	Limitations and Sources of Error in d-LbL Experiments	161
5.4.4	New Questions Raised	162
CHAPTER 6 CONCLUSIONS AND FUTURE WORK		164
6.1	Evaluation of Hypotheses	164
6.1.1	Hypothesis 1	164

6.1.2	Hypothesis 2.....	165
6.1.3	Hypothesis 3.....	165
6.1.4	Hypothesis 4.....	166
6.2	Future Work.....	166
6.2.1	Platelet Adhesion	167
6.2.2	Fluid Dynamics.....	168
6.2.3	Surface Design.....	168
APPENDIX A MATLAB PROGRAMS		169
APPENDIX B COMPLETE DIGITAL ARCHIVE RECORD.....		173
APPENDIX C TECH DAIRY COW RECORD		174
APPENDIX D STATISTICAL SAMPLES: t-TEST		176
APPENDIX E STATISTICAL SAMPLES: F-TEST.....		178
APPENDIX F PARTICLE TRACKING TEMPLATE.....		181
APPENDIX G MICROSCOPE SETTINGS FILE DETAILS		183
REFERENCES		185

LIST OF FIGURES

Figure 1	Intrinsic pathway for the coagulation cascade, initiated by injury to the blood or exposure of the blood to collagen (18).....	11
Figure 2	Extrinsic pathway for the coagulation cascade, initiated by injured tissue in contact with the blood expressing tissue clotting factor (18)	12
Figure 3	The polymerization of fibrinogen into cross-linked fibrin fibers in the presence of prothrombin and thrombin from the coagulation cascades (18).....	14
Figure 4	The LbL electrostatic multilayer process. A charged substrate is exposed to a solution with an oppositely charged polyion (top left) allowing the polyion to adsorb to the surface via electrostatic attraction. After a rinsing and drying cycle to remove unadhered polyions, the newly coated surface is exposed to an alternate polyion of opposite charge to the first (top right). This process is repeated as many times as necessary to achieve an engineered set of layers (bottom).....	15
Figure 5	Layout of glass slides in the Pyrex containers. The location on the slide for forceps manipulation is marked	31
Figure 6	Typical s-LbL layout. The solutions, left to right, were PDDA, Rinse, PSS, Rinse (for the polyion layers), and PDDA, Rinse, Fibrinogen, Rinse (for the biointerface layers).....	31
Figure 7	Controlled environment chamber (CEC) with the front cover removed	35
Figure 8	Temperature (right) and humidity (left) controllers located on top of the CEC.....	40
Figure 9	Basic equipment layout spaces in the CEC. Shown with the front plate removed for clarity.....	41
Figure 10	A sample experiment, with the Petri dishes laid out for their respective experiments, dynamic on the orbital shaker (left), and static on the CEC floor (right).....	41
Figure 11	Transferring the collected whole blood into a centrifuge tube	46

Figure 12	Centrifuge interior showing the two different types of buckets available for the 50 mL tubes (left and right) and the 15 mL tubes (top and bottom)	47
Figure 13	Centrifuged whole blood showing a clear separation into the pellet and plasma	48
Figure 14	Centrifuged whole blood an unsuccessful centrifuge run, showing cloudy plasma and a lack of thorough pelleting of the erythrocytes	49
Figure 15	Separated plasma, presumed to be PRP at this point, and collected into a 50 mL tube	50
Figure 16	Estimated cross-section of the waveform circulating around the Petri dish during oscillatory motion while over the Petri dish only. Graph shows the third order polynomial best-fit line from measured points at the dish wall, and an estimated point 0.5 mm inside the dish that estimated the slope at the wall.....	52
Figure 17	Estimated cross-section of the waveform circulating around the Petri dish during oscillatory motion while over the slide region only. Graph shows the third order polynomial best-fit line from measured points at the dish wall, and an estimated point 0.5 mm inside the dish that estimated the slope at the wall	53
Figure 18	Imaging locations on a slide. Shear regions from which images were captured are highlighted, The mark for the forceps handling edge is indicated on the left side	62
Figure 19	Image in which a fibril is visible on the lower left hand side, used as a criterion for excluding a region from imaging.....	63
Figure 20	Example of an image where there is a malformation of the d-LbL or a drying ring area	64
Figure 21	Flowchart for standard image processing program, <i>improcess_FINAL.m</i>	69
Figure 22	Flowchart for standard image processing program, <i>improcess_FINAL.m</i>	70
Figure 23	Equipment used to prepare for a Bioanalyzer run. Shown from left to right, 10 μ L and 200 μ L pipette tips, a new cell chip, the reagents box, a 1 mL centrifuge tube, and the two micropipettes	79
Figure 24	Slide with blackened back placed in the Petri dish aligned with the vertical axis markers. The template and its two horizontal axis markers and lower vertical axis marker can be seen in the image.....	85

Figure 25	Container with a hole cut in the bottom, set over the template and Petri dish. This setup allowed for filming of the fluid in the dynamic flow condition with no relative motion between the camera and the Petri dish	86
Figure 26	Flowchart 1 of 2 for particle tracking program, <i>ParticleTrack_FINAL.m</i>	87
Figure 27	Flowchart 2 of 2 for particle tracking program, <i>ParticleTrack_FINAL.m</i>	88
Figure 28	Local flat-plate transport model boundary conditions, calculated for a unit width and depth (into page). The top view shows one of the localized areas calculated for transport given a particle location, with the detail view shown from a side view for section A.....	90
Figure 29	Local transport model, shear stress definition, linear shear stress model	90
Figure 30	Still frame from the “Run 1” video for particle tracking. The Petri dish, slide with blackened silicone backing, template with position and sizing markers, and particles can be seen	100
Figure 31	Still frame from the “Run 1” Tagged Vector video for particle tracking. Particles are tagged with identifying numbers, and velocity vectors are extended from the particle centroids. The alignment markers, Petri dish outline, and exclusion zone can also be seen	100
Figure 32	Sample frame showing paths for all tracked particles, from 21s-28s of the original video, “Run 1”	101
Figure 33	Sample frame showing paths for all tracked particles, from 7s-14s of the original video, “Run 1”	102
Figure 34	Velocities over each slide region as a function of time, from 7s-14s of the original video, “Run 1”	103
Figure 35	Velocities over each Petri dish region as a function of time, from 7s-14s of the original video, “Run 1”	104
Figure 36	Radial velocities averaged over time and angular position, from 7s-14s of the original video, “Run 1”	105
Figure 37	Angular velocities averaged over time and angular position, from 7s-14s of the original video, “Run 1”	106
Figure 38	Velocity magnitudes averaged over time and angular position, from 7s-14s of the original video, “Run 1”	106
Figure 39	Shear stress magnitudes averaged over time and angular position, from 7s-14s of the original video, “Run 1”	107

Figure 40	Localized mass transport coefficient averaged over time and angular position, from 7s-14s of the original video, “Run 1”	108
Figure 41	Ratio of localized mass transport of NO to NO diffusion constant, from 7s-14s of the original video, “Run 1”	109
Figure 42	Flow cytometry results summary on the two reported days, showing the total number of reported events for high and low dilution, and the ratio between the two dilutions for each day.....	111
Figure 43	Sample wells 1-3 for the high-concentration stained PRP suspension, 2X the diluted concentration in wells 4-6, 6-2-2010 experiment	113
Figure 44	Sample wells 4-6 for the low-concentration stained PRP suspension, 0.5X the diluted concentration in wells 1-3, 6-2-2010 experiment	114
Figure 45	Sample wells 1-3 for the high-concentration stained PRP suspension, 2X the diluted concentration in wells 4-6, 6-16-2010 experiment	115
Figure 46	Sample wells 4-6 for the low-concentration stained PRP suspension, 0.5X the diluted concentration in wells 1-3, 6-16-2010 experiment	115
Figure 47	A sample montage image, in original color. AO fluorescence of adhered platelets on a d-LbL fibrinogen surface, with no L-a under high-shear dynamic flow	117
Figure 48	The black and white (B/W) of the color montage in Figure 47	118
Figure 49	The negative black and white (W/B) montage of Figure 47.....	118
Figure 50	s-LbL static exposure to PRP condition, montage of all thresholded negative black and white (W/B) images for experiment “3-31-2010 Static-Dynamic”. A: no chemical additive, B: chemical additive, 20 μ M L-a.....	119
Figure 51	s-LbL dynamic flow condition, montages of all thresholded negative black and white (W/B) images for experiment “3-31-2010 Static-Dynamic”. A, C, and E: no chemical additive; B, D, and F: 20 μ M L-a. A, B: low shear; C, D: mid shear; E, F: high shear.....	120
Figure 52	s-LbL experiment results for the “3-31-2010” experiment set	121
Figure 53	s-LbL static exposure to PRP condition, PBS with no d-PRP, stained with AO. Result shown from the “3-19-2010 Static-Dynamic” experiment data set. There was retention of AO stain on the LbL surface in the absence of platelets	122

Figure 54	s-LbL static exposure to PRP condition, PBS with no d-PRP, stained with AO, montage of all W/B images for the “3-19-2010 Static-Dynamic” data set	123
Figure 55	s-LbL Dynamic flow condition, PBS with no d-PRP, stained with AO, montage of all images for the “3-19-2010 Static-Dynamic” experiment data set. A, C, and E: no chemical additive; B, D, and F: chemical additive, 20 μ M L-a. A, B: low shear; C, D: mid shear; E, F: high shear.	124
Figure 56	s-LbL with PBS (no d-PRP) percent surface area coverage in static and dynamic flow conditions, with and without chemical additive in the dynamic condition, stained with AO and imaged in both FITC and TRITC	125
Figure 57	d-PRP on plain glass slide from the “3-31-2010 Static-Dynamic” experimental set, montage of set “Static Plain 0uM...”	126
Figure 58	A: Sample d-LbL microscopy result for the high-shear, no chemical additive condition in the “6-4-2010” set. B: Sample platelet adhesion from a microfluidics device as reported by Tsai, et al. (68), with a morphology of small, mostly circular areas of adhesion	127
Figure 59	s-LbL static exposure to PRP condition, FITC-fibrinogen and AO-platelet staining, images taken in FITC/TRITC filter pairs	128
Figure 60	A: One false-color red image (fc-red-image008) generated by thresholding the TRITC filtered AO fluorescence results, and then mapping the thresholded areas to the RGB Red [1,0,0]. B: Corresponding false-color green image (fc-green-image007) generated by thresholding the FITC filtered FITC-fibrinogen fluorescence results, and then mapping the thresholded areas to the RGB Green [01,0]	129
Figure 61	The superposition of the two false color images in Figure 60. The summed image produces RGB Yellow [1,1,0] in areas where the thresholded areas overlap.....	129
Figure 62	The superposition of the two false color images from the dynamic, no chemical additive condition. A: Low-shear region, B: Mid-shear region, C: High shear region	131
Figure 63	Montages of d-LbL surfaces exposed to d-PRP under static conditions, and stained with AO. A: no chemical additive; B: 20 μ M L-a. “5-17-2010 dLbL” data	132
Figure 64	Montages of d-LbL surfaces exposed to d-PRP under dynamic flow conditions, and stained with AO. A, C, and E: no chemical additive; B, D, and F: chemical additive, 20 μ M L-a. A, B: low shear; C, D: mid shear; E, F: high shear. “5-17-2010 dLbL” data	133

Figure 65	Montages of d-LbL surfaces exposed to d-PRP under static conditions, and stained with AO. A: no chemical additive; B: 20 μM L-a. “6-19-2010 dLbL” data	134
Figure 66	Montages of d-LbL surfaces exposed to d-PRP under dynamic flow conditions, and stained with AO. A, C, and E: no chemical additive; B, D, and F: chemical additive, 20 μM L-a. A, B: low shear; C, D: mid shear; E, F: high shear. “6-21-2010 dLbL” data	135
Figure 67	Percent surface area coverage data in each condition category-for the “5-17...”, “6-4...”, “6-19...”, and “6-21...” fibrinogen compared to collagen experiment results.....	136
Figure 68	Percent differences between the control (0 μM L-a) and the experimental (20 μM L-a) chemical additive conditions at different shear rates.....	137
Figure 69	s-LbL, fibrinogen surface, FE-SEM image, 15.0K magnification, scale marks 3.00 μm	138
Figure 70	d-LbL, fibrinogen surface, FE-SEM image, 9.0K magnification, scale marks 5.00 μm	138
Figure 71	d-LbL, collagen surface, FE-SEM image, 12.0K magnification, , scale marks 4.00 μm	139
Figure 72	Percent surface area coverage in each condition category-for the “5-17...”, “6-4...”, “6-19...”, and “6-21...” fibrinogen experiment data sets only, averaged over each day’s results	140
Figure 73	The total change, $\Delta_{L,a}$, in fluorescent percent surface coverage for the static exposure to PRP and the dynamic flow condition, for the d-LbL fibrinogen and collagen experiments.....	144
Figure C-1	Tech Dairy Cow Record for Cow #41, scanned image of datasheet.....	175
Figure F-1	Template used as a background for filming particle tracking videos.	182

LIST OF TABLES

Table 1	Clotting factors in blood and their synonyms, from Guyton and Hall (18).....	10
Table 2	Quantities of adhesion chemical additive, 1 mM L-a solution, to be added to each prepared tube of d-PRP for the two different flow conditions and two different chemical additive conditions.....	51
Table 3	The slides stained with fibrinogen-FITC stain, showing the flow condition (static/dynamic) and the concentration chemical additive, L-a	60
Table 4	Pairings for statistical testing of results used to compare s-LbL and d-LbL percent surface coverage by AO stain.....	94
Table 5	Pairings of statistical tests used to compare d-LbL Fibrinogen and d-LbL Collagen for percent surface coverage.....	95
Table 6	Pairings of statistical tests used to examine d-LbL surfaces under different flow and chemical additive conditions.....	96
Table 7	t-Test comparisons for means and F-test comparisons for variances. Items above the 0.05 threshold are in bold	141
Table 8	t-Test comparisons for means and F-test comparisons for variances. Items above the 0.05 threshold are in bold	142
Table 9	t-Test comparisons for means and F-test comparisons for variances. Items above the 0.05 threshold are in bold	145
Table D-1	Sample t-test to validate statistical process comparing data that are similar in means and data that are significantly different, with an α of 0.05.....	177
Table E-1	Sample F-test to validate statistical process comparing data that are similar in variance/means and data that are significantly different in variance, with an α of 0.05.....	179
Table E-2	Sample F-test to validate statistical process comparing data that are similar in variance with different means and data that are significantly different in variance, with an α of 0.05	180

ACKNOWLEDGMENTS

I would like to acknowledge all the people that have contributed so much to my professional development and my work. To Dr. Melanie Watson, my constant friend and lab mate, our work would not have had the depth and quality without you. To Dr. Gonzalez: my roots in science and investigation are firmly rooted in the opportunity you gave me to start along this path and your encouragements towards excellence. To Dr. Roy Henk: thank you for your example of integrity and thoroughness in research, along with your example of humble wisdom. To my brothers on 41: you helped shape me and mold me into the man I am today, and I owe you an indelible debt of friendship, especially Soo-Jin Lee, Brian Marianelli, and Nathaniel Miller. To my committee, Dr. Steven Jones, Dr. Eric Guilbeau, Dr. James Spaulding, Dr. June Feng, Dr. Stan Cronk: thank you for your support and mentorship, the scientist and academic I become will always have its roots in the opportunities you provided for me at Louisiana Tech. To my friends, George Hernandez, Brian Gist, Leandro Bruno, Marlin Sinville, Eduardo Lesser, Juan Fontana, Cristian Pasluosta, Bill Gibson, Jerome Saltarelli: you have each contributed so much to my own personal and professional development, been examples in your own right, and been constant sources of joy and encouragement, no thanks will ever be sufficient.

CHAPTER 1

INTRODUCTION

1.1 Hemostasis and Cardiovascular Disease

Hemostasis is one of the principal processes involved in maintaining homeostasis. Dysfunction in hemostatic processes is closely related to many forms of cardiovascular disease (CVD). A 2010 report by the American Heart Association's Lloyd-Jones et al. [1] states that as of 2005 CVD was the cause of death for ~275 per 100,000 in the US population, and was expected to be ~250 deaths per 100,000 population by 2010. According to the U.S. Census [2], 830 deaths occurred per 100,000 population in 2005, making CVD responsible for ~33% of all deaths that year.

The study of Lloyd-Jones et al. was conducted to establish metrics for health statistics, treatment impact and treatment outcomes, with the goal of reducing CVD by 25% of current levels by 2020. To achieve this goal, new approaches to medication, preventative therapies, and diagnostic tools will be needed. The research presented in this dissertation examines a physical process associated with a wide range of CVD problems, platelet activation and adhesion – thrombus formation.

1.2 Platelet Adhesion

The principal non-pathological function of thrombi is to form a plug at the site of an injury to plug the vascular leak and allow the body to begin healing. Pathological

thrombi cause embolisms, ischemia, and myocardial infarctions [3] [4]. Platelets can be activated by excessive shear stress as they move through a stenosed vessel [5], or by interaction with collagen/von Willebrand factor (vWF) from a damaged vessel endothelium [6] [7]. Platelet activation begins a chain reaction releasing a variety of chemicals to regulate thrombus formation. Thrombogenic factors such as platelet-derived growth factors, coagulation factors, and activation of nearby platelets, as well as thrombolytic factors such as platelet-derived nitric oxide (pd-NO), are all generated by activated platelets. Platelet activation, signaling, receptors, thrombogenesis, and the various pathologies associated with the subsequent thrombi have been areas of constant investigation over the years [8] [9] [10].

1.3 Nanotechnology Biointerfaces/Lab-on-a-Chip

The work presented in this dissertation stemmed from a continuation of work begun in our laboratory by Frilot [11] and Eshaq [12], who were studying platelet adhesion on biointerface surfaces under static (Frilot) and dynamic (Eshaq) flow conditions. This earlier work was conducted to establish the link between shear stresses and the effect of various platelet chemical additives on thrombogenesis and platelet adhesion to the LbL surface.

While attempting to replicate these earlier results, questions arose over the functionality of the LbL surface from Eshaq's work and the imaging techniques being used to quantify adhesion on those surfaces (see §1.4). Therefore, this study did not aim to shed new light on platelet adhesion behavior, but rather to validate an LbL surface manufacturing process and an assay method to determine platelet adhesion. This type of design is related to Lab-on-a-Chip (LoC) technologies.

LoC technology is the concept of integrating an entire assay into a micro-scale environment that could allow for the assay or multiple assays to be performed on a single device, or “chip.” Eliminating the need for large-scale laboratory equipment and multiple assay steps requiring human interaction is attractive for both the ability to increase research throughput and the reduced possibility of human error. Chin et al. [13] have identified 18 communicable and 17 non-communicable diseases or disease groups that would benefit greatly from specific assays being given LoC technology emphasis; among these is CVD. Dittrich and Manz [14] describe how LoC technology can be exploited to greatly increase throughput in drug function tests, and suggest that the throughput using LoC technology could eventually outperform conventional robotic techniques.

The benefit of performing platelet adhesion tests on nano-scale engineered biointerfaces is that specific physiological conditions can be tested in repeatable, controllable scenarios. While the same technology could be used to generate a surface with an endothelial cell layer, the current biointerface approach eliminates the additional variables introduced by cellular signaling pathways, and reduces the interactions to those being studied. This simpler surface is a polymeric multilayer base material under the desired biointerface.

1.4 Limitations of Prior Approaches

The initial research focus in our laboratory had been to replicate the Eshaq [12] and Frilot [11] work to validate the experimental methodology, and then expand on that work with controlled shear stresses, different chemical additives, and chemical additive concentrations on the standard or “static” manufactured LbL surfaces (s-LbL). During

attempts to repeat the work of Eshaq and Frilot, questions arose about the validity of the microscopy results.

The initial questions stemmed from the fluorescence microscopy (FM) images that were taken from slides that had been exposed to platelet-rich plasma (PRP), stained with acridine orange (AO), and then rinsed to remove excess AO. For s-LbL imaging, each FM image was generated by integrating 66.67 to 166.67 ms of optical data for a single frame. A longer integration time often caused the images to wash out into a bright red that could not be processed by the image processing program. The exact time integration setting varied from experiment to experiment, however, and a few experiments required much higher time integration, some as high as 666.67 ms.

This brightness issue meant that the researchers needed to vary integration time for each experimental slide to be imaged. The different integration times led to difficulties in comparing results from experiment to experiment. Images in the 66.67 ms integration range were rejecting data that would have been considered “platelet adhesion” at 166.67 ms. This type of qualitative, value judgment setting based more on the experience of the researcher than on a replicable process was a problem that needed to be overcome.

A proposed homogenizing process was to stain a slide from each s-LbL generated lot that had never been exposed to PRP. A control slide was used that was exposed to the buffer, phosphate-buffered saline (PBS), instead of the dilute-PRP (d-PRP). This slide was processed alongside the rest of a day’s experiments, all the way through the staining and microscopy. It was hypothesized that the fluorescence results from the control slide could then be used to normalize the results from all microscopy versus a common

background fluorescence quantity. The results from the initial attempts at this process were surprising, and led to a series of experiments that eventually invalidated the use of s-LbL surface in platelet adhesion studies where AO fluorescence would be used as the quantifying process (Red-Green tests, §3.4.3.2, 3.4.4.4.3). In short, the s-LbL surfaces, under AO staining conditions, provided strong false positives for platelet adhesion (§4.4.2).

1.5 Current Work

With the viability of the platelet adhesion experimental protocols and assays in question, the work presented for this dissertation sought to establish an improved methodology that would allow for unambiguous identification of platelets on an engineered biointerface. Because the s-LbL surface was retaining AO stain, it was hypothesized that some physical characteristic of the surface was contributing to this stain retention. The original surfaces needed to be tested to confirm this false positive bias, and an alternative surface needed to be designed and similarly tested. Other researchers have proposed using dynamic techniques such as flow [15] and vibration [16] to homogenize the deposited surfaces, and it was theorized that a similar approach could be taken to generate a smoother, more homogenous and repeatable surface than with the s-LbL method.

The work by Eshaq [12] had taken place in a microfluidics environment, where shear stresses could be controlled tightly with a digitally controlled infusion. However, in designing and testing a new surface, the additional variables introduced by the manufacture and assembly of the microchannels were eschewed for a simpler test bed, whole glass slides in a Petri dish, a simplification that was introduced while mentoring a

summer research student in our laboratory, Veverka [17]. In mentoring Veverka, we discovered the sensitivity of the existing microchannel approach to factors such as bolt tightness, spacing between microchannels, and bubbles in the flow. All of these factors led to varying pressure conditions within the microchannels, and could produce “cross-talk” between test channels by allowing leak-through. The alternative approach was to place a Petri dish on an orbital shaker to produce oscillatory flow and a shear gradient. This shear gradient was expected to provide an uncalibrated rough estimate of shear-stress dependent effects on adhesion on a single surface, without the need for microchannel and multiple infusion pumps or infusion runs.

A new LbL surface generation protocol was proposed and tested, dynamic LbL (d-LbL). This protocol differed from the original s-LbL in that the layering solutions were constantly washed over the glass slides. It was theorized that this dynamic aspect to the layering process would generate a more homogeneous surface coating as reported by other d-LbL processes, and would provide a biointerface with fewer pockets that could trap the AO stain that is incorrectly interpreted as platelet adhesion. To compare the new flow system and the d-LbL process to the previously standard methods in the laboratory, the following four hypotheses were proposed (§1.5.1, 1.5.2, 1.5.3 and 1.5.4), and tested as described in Chapter 3.

1.5.1 Hypothesis 1

When s-LbL and d-LbL fibrinogen surfaces are exposed to either PBS or PRP and then stained with AO, the percent surface area that fluoresces will be smaller for the d-LbL surface than for the s-LbL surface.

If Hypothesis 1 is demonstrated, it suggests that d-LbL surfaces retain significantly less anomalous AO stain, increasing the likelihood that the observed fluorescent peaks are associated with platelets or cellular material on the surface.

1.5.2 Hypothesis 2

The shear stress on a glass slide that is placed in a Petri dish, covered with fluid, and agitated to generate a swirl flow will increase as the location on the slide changes from the center of the Petri dish to the edge, and the AO fluorescence percent surface coverage of d-LbL fibrinogen-coated slides that are exposed to PRP, with and without added L-arginine (L-a) will be significantly different on regions of the slide corresponding to different shear stresses.

If Hypothesis 2 is demonstrated, it suggests that a swirl flow configuration could be used as an initial screening approach for shear-dependent properties, to isolate properties that may be tested in more controlled conditions such as microchannel infusions.

1.5.3 Hypothesis 3

The addition of L-a to platelets in plasma will decrease observed fluorescent percent surface coverage of d-LbL surfaces under shear conditions.

If Hypothesis 3 is demonstrated, it suggests that the observed fluorescent percent surface area coverage, if it is indicative of platelet adhesion (Hypothesis 1), may be affected by released pd-NO, as stimulated by the presence of the pd-NO precursor, L-a.

1.5.4 Hypothesis 4

When d-LbL surfaces are exposed to PRP, without flow, the fluorescence percent surface coverage will be smaller when L-a is added to the PRP, but the reduction of surface coverage will be significantly less than observed under shear flow of PRP.

If the percent surface coverage decreases for dynamic flow, but does not decrease for static flow, as suggested by Frilot's results [11], a possible explanation is the enhanced transport of L-a or NO caused by the flow condition.

CHAPTER 2

BACKGROUND

2.1 Thrombi

2.1.1 Coagulation Overview

The body regulates its blood supply in different ways to achieve hemostasis. Hemostasis is the process through which blood loss is prevented, and blood-loss injuries stabilized and repaired. While several mechanisms contribute to hemostasis, such as vascular constriction, platelet plugs, and fibrous tissue growth to seal a rupture permanently, the mechanism of interest for the research presented here is blood clotting. Blood clotting, or coagulation, is the process through which 1) platelets become activated, 2) prothrombin activator is generated, 3) prothrombin activator catalyzes prothrombin into thrombin, and 4) thrombin polymerizes fibrin fibers from fibrinogen to form a fibrous mesh in which platelets and red blood cells (RBC) are trapped, resulting in coagulated blood, or a clot. Coagulation occurs in the body at the site of a vascular injury, where collagen has been exposed, at a site where elevated shear rates activate platelets, on non-biocompatible materials, and from damage to the cells in the blood [6] [18] [19].

Blood coagulation is a complex process that involves ~50 substances, divided into clotting promoters (procoagulants) and inhibitors (anticoagulants) [18] [20]. Fifteen of these substances (Table 1) are a part of both principal chemical processes that lead to

coagulation: the intrinsic and extrinsic pathways. These chemical pathways are collectively known as the coagulation cascade [18].

Table 1 Clotting factors in blood and their synonyms, from Guyton and Hall [18]

CLOTTING FACTOR	SYNONIMS
Fibrinogen	Factor I
Prothrombin	Factor II
Tissue Factor	Factor III; tissue thromboplastin
Calcium	Factor IV
Factor V	Proaccelerin; labile factor; Ac-globulin (Ac-G)
Factor VII	Serum prothrombin conversion accelerator (SPCA); proconvertin; stable factor
Factor VIII	Antihemophilic factor (AHF); antihemophilic globulin (AHG); antihemophilic Factor A
Factor IX	Plasma thromboplastin component (PTC); Christmas factor; antihemophilic factor B
Factor X	Stuart factor; Stuart-Prower factor
Factor XI	Plasma thromboplastin antecedent (PTA); antihemophilic factor C
Factor XII	Hageman factor
Factor XIII	Fibrin-stabilizing factor
Prekallikrein	Fletcher factor
High-molecular-weight (HMW) kininogen	Fitzgerald factor; HMWK (high molecular weight) kininogen
Platelets	

The intrinsic pathway (Figure 1) is initiated when the blood itself is injured or exposed to collagen, while the extrinsic pathway (Figure 2) is initiated when injured tissues are exposed to blood. These two pathways are positive feedback systems in which the generated thrombin further increases coagulation. This feedback causes the coagulation to occur rapidly when necessary, but when it is unchecked, it can be disastrous. Production of pd-NO and other anticoagulant processes control these positive feedback pathways so that they do not coagulate the entire blood supply. Some of these

include the sequestering of thrombin on the endothelial surface and the endothelial surface expression of glycocalyx, which repels platelets and clotting factors [18].

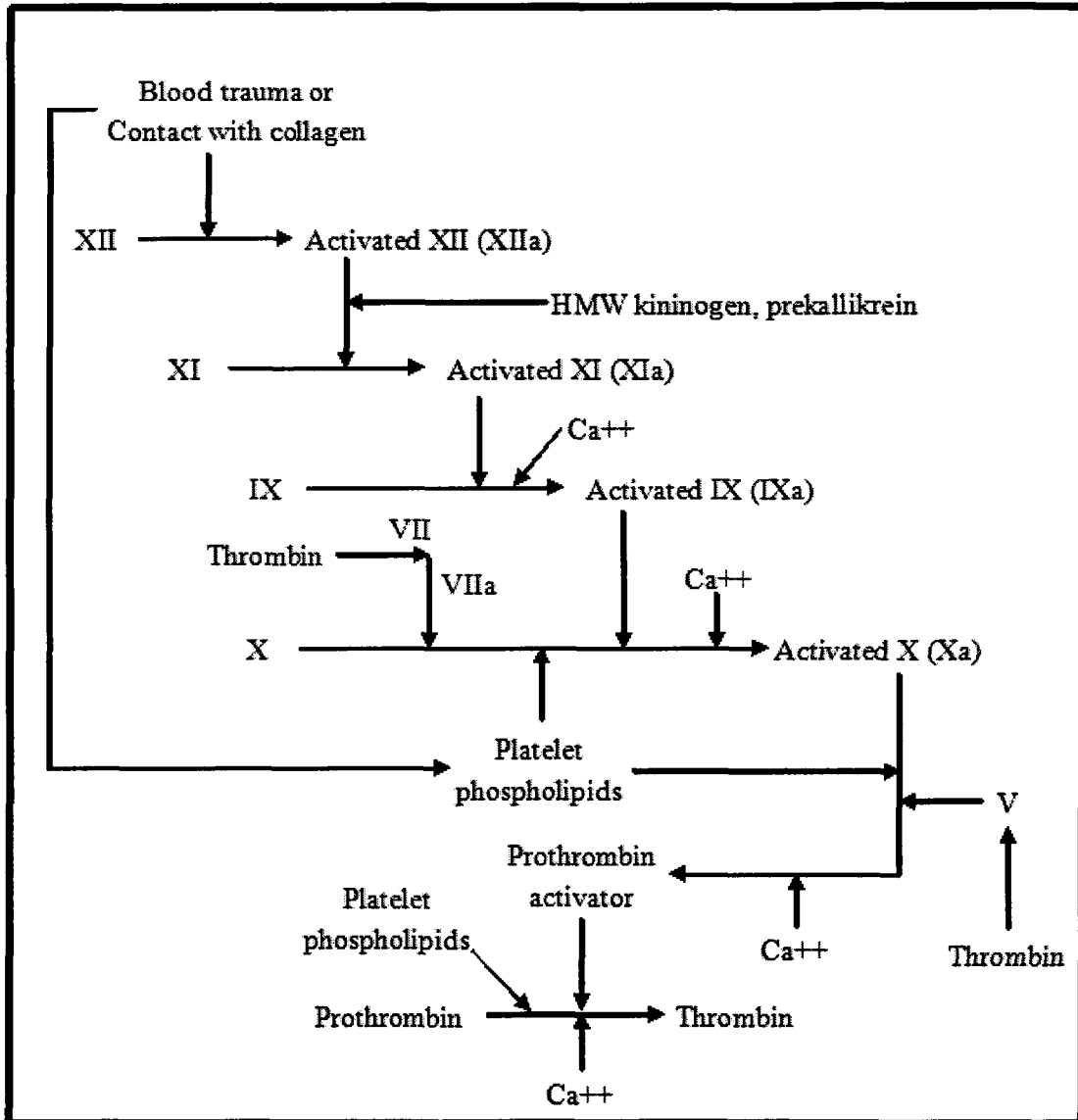


Figure 1 Intrinsic pathway for the coagulation cascade, initiated by injury to the blood or exposure of the blood to collagen [18]

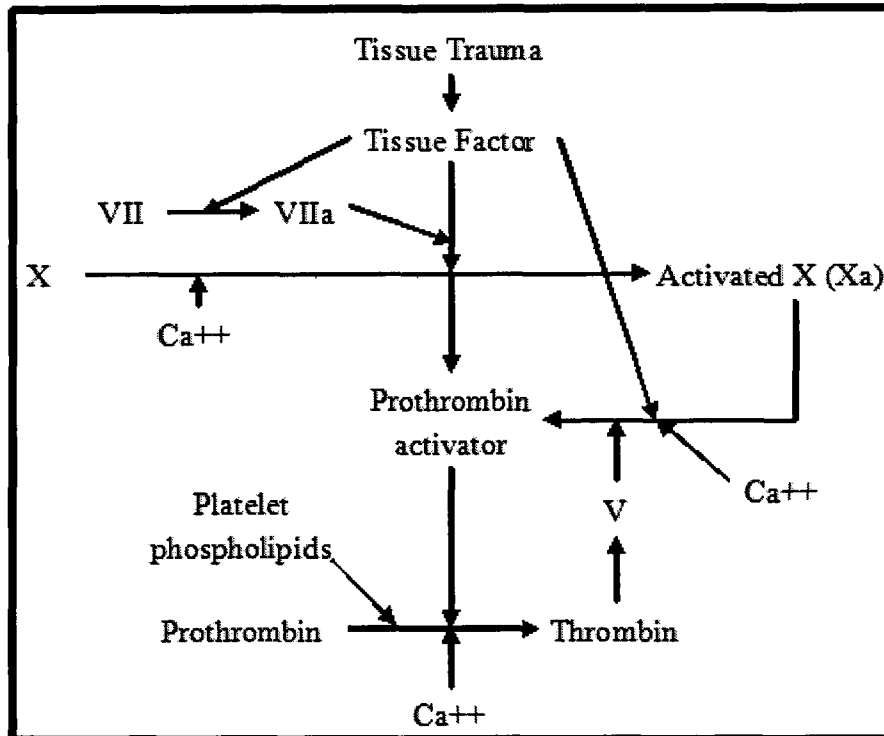


Figure 2 Extrinsic pathway for the coagulation cascade, initiated by injured tissue in contact with the blood expressing tissue clotting factor [18]

The protein von Willebrand Factor (vWF) is involved in retaining the platelets at the site of adhesion, even under shear stress. vWF is produced in the endothelium and subendothelial cells. It can adhere to the endothelial layer, but has a greater affinity for the collagen under the endothelium. Thus, when an injury exposes the endothelium, vWF adheres to the collagen and arrests platelets by interacting with various receptor sites on platelets, including glycoprotein IIb and IIIa [21] [22] [23] [24]. While it is an important factor in coagulation, it was not a principal area of study in this dissertation.

2.1.2 Nitric Oxide and L-Arginine

One of the anticoagulants involved in the clotting process is Nitric Oxide (NO). NO is continuously produced at low levels by the endothelium along the inner walls of vessels, inhibiting clotting in non-injury conditions, but is also produced by the platelets

in the form of pd-NO as a self-limiter of the retention of platelets during the coagulation cascade [19] [20] [25].

NO and L-a are directly linked in various NO pathways. NO can be synthesized from L-a by NO synthase. The L-a-NO pathways can directly inhibit platelet activity through both the release of NO from the L-a/NO synthase reaction and the increase of cyclic guanosine monophosphate (GMP) in the platelet cytosol. The L-a does not increase baseline cyclic GMP, but only acts on the cyclic GMP in the presence of collagen [26] [27] [28]. Because the cyclic GMP action would be a nuisance variable when attempting to isolate the effects of pd-NO on aggregation, the biointerface was changed from collagen to fibrinogen.

2.1.3 Fibrinogen

Fibrinogen is a precursor to fibrin fibers, which are generated because of the coagulation cascade in the presence of prothrombin and thrombin (Figure 1, Figure 2). The transformation process is shown in Figure 3.

Fibrinogen is found in the blood plasma, being originally manufactured in the liver [18]. In physiological conditions, fibrinogen is in solution, and added to the coagulation reaction as shown in Figure 3. However, fibrinogen coatings have been shown to initiate platelet adhesion in various studies, including Eshaq [12] from our own laboratory [29] [30] [31]. Heemskerk et al. [29] showed that platelets adhered to fibrinogen tended to spread out on the surface, while those adhered to collagen tended to bleb or form balloon-like structures. Savage et al. [30] showed how platelet integrin $\alpha_{IIb}\beta_3$ could arrest platelets onto fibrinogen, though this function is limited to shear rates below $600\text{-}900\text{ s}^{-1}$. These shear rates were larger than those used in our tests and in the tests

previously performed by Eshaq, so fibrinogen was presumed to be an adequate surface for arresting platelets under the shear conditions to be tested.

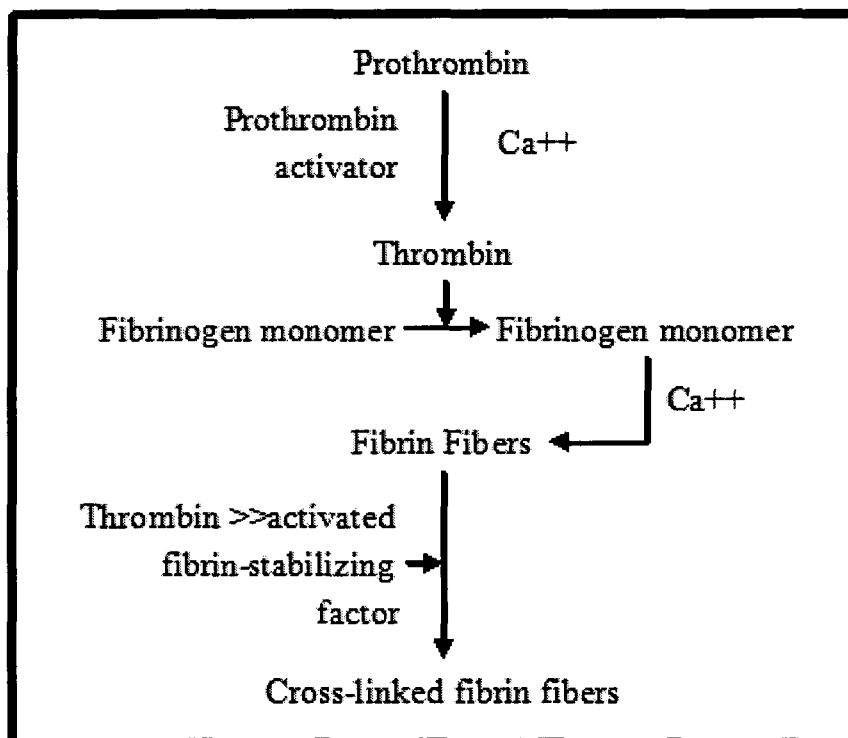


Figure 3 The polymerization of fibrinogen into cross-linked fibrin fibers in the presence of prothrombin and thrombin from the coagulation cascades [18]

2.2 Layer-by-Layer Self-Assembly (LbL) in Biomedical Applications

LbL is a powerful and simple process to generate engineered structures on a nanometer scale [32] [33]. The films can be categorized as roughly thin films [34] [35], particles and particle coatings [36] [37] and additional three-dimensional coatings such as those covering carbon nanotubes [38]. The process exploits electrostatic attraction to form nanometer thickness coatings by exposing a surface to alternating solutions with dissolved charged polymers (polyions), as shown in Figure 4.

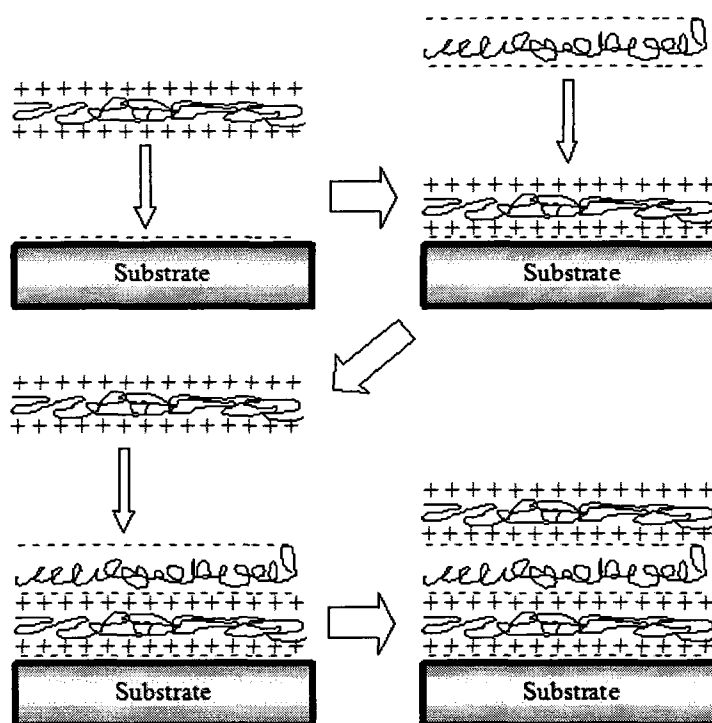


Figure 4 The LbL electrostatic multilayer process. A charged substrate is exposed to a solution with an oppositely charged polyion (top left) allowing the polyion to adsorb to the surface via electrostatic attraction. After a rinsing and drying cycle to remove unadhered polyions, the newly coated surface is exposed to an alternate polyion of opposite charge to the first (top right). This process is repeated as many times as necessary to achieve an engineered set of layers (bottom)

This simple process has been employed in a wide range of applications, and has gained popularity as a tool for generating biologically active surfaces or altering biological surfaces to meet specific needs [35]. Platelets have been coated with LbL and nanoparticles to aid in microscopy detection of single cells [36]. Collagen and fibrinogen films have been engineered, and some have been used for platelet adhesion studies [11] [12] [34]. The fundamental LbL structure pursued for this research was different from the engineered films tried before in one principal way: the introduction of a dynamic process to the layering step in an attempt to generate smoother surfaces. The layer constituents,

number of layers, and rinsing and drying steps remained the same to isolate the addition of a dynamic component as the principal cause of morphology changes.

Other researchers have shown that LbL surfaces generated under dynamic rather than static conditions generate more homogenous, functional surfaces. Grzybowski and Campbell [39] have reviewed processes that can be used in dynamic layering, including magnetic, electrostatic, and vortexing approaches. Jiang et al. [40] used spinning as the dynamic component, rapidly producing uniform layers of high integrity. Deng et al. [41] combined d-LbL with varying pH of the polyion solutions to generate nonporous membranes that were more efficient in their filtration than the standard s-LbL process. Other dynamic approaches have included vibration [16], laminar flow [15], and pervaporation [42]. Yin et al. [16] used vibration as the dynamic component to layer poly(diallyldimethylammonium chloride) PDDA and poly(styrene sulfonate) (PSS), the two non-biological materials used in the LbL processes used for this dissertation. They report that multiple bilayers of these polyions deposited under the vibration dynamic condition showed dense and smooth films with an improved pervaporation in the dehydration of isopropanol compared to s-LbL surfaces.

The literature review did not produce a group attempting a d-LbL process like the one used for the work presented in this dissertation. However, the literature demonstrates that improved surface performance and other benefits are gained when a dynamic component is added to the LbL process. The work in this dissertation was therefore conducted to test the function of a simple dynamic condition that did not require flow chambers, pumping equipment, magnetic or electric field controls, or a method of securing slides during vibration.

2.3 Lab-on-a-Chip (LoC)

While LbL modified surfaces have strong potential in biomedical and other applications, they have not yet been used in contexts beyond the research laboratory. A motivation for improved LbL techniques is the application to LoC technologies. A variety of biomedical applications are being developed that combine microfluidics with engineered surfaces to create LoC technologies. Examples include clinical diagnostics of human physiological fluids [43], optical transducers [44], cell differentiation and cell culture [45], cell injection, lysis, separation, and detection on a single chip [46], isolation of plasma from blood [47], and fully-integrated PCR for DNA analysis [48].

The analysis of physiological fluids and the study of cellular behavior, such as platelet adhesion and thrombus aggregation, are natural extensions of previous LoC studies. Not only do LoC technologies simplify complicated analyses, but they also help reduce the size of the sample required to make a useful measurement. The focus of this dissertation was to design and test a new LbL surface, so the microchannel approach by Eshaq [12] was temporarily replaced by the whole-slide approach initially attempted in our laboratory with Veverka [17]. However, once the surface fabrication processes are validated, subsequent researchers can combine them with the microfluidics approach as a LoC technology. The whole-slide tests required sample sizes of 5 mL to 15 mL, while a microfluidics approach could perform the same assays with samples smaller than 5 mL. Smaller samples become advantageous in the laboratory setting because all of the blood can be processed at the same time instead of in separate batches, reducing sources of variability in the experiments.

2.4 Previous Studies from our Laboratory

2.4.1 Collagen/Static Studies – Frilot

Frilot [11] used a fibrillar collagen film (not an LbL process) coated on the bottom of a Petri dish as a bioactive surface to promote platelet adhesion and activation. The production and diffusion of serotonin were studied via voltammetry. Serotonin-specific electrodes were used to measure the signal from the adhered platelets, and the results were compared to chemical additive release computed from a mathematical model of platelet activity, including the release of pd-NO, under static exposure to PRP/diffusion conditions. The measured values were several orders of magnitude lower than the mathematical model predicted. Electrode fouling, limitations in electrode distance from thrombi, and a stochastic distribution of thrombi across the surface were all suspected to contribute to this difference. Frilot's images of platelet adhesion on the collagen surface correlated well with our own plain glass (§4.4.3.2) and d-LbL results (§4.5). Frilot did not observe a measurable change of serotonin in the presence of platelet chemical additives, suggesting that a dynamic flow condition would be necessary to have these effects amplified to a measurable level.

2.4.2 Fibrinogen/Dynamic Studies – Eshaq

Eshaq [12] extended Frilot's studies attempting to test platelet response to chemical additives under dynamic conditions. She infused dilute PRP (d-PRP) through microchannels that had been fibrinogen coated with the s-LbL method to model physiological flow conditions. Eshaq tested the effects of ADP, a platelet activator, and L-a, a precursor to the platelet adhesion inhibitor NO, on the percent surface coverage by platelets under flow conditions. The hypothesis was that the effects of both ADP and L-a

would increase with increasing shear rates. The results supported the hypothesis, but as discussed in §1.4, problems inherent to the s-LbL surface used necessitated a redesign of the bioactive surface, and will require revisiting this work in the future with the improved surface.

For the current work, the literature review indicates that exposure to collagen opens additional nuisance variables when attempting to isolate pd-NO effects on thrombus formation (§2.1.2), and fibrinogen has been shown to arrest platelets adequately within the shear regions tested (§2.1.3). This further supported the use of fibrinogen as the bioactive surface in the LbL process.

CHAPTER 3

METHODS

3.1 Experimental Workflow for Hypotheses Tests

The generalized workflow for this study is described here, broken down by the hypotheses (§1.5).

3.1.1 Hypothesis 1

Before it could be shown that d-LbL surfaces reduced the amount of anomalous staining caused by the pooling of AO, it was necessary to determine whether observed AO signals were present that were not associated with platelet adhesion. Therefore, s-LbL was used to coat slides with fibrinogen. Some of these slides were exposed to PBS only, with no platelets, and others were exposed to d-PRP. The experiments were performed under both static and dynamic conditions. Also, because L-a itself could affect the staining, experiments with and without L-a were compared.

As a positive control for adhered platelets, plain glass slides were exposed to d-PRP, stained, and imaged (§3.4.3.2). The glass surface is a known activator of platelets [49]. The specific questions to be answered with these experiments were whether AO stained s-LbL slides that were never exposed to d-PRP generated fluorescent signals, and whether the calculated percent surface coverage from these slides was statistically different from the calculated percent surface coverage from slides that were exposed to d-PRP.

To determine whether the d-LbL process creates surfaces with less anomalous AO staining than the s-LbL process, fibrinogen surfaces were prepared with both s-LbL (§3.2) and d-LbL (§3.5). These surfaces were subjected to static and dynamic flow conditions of platelet-laden d-PRP with and without the platelet chemical additive L-a following the same procedures for both LbL types (§3.2.4.6). The anomalous adhesion (AO accumulation not caused by platelets) was established by tests without platelets, as described earlier in this section. The platelet count of the d-PRP was analyzed with a form of flow cytometry (§3.6) to quantify the concentration of platelets across the various days of d-PRP experiments.

The distribution of fibrinogen on the final LbL surface generated with the standard, static process (s-LbL) was imaged by tagging the fibrinogen with an anti-fibrinogen antibody tagged with fluorescein isothiocyanate (FITC). FITC FM images and AO FM images were taken sequentially in individual spots to generate a composite overlap of presumed platelet adhesion as a function of fibrinogen distribution in a series of tests called the Red-Green tests (§3.4.3.2).

The d-PRP slides were stained with AO following the laboratory's standard methods (§3.3.4.5), and then imaged under fluorescent microscopy (§3.4.4). The images were processed with a MATLAB® program to calculate the percent surface coverage (§3.4.5). The percent surface coverage for d-LbL (§4.5) and s-LbL (§4.1) were compared with a t-test for means and an F-test for variances. The surface morphologies of the s-LbL and d-LbL surfaces were also compared through FE-SEM imaging (§3.7).

3.1.2 Hypothesis 2

To test the shear-dependent properties of platelets, d-LbL slides were subjected to a control flow condition, static (§3.3.4.1), and a test flow condition, dynamic (§3.3.4.1.2), on different slides from a single batch of d-LbL slides. The staining, fluorescence microscopy, and data processing remained the same as for Hypothesis 1. The means and variances of surface coverage by platelets indifferent shear regions for the dynamic flow condition and the static exposure to PRP condition were compared with the t-test and F-test methods described in §3.9.

An additional control experiment was performed on d-LbL surfaces prepared with a collagen biointerface (§3.5.4.4). This test was used to validate the static control condition in fibrinogen d-LbL against previous work by Frilot [11] through a series of statistical tests. By extending the comparison to the dynamic flow condition, the observed patterns in total calculated percent areas as a function of shear with fibrinogen d-LbL surfaces were further supported.

Approximate velocities and shear stresses on the slides under dynamic flow conditions were obtained from a particle tracking experiment (§3.6). A MATLAB program was used to track particles at the surface of the liquid in a Petri dish to obtain statistics for velocity as a function of position within the dish. These velocities were combined with a surface profile, estimated from photographs, as the fluid wave moved around the dish, to estimate shear rates and local transport coefficients for NO (§3.8.4).

3.1.3 Hypothesis 3

To test the effect of adding L-a to the d-PRP under dynamic conditions, the dynamic flow procedures from Hypothesis 2 were performed for a control condition (no

L-a), and a chemical additive condition (with L-a). The means and variances of percent surface coverage for the two conditions were compared with the t-test and F-test, respectively.

3.1.4 Hypothesis 4

To test whether the addition of L-a affected adhesion under static conditions, the static exposure to PRP procedures in Hypothesis 2 were performed for a control condition (no L-a) and a chemical additive condition (with L-a). The means and variances of percent surface coverage for the two conditions were compared with the t-test and F-test, respectively.

3.2 s-LbL and d-LbL Biointerfaces for Platelet Adhesion Studies

3.2.1 Overview

This section describes the protocols for s-LbL and d-LbL coating. The s-LbL processes were the previous standard in our laboratory to manufacture biointerfaces for platelet adhesion studies. The two coating methods were similar, except for the addition of the dynamic component in d-LbL. Therefore, this section follows the sequence required for s-LbL, with differences required for d-LbL indicated as needed.

3.2.2 Process Summary

Prior to the day on which slides were to be layered, the chemicals were prepared and balanced to the required pH levels (§3.2.3), and glass slides for the LbL base substrate were cleaned (§3.2.4.2). On the day of LbL generation, the polyion chemicals and rinses were laid out in rectangular Pyrex containers (§3.2.4.3). The slides alternatively immersed in solutions of PDDA and PSS (§3.2.4.3.1) with a rinse and drying step (§3.2.4.3.2 and 3.2.4.3.4) between each polyion immersion. This process was

repeated five times to form a five-bilayer substrate for the biointerface. The slides could be stored at this point to add the biointerface the following day, or the biointerface could be added immediately. To add the biointerface, the slides were alternatively immersed in solutions of PDDA and fibrinogen (§3.2.4.3.3) with a rinse and drying step (§3.2.4.3.2 and 3.2.4.3.4) between the PDDA and fibrinogen immersions. This process was repeated three times to generate a final coating of eight bilayers. The leftover reagents were disposed of following an approved waste handling procedure (§3.2.4.4). The prepared slides were stored (§3.2.4.5) for use in subsequent d-PRP experiments to test platelet adhesion under various conditions (§3.2.4.6).

The procedures for d-LbL differed from the s-LbL method only in the replacement of static immersion with immersion in individual centrifuge tubes that could be placed on an orbital shaker to flow the LbL solution continuously over the glass slide.

3.2.3 Solution Preparations

All solutions were mixed with room-temperature reagents and liquids except for the biological surfaces, which were kept in -4°C storage until ready to be measured for mixture. However, because the volumes were small, these reagents came up to ambient temperature quickly.

Before storage, all solutions were labeled with the date of preparation, who prepared them, which laboratory they belonged to, the final pH (if applicable), and the name of the solution. No solutions were stored without labeling.

3.2.3.1 *Equipment and reagents List*

The following equipment was used in the procedures for preparing the chemical solutions used throughout the experiments:

- 1 – Acculab Vicon Scale: 120g limit, 0.001g resolution, serial number 21554350.
- 2 – Bio-Rad Vortexer: Model BR-2000, serial number 70308196
- 3 – Micropipettes: Rainin-Gilson: W64685C, 200-P, 200 μ L; and W56654D, 20-P, 20 μ L; plastic transfer disposable 3 μ L pipettes, Premiere® non-sterile
500pcs-PTP-01-Lot: 28091020
- 4 – pH Meter: Mettler Toledo, Seven Easy, serial number 1228175340
- 5 – 50 mL centrifuge tubes: Becton Dickson polypropylene conical tubes, 30x115 mm, non-pyrogenic
- 6 – Assorted beakers and glassware
- 7 – Paraffin film: “M” Laboratory film – Pechiney Plastic Packaging, 4”x125’.

The following reagents were required to produce the chemical solutions:

- 1 – De-ionized water: Wal-Mart Great Value® 1-gallon lots, steam processed.
Used as the principal dilution agent in all of the chemical preparations.
- 2 – Fluka Item #82597, pH 10 \pm 0.01 pH calibration liquid
- 3 – Fluka Item #82596, pH 7 \pm 0.01 pH calibration liquid
- 4 – Fluka Item #82596, pH 4 \pm 0.01 pH calibration liquid
- 5 – NaOH, Fluka 53339, pellets, 10g, puriss. P.a. ACS, \geq 98.0%; lot and filling
code: 93741/1 10603162
- 6 – HCl, laboratory stock, 2 Molar HCl in H₂O
- 7 – Polystyrene sulfonate (PSS), Sigma-Aldrich, Item #243051-500G, powdered
form of poly(sodium 4-styrene-sulfonate)

- 8 – Poly(diallyldimethylammonium chloride), low molecular weight, 20% wt. in H₂O, typical MW 100,000-200,000; sold by Aldrich, Item# 409014-4L, Batch #08520HB
- 9 – Phosphate-buffered saline (PBS), Sodium phosphate. Sigma-Aldrich, Item #S2554-500G.
- 10 – Tris buffer: Tis tablets, Sigma-Aldrich, Item #T5030-100TAB
- 11 – Fibrinogen: powdered form, Sigma Life Science #F8630-5G, Fraction I type I-S from bovine plasma, contains 10% sodium citrate and 15% NaCl, 76.5% protein (Biuret), 91.2% clottable protein, stored at -20°C
- 12 – Isopropyl alcohol (IPA), 97%

3.2.3.2 *Measuring pH*

The pH meter (Mettler Toledo) was calibrated before each chemical generated for this section was pH balanced. The probe was first rinsed in DIW, and then calibrated following the manufacturer's recommended process, listed on an instruction sheet stored at the instrument bench in the general laboratory. After calibration mode was enabled, the probe was dipped into the pH 4.0 calibration solution (Fluka) until the meter registered the 4.0 pH calibration point, rinsed, and then dipped in the pH 7.0 calibration solution (Fluka) until the correct calibration was indicated by the meter. If the calibration was incorrect, the calibration process was repeated.

The pH of each solution to be balanced was measured in a similar fashion. The probe was first immersed in DIW to rinse the probe, and then immersed in the liquid to be tested. The measurement button was pushed, and a reading was taken after the output

stabilized. After the reading, the probe was re-rinsed in DIW. If necessary, the proper acid or base was added to the solution to adjust the pH measurement to the desired level.

PSS (§3.2.3.5) and PDDA (§3.2.3.6) showed strong buffering characteristics, requiring large quantities of balancing solution, typically NaOH (§3.2.3.3), to bring the pH levels close to the desired levels, and then suddenly moving quickly along the pH scale with small quantities added. The pH change could quickly overshoot, requiring the use of the alternate pH solution to correct.

3.2.3.3 *NaOH – Basic solution*

A pH ~12 solution of NaOH was prepared as follows: 400 mL of DIW were placed into a 500 mL flask. Four NaOH tablets were added to the DIW and thoroughly mixed by manually oscillating the flask. The pH was measured (§3.2.3.2), and marked on the label for the flask. The labeled flask was sealed with a paraffin film, and stored on the appropriate laboratory shelf.

3.2.3.4 *HCl – Acid solution*

A pH ~2 solution of HCl was prepared as follows: a small quantity of stock HCl (~200-300 mL) was placed in a 500 mL flask. The pH was measured (§3.2.3.2), and marked on the label for the flask. The labeled flask was sealed with a paraffin film, and stored on the appropriate laboratory shelf.

3.2.3.5 *PSS – polyion, negatively charged at pH 7.5*

A 3 mg/mL solution was prepared as follows: 3g of PSS powder (Sigma Aldrich) was measured then added to a 1000 mL flask. DIW was added to the 1000 mL mark on the flask, and stirred thoroughly until the powder was completely dissolved. The pH was measured (§3.2.3.2), and was adjusted to the desired pH 7.5 with HCl (§3.2.3.4) and/or

NaOH (§3.2.3.3). The final pH was marked on the label for the flask. The labeled flask was sealed with a paraffin film, and stored on the appropriate laboratory shelf.

3.2.3.6 *PDDA – polyion, positively charged at pH 7.5*

A 9.46% solution was prepared as follows: 94.6 mL of PDDA liquid solution (Aldrich) was added to a 1000 mL flask. DIW was slowly added to complete 1000 mL in the flask. The solution was mixed thoroughly by stirring and manually oscillating the flask. The pH was measured (§3.2.3.2), and adjusted to pH 7.5 with HCl (§3.2.3.4) and/or NaOH (§3.2.3.3). The final pH was marked on the label for the flask. The labeled flask was sealed with a paraffin film, and stored on the appropriate laboratory shelf.

3.2.3.7 *PBS – solution buffer*

A 12 mg/mL standard PBS solution was prepared as follows: 10.8 g of sodium phosphate powder (Sigma-Aldrich) was measured and added to a 1000 mL flask. 900 mL of DIW were added to the flask, and the contents mixed thoroughly by stirring and manually oscillating the flask. The pH level was not adjusted for this solution. The labeled flask was sealed with a paraffin film, and stored in the refrigerator at 4°C.

3.2.3.8 *Tris saline buffer*

Standard Tris saline buffer was prepared as follows: 1 Tris tablet (Sigma-Aldrich) was added to 37.5 mL of DIW in a 50 mL centrifuge tube. The tube was vortexed with the Bio-Rad vortexer until the tablet was fully dissolved. The Tris solution was placed in a 500 mL flask. This process was repeated 12 times to generate 450 mL of Tris solution. The pH level was not adjusted. If the buffer was not to be used immediately to prepare fibrinogen (§3.2.3.9), the flask was sealed with a paraffin film and stored in the refrigerator at 4°C.

3.2.3.9 Fibrinogen – bioactive surface, negatively charged at pH 7.5

A 1 mg/mL solution of fibrinogen was prepared as follows: 450 mg of fraction I type I fibrinogen from bovine plasma in powdered form (Sigma), stored at -20°C, were added to a 1000 mL flask and mixed with 450 mL of previously prepared Tris buffer (§3.2.3.8). The flask was stirred and oscillated to prevent the formation of excessive foam. The pH level was not adjusted for this solution. The labeled flask was sealed with a paraffin film, and stored in the refrigerator at 4°C.

3.2.4 Surface Preparation

Glass slides were cleaned prior to layering with IPA, and dried in the Controlled Environment Chamber (CEC) (§3.2.4.6). Cleaned slides were then alternately dipped in the layering solutions to generate the LbL surfaces (§3.2.4.3).

3.2.4.1 Equipment and reagents List

The equipment and reagents required to clean and layer the surface were:

- 1 – Glass slides: Premiere® microscope slides, 9101 plain fine ground, 3”x1”x1 mm, 72 piece boxes
- 2 – IPA, 97%
- 3 – Pyrex® containers, 7”x5”x1.5”, model 7210, with lids.
- 4 – Forceps
- 5 – Timers: Good Cook® kitchen timers
- 6 – Splatter screens
- 7 – Solutions, described in §3.2.

3.2.4.2 *Cleaning*

The surfaces to be layered were cleaned to remove contamination such as debris, oil, and cellular material accumulated from handling. After cleaning, the substrates were handled with latex gloves or alcohol-cleaned forceps to minimize further contamination.

Glass slides were individually selected in batches of seven, and arranged into a rectangular Pyrex container filled with a 97% isopropyl alcohol cleaning bath. The arrangement in the container was the same arrangement used in the LbL dipping process (Figure 5). This layout maximized the number of slides that fit in the container, while allowing sufficient room between the slides to be extracted with the forceps.

The slides were allowed to soak in the solution for 4 minutes. At the end of the cleaning soak, they were transferred to a similar container filled with DIW and allowed to rinse for 4 minutes. Once rinsed, the slides were extracted, and set on a sheet of wax paper. The slides were then individually dried under a forced dry nitrogen flow, from a dry compressed nitrogen source.

The cleaned slides were placed into the Controlled Environment Chamber (CEC), described in §3.2.4.6, to ensure they were completely dry before storage or layering.

3.2.4.3 *s-LbL assembly*

For each of the layering steps, the glass slides were placed in the Pyrex containers as shown in Figure 5. This arrangement allowed for the maximum number of slides to be placed in the containers while still providing room for the slides to be manipulated with the forceps without interfering or damaging the other slides. Seven 1"x3" slides could be arranged in the dish by following this layout pattern.

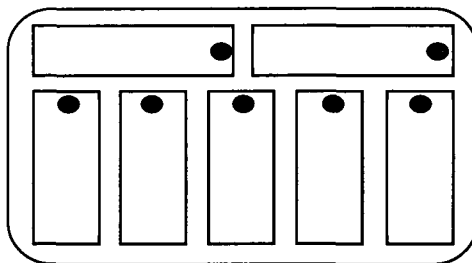


Figure 5 Layout of glass slides in the Pyrex containers. The location on the slide for forceps manipulation is marked

The arrangement also allowed us to identify which side of the slide was to be manipulated by the forceps. Handling the slides in the same location with forceps allowed the other end of the slide to remain undamaged by the forceps – an important requirement for the dynamic flow condition experiments. Figure 6 shows a typical layout for an s-LbL run. My laboratory partner, Melanie G. Watson, and I ran many of the processes described in this dissertation concurrently, as the areas of research were closely tied [50]. This cooperation reduced the amount of redundant work, and increased the throughput.

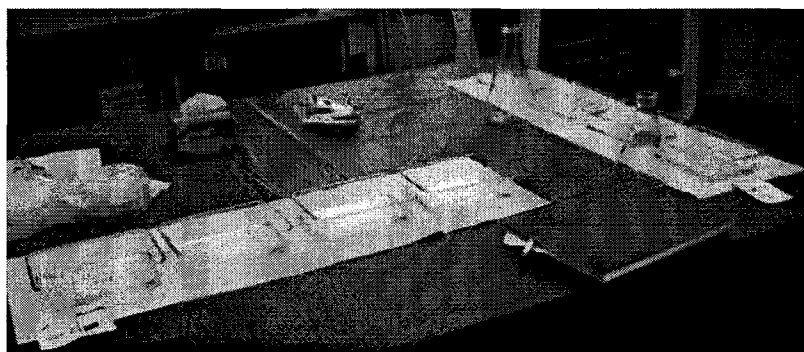


Figure 6 Typical s-LbL layout. The solutions, left to right, were PDDA, Rinse, PSS, Rinse (for the polyion layers), and PDDA, Rinse, Fibrinogen, Rinse (for the biointerface layers)

The s-LbL process was divided into two principal stages, construction of a polyion precursor and the addition of the active fibrinogen layers, as follows:

1 – To construct a polyion substrate, five bilayers of PDDA and PSS were formed, 5-(PDDA-PSS). For each bilayer, the slide was immersed in the first polyion solution (§3.2.4.3.1), rinsed (§3.2.4.3.2), dried (§3.2.4.3.4), immersed in the second polyion solution (§3.2.4.3.1), and rinsed and dried again.

2 – To construct the biointerface over the 5-(PDDA-PSS) substrate, the procedure used to construct the polyion substrate was applied three times, with fibrinogen substituted for the second polyion until a 3-(PDDA-Fibrinogen) structure had been added (§3.2.4.3.3). The final surface coating consisted of eight bilayers 5-(PDDA-PSS) +3-(PDDA-Fibrinogen).

The d-LbL process followed the same breakdown, but used slides inside solution-filled centrifuge tubes in motion rather than immersion in a static solution during the layering process.

3.2.4.3.1 Layering technique – polyion immersion

PDDA solution (§3.2.3.6) and PSS solution (§3.2.3.2) were placed in individual Pyrex containers to a depth of approximately $\frac{1}{2}$ of the container height, or at least $\frac{1}{2}$ ". For the current polyion on any given dip (PDDA or PSS), the slides were placed in the solution in the arrangement shown in Figure 5. Once in the solution, a timer was set for 10 minutes, during which the slides were allowed to sit in the solution undisturbed.

3.2.4.3.2 Layering technique – rinsing

DIW (§3.2) was placed in two rinse Pyrex containers. The slides were quickly transferred into the rinse containers, following the same layout pattern as the polyion dipping. For rinsing during the polyion dipping phase (5-(PDDA-PSS)), rinse time was 1

minute. For rinsing during the biointerface phase (3-(PDDA-Fibrinogen)), the rinse was set to 4 minutes.

3.2.4.3.3 Layering technique – bioactive surface immersion

The same procedure as the polyion dipping (§3.2.4.3.1) was followed, with PSS replaced by fibrinogen solution. The immersion time for PDDA (§3.2.3.6) was 10 minutes, while the immersion time for fibrinogen (§3.2.3.8) was 20 minutes.

3.2.4.3.4 Layering technique – drying

After each rinse cycle, the slides were placed on a clean wax paper surface, top side up. The slides were held with forceps and dried as completely as possible with pressurized dry N₂ gas. The nitrogen flow was directed initially to the top of the slide, and then swept down towards the bottom of the slide to sweep the bulk of the liquid off. The slide was then turned over, and the process repeated. Afterward, the nitrogen flow was washed back and forth over the slide until it appeared dry. The dry slide was placed on a drying tray, and placed into the CEC (Figure 7) to dry at 35C and 20% relative humidity for at least 7 minutes, or as long as another round of slides may take if there was more than one series of slides being run at one time.

The drying tray was a repurposed grease splatter screen. Made of aluminum formed into a fine open mesh, the tray allowed circulation on both sides of the slide.

3.2.4.4 *Waste disposal*

For these s-LbL procedures based on Eshaq's work [12], the solutions were kept until the end of a round of LbL – all 8 bilayers. The Pyrex containers had secure lids that permitted the solutions to be stored in them if the polyion stage had to be performed on a

different day than the biointerface day. The rinses were disposed of between days. The various solutions were not discarded until the end of a full round of LbL, 8 bilayers.

However, in later trials with d-LbL the solutions were changed whenever they showed excessive cross-contamination via fibrils or milky cloudiness, and the rinses were changed after each bilayer round.

Waste chemicals were disposed of in a container labeled with “WASTE”, and a list of the chemicals being disposed (PDDA, PSS, and Fibrinogen). Mixing these chemicals together into a single waste container generated no undue interactions, and was determined to be safe. PSS and PDDA reacted together to form a milky white substance of suspended polymers, and the fibrinogen simply added a biological hazard aspect. After checking with Dr. James Spaulding, in charge of safety for the Biomedical Engineering Center (BEC) at Louisiana Tech, this approach was determined to be adequate. The combined waste solutions were processed by the safety staff of the BEC by autoclaving first and then putting into the normal chemical disposal system.

3.2.4.5 *Slide storage*

The slides were stored in a rectangular dish, of the same style as used for LbL. Wax paper was placed on the bottom of the dish, and the slides were laid out in the pattern shown in Figure 5. If more than one set of seven slides was to be stored, a layer of wax paper was placed over the bottom layer of slides, and a new layer of slides was placed on top. The slides could be stored in the laboratory at ambient temperature after the polyion stage (§3.2.4.3.1), but needed to be stored at 4°C after the biointerface was applied (§3.2.4.3.3).

3.2.4.6 *Controlled environment chamber (CEC)*

The CEC is a polycarbonate box, shown in Figure 7. The box has a large front opening and two smaller side openings. The following equipment was used to turn the box interior into a controlled environment:

- 1 – Electric resistance heater, Marley Electric Heating
- 2 – Automatic Humidity Controller: Model 514-ETS, Electro-tech systems, serial number 405, along with a humidity sensor.
- 3 – Automatic Temperature Controller: Model 513A-ETS, Electro-tech systems, serial number 1071, along with a temperature sensor
- 4 – Gas drying unit: Drierite Anhydrous CaSO_4 Hammond
- 5 – Air pump, Aqua Culture® aquarium air pump, Model MK-1504-110508
- 6 – Electric fan – Westpointe®

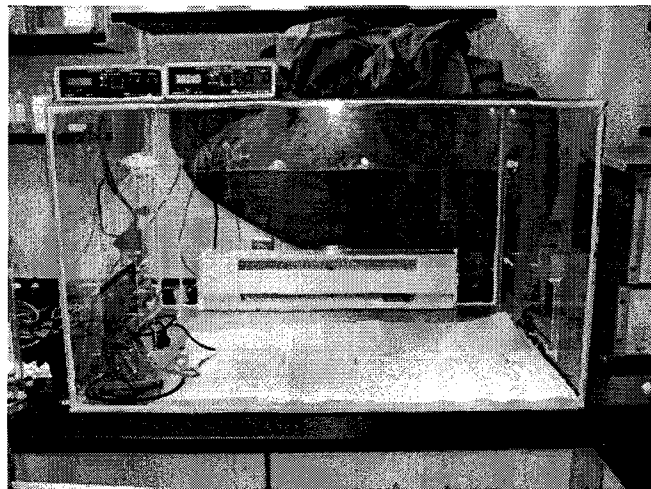


Figure 7 Controlled environment chamber (CEC) with the front cover removed

Temperature and humidity controls are on top of the chamber. The back of the chamber contains a heater along the bottom, sensors for the temperature and humidity

controls, and the air circulation loop into the desiccant. A side-access panel can be seen on the left side of the chamber. The front panel can be a polycarbonate sheet with built-in handling gloves, or can simply be covered with a heavy drape for simple access. The chamber was controlled for temperature and humidity to ensure a thoroughly dry surface. The temperature and humidity controllers have electrical outlets to which equipment may be connected for raising and separately for lowering the condition being measured by the individual controller.

Since the humidity was meant to be kept as low as practical, there was no humidification system connected, only the desiccant system listed above. The desiccant system was operated by using the air pump to force air through the desiccant and into the CEC, lowering the relative humidity within the chamber. A one-way check valve, a part of the air pump, was installed as an exhaust to the CEC, allowing air from the CEC to escape as new, dry air was pumped in.

Likewise, the temperature was to be controlled to a point higher than the air-conditioned temperature of the room, so no cooling system was connected. The electric heater was connected to the heating electrical outlet of the temperature controller.

The electric fan constantly circulated and homogenized the air in the CEC. Because only one controlling factor was used for each variable (temperature and humidity), the controllers kept a 2-3% relative humidity (RH) and 2-3°C temperature variance about the desired set points. However, this variance was considered sufficient for the purposes of these experiments.

3.3 Platelet Adhesion Tests

3.3.1 Overview

The platelet adhesion tests were at the heart of all four hypotheses (§1.5). All four were developed and tested to allow construction of a biointerface that would allow the reliable quantification of platelet adhesion. The platelet adhesion tests were divided into two sets of control cases and two sets of test cases. The first control case was a static exposure to PRP condition (§3.3.4.1) and the second control case was a no platelet chemical additive condition (0 μM L-a, §3.3.3.5). The first experiment case was a dynamic flow condition (§3.3.4.1.2), and the second control case a platelet chemical additive condition (20 μM L-a, §3.3.3.5). The slides exposed to these conditions were stained with AO (§3.3.4.5), and stored for experiment post-processing (§3.4).

Prior to blood collection, the CEC was set up (§3.3.2.3), prepared slides were retrieved from storage, given silicone backings, and placed in labeled Petri dishes (§3.3.2.4), a kit for blood collection was prepared (§3.3.2.5), the platelet chemical additive, a 1 mM L-a solution was prepared (§3.3.2.6), and the AO was prepared (§3.3.2.7).

Bovine blood was collected at the Tech Dairy (§3.3.3.2). The collected blood was returned to the lab and processed by: dividing into centrifuge tubes, centrifuging and separating out the supernatant (PRP), diluting the PRP with PBS to generate d-PRP (§3.3.3.4), dividing the d-PRP into tubes for individual slides, loading the chemical additive condition tubes with 1 mM L-a solution for the 20 μM L-a chemical additive conditions (§3.3.3.5), and preparing PBS rinses for each of the slides (§3.3.3.6).

To control the temperature of the collected blood and subsequent PRP and d-PRP, whole blood was transported from the farm to the laboratory in the insulated ice chest, the centrifuge was operated in a heated mode, and all PRP experiments were performed in the CEC.

3.3.2 Pre-Experiment Preparation

3.3.2.1 *Overview*

Pre-experiment preparations required at least 2 hours. Because daily blood draws at the dairy farm needed to occur between 1:30 and 2:00 PM, it was necessary to begin the pre-experiment preparations by 11:30 AM on an experiment day.

3.3.2.2 *Equipment list*

The following equipment and supplies were needed to be available for the platelet adhesion tests:

- 1 – CEC (§3.2.4.6 and 3.3.2.3)
- 2 – Plastic transfer micropipettes (§3.2)
- 3 – 3.5” Disposable Petri Dishes
- 4 – s-LbL slides (§3.2.4.3)
- 5 – 50 mL centrifuge tubes (§3.2)
- 6 – 15 mL centrifuge tubes: VWR International, Catalog #21008-216-50
- 7 – Orbital shaker: VWR Advanced Digital Shaker, Cat. #89032-096, Model 3600
Adv., Orbital shaker 980303, serial number 090408003
- 8 – Silicone elastomer, McMaster BIHT6135 011212:12”x12” Solid Sil, cut into
1”x3” strips as backing for the glass slides
- 9 – Insulated ice chest: Igloo® Model 462

- 10 – Latex gloves: Safe-Touch Latex Examination Gloves, non-sterile, disposable.
- 11 – Needle, 16 gauge: Becton Dickson 16G1 precision guide needles, disposable, Lot#305197
- 12 – Sodium citrate: Tribasic solution 4% (w/v) Sigma Life Science, 088K827, Item #S577-50ML
- 13 – PBS (§3.2.3.7)
- 14 – Forceps
- 15 – Waste container
- 16 – Acculab scale (§3.2)
- 17 – Syringe filters: Whatman GD/X, item #WU-29705-20, polyethersulfone 25 mm GD/X, and pore size 0.2 μm
- 18 – Syringe: BD, 10 mL, Luer-lok™ tip, Ref. 309604, Lot 8253407

In addition, it was necessary to verify that the following reagents were available:

- 1 –AO: hemi(zinc chloride) salt, for molecular biology, Sigma item #A6014-25G, hygroscopic.
- 2 – L-a: powdered form, minimum 98%, Sigma TLC-A5006-500G, Batch #103K0033

3.3.2.3 *Controlled environment chamber (CEC)*

To ensure that the experiments could be performed efficiently, it was necessary to set up the CEC and configure the instrumentation and supplies so that they would be readily available when needed.

3.3.2.3.1 Temperature and humidity settings

The CEC needed time to come to a controlled temperature and humidity, at least 30-45 minutes. Figure 8 shows the control section of the CEC. The relative humidity was set to 20%, and the temperature to 35°C. The air pump (not shown) and electric resistance heater (bottom) were actuated by electrical outlets on the back of the controllers.

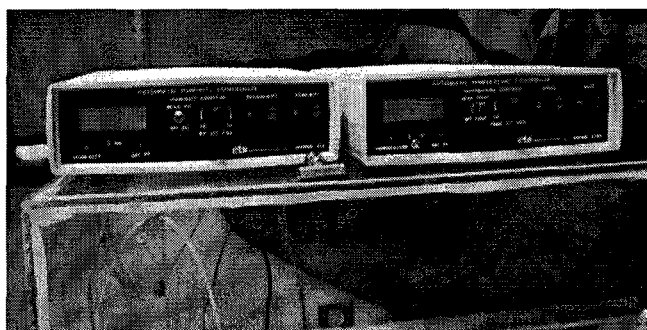


Figure 8 Temperature (right) and humidity (left) controllers located on top of the CEC

3.3.2.3.2 Equipment layout in CEC

Static condition (§3.3.4.1) and dynamic condition (§3.3.4.1.2) experiments were performed simultaneously to ensure that comparisons across conditions were done with the same batch of d-PRP. Therefore, the interior of the CEC was organized to accommodate both experiment types.

Figure 9 shows the initial layout of equipment within the CEC. The orbital shaker was placed on the left hand side, and was used for the dynamic condition experiments (§3.3.4.1.2). The right hand side contains a space for the static condition experiments (§3.3.4.1), the rinses (§3.3.4.3), and the waste container (§3.2.4.4). The bottom was covered with wax paper and paper towels to contain any spills and reduce the potential for biohazard contamination.



Figure 9 Basic equipment layout spaces in the CEC. Shown with the front plate removed for clarity

Figure 10 shows one arrangement of experiments within the sealed CEC. The Petri dishes are arranged on the orbital shaker for the dynamic experiments and on the space next to the orbital shaker for static experiments.

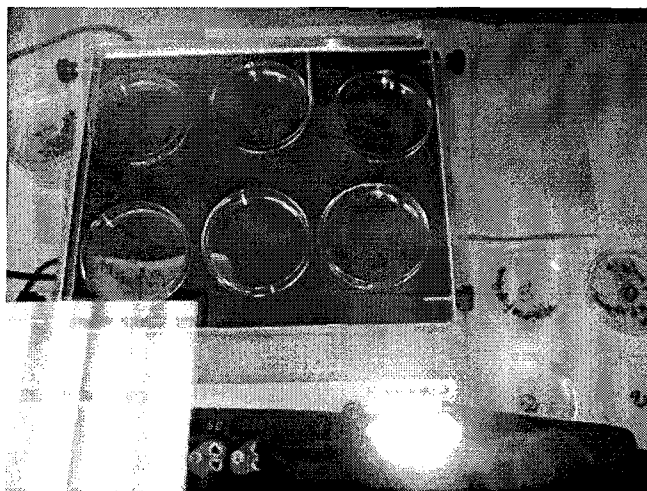


Figure 10 A sample experiment, with the Petri dishes laid out for their respective experiments, dynamic on the orbital shaker (left), and static on the CEC floor (right)

3.3.2.4 *Slides*

The Petri dishes shown in Figure 10 were typical for the experiments. Each dish was labeled with the following information: 1) “Static” or “Dyn.” to indicate the flow condition, 2) “XX μ L” to indicate the quantity of chemical additive (Table 2, §3.3.3.5), 3) “s-LbL” or “d-LbL” the type of LbL. The dishes were labeled on both the lid and the base, as the base will be used during the drying process (§3.3.4.4). A “+” mark on one side of the dish indicated where an individual slide’s forceps-manipulated side was to be placed.

The LbL-prepared slides were retrieved from storage, and given a silicone elastomer backing. This backing performed two basic functions: 1) it prevented the slides from moving relative to the Petri dish surface during dynamic tests, preserving the consistency of the dynamic flow condition; 2) it protected the back of the slide from being contaminated with d-PRP and staining, improving the results during imaging.

3.3.2.5 *Blood collection kit preparation*

The blood collection kit was assembled each time an experimental run was performed. The kit was transported in the ice chest and contained redundant pieces of equipment in case of a problem at the dairy, where replacement pieces could not be obtained. The kit consisted of:

- a) 2 needles
- b) 2 pairs of latex gloves
- c) Paper towels
- d) A logbook to detail each of the blood draws
- e) 50 mL centrifuge tubes prepared as discussed below

The centrifuge tubes were ideal for collection because of their sterile polypropylene construction (non-thrombogenic, as opposed to glass), and their volume. Sodium citrate was retrieved from the refrigerator, and 5 mL added to each tube. This volume, when combined with 45 mL of blood to complete 50 mL of fluid in the container provided the standard 9:1 whole blood to sodium citrate ratio required to prevent coagulation during transport and processing, allowing the extraction of PRP in the laboratory [51].

The number of prepared tubes depended on the number of individual slide experiments to be performed. In all situations, one extra tube was taken. On average, 150 mL of whole blood was required, resulting in four tubes being prepared, three for blood, and one spare.

3.3.2.6 *Chemical preparation – L-a*

A 1 mM solution of L-a was prepared days ahead of the experiments, and a single preparation of L-a could be used on many subsequent experiments. The solution was prepared as follows: 87 mg of L-a powder (Sigma) were added to a 50 mL tube. The tube was filled with 50 mL of DIW and thoroughly mixed, generating a solution 10X the desired concentration, 10 mM. 5 mL of the solution were transferred into another 50 mL tube, and filled to the 50 mL mark with DIW, to achieve the desired final 1 mM concentration.

3.3.2.7 *Chemical preparation – AO*

A 1 mg/mL solution was prepared days ahead of most experiments, as one preparation was sufficient for multiple days of experiments. In a darkened work area, 500 mg of AO (Sigma) were added to a 500 mL flask of DIW. The solution was thoroughly

mixed by stirring and manually oscillating the flask. A 10 mL syringe (BD) and 0.2 μm pore size syringe filter (Whatman) was used to filter the mixture into a 500 mL flask covered in aluminum foil to protect against ambient light. The flask was sealed with a paraffin film, and the film was covered with aluminum foil. The flask was labeled and stored at ambient temperature.

AO fluoresces red ($\lambda \approx 650 \text{ nm}$) given a green ($\lambda \approx 465 \text{ nm}$) excitation when it is associated with RNA. It can also fluoresce green ($\lambda \approx 525 \text{ nm}$) given a cyan ($\lambda \approx 502 \text{ nm}$) excitation when bound to DNA. The green fluorescence was not expected to be significant because the target cells, platelets, contain only micro-RNA (mRNA) and no DNA. This assumption had been used throughout the Eshaq [12] and Frilot [11] work in our laboratory. Fibrinogen surface staining tests (§3.4.3.2.1) and subsequent literature review would demonstrate that this assumption was too simplistic [52] [53].

3.3.3 Blood Collection and Processing

Before the platelet adhesion tests, it was necessary to collect the blood, prepare the d-PRP, and load the d-PRP with the chemical additives under study. Blood was collected from cows housed at the Louisiana Tech Dairy. It was centrifuged to separate the plasma, re-suspended in PBS, and modified with chemical additives, as needed.

3.3.3.1 *Equipment list*

The following equipment and supplies were used to collect and process the blood:

- 1 – Blood collection kit (§3.3.2.4)
- 2 – Centrifuge tubes (§3.2)
- 3 – Transfer pipettes (§3.2)

4 – Centrifuge: Eppendorf, Model 5804-R, 15 amp version, serial number
5805XJ334709

3.3.3.2 *Collection at the dairy*

All animal procedures were reviewed and approved by the IACUC at Louisiana Tech University. On a blood collection day, the LaTech Dairy manager was contacted by 11 am so that the cow being used for research (Appendix D) could be separated from the herd before the blood collection time. The blood collection kit and boots or spare shoes in a plastic bag were placed into a vehicle, and transported to the dairy.

At the dairy, contact was made with the dairy manager who would lead the way to the isolation pen where the cow had been placed. The researcher donned gloves and removed the collection tubes and a needle from the blood collection kit. The dairy manager used the needle to puncture the main vein near the cow's udder, referred to by the dairy as the "milk vein." If done properly, a rapid flow of blood would ensue. The tubes were handed to the dairy manager who opened them and handed them to the researcher as needed. The researcher filled each tube carefully to the 50 mL mark, and capped it.

After a tube was filled and capped, it was rocked gently back and forth multiple times to mix the sodium citrate and blood thoroughly. Improper mixing would result in early coagulation of the blood. Once the adequate number of tubes were collected, capped, and safely mixed, the dairy manager would remove the needle, and staunch the blood flow with pressure applied at the puncture site. At no time did the researchers involved manipulate the needles in the animal.

The paper towels were used to clean the bulk of the blood off the exterior of the tubes, and then the latex gloves were inverted over the tubes as they were removed from the researcher's hands. This wrapping provided a latex seal around the tubes for additional protection on the way to the laboratory. The wrapped tubes were placed back into the ice chest and transported back to the laboratory.

3.3.3.3 Platelet-Rich-Plasma (PRP) extraction

Once collected, the ideal time to first centrifuging was 30-45 minutes. Back in the laboratory, the tube exteriors were washed and dried with paper towels. The collected blood was separated into centrifuge tubes manually with 3 mL transfer pipettes (Figure 11). This process was performed carefully and slowly to prevent the exposure of the whole blood to undue shear stresses that could lead to coagulation. If transferring to a 50 mL centrifuge tube (when low quantities of blood were being processed), 12.5 mL of whole blood were put into each tube to be centrifuged. If being transferred into 15 mL tubes (for large volume processing), 7 mL of whole blood were placed in each centrifuge tube.

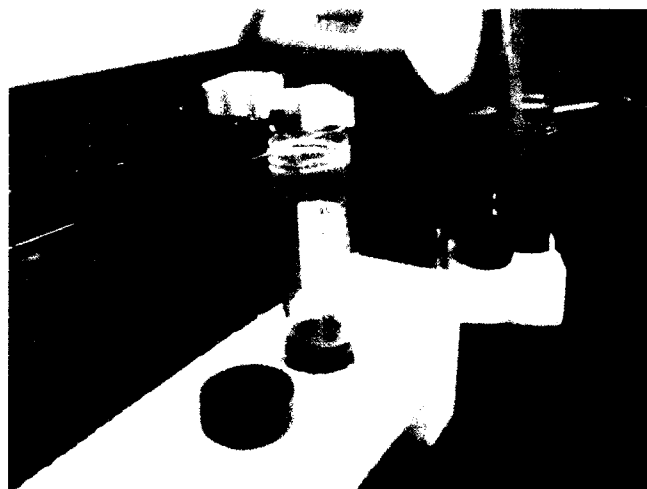


Figure 11 Transferring the collected whole blood into a centrifuge tube

The whole blood tubes were loaded into the centrifuge. The centrifuge settings were as follows: 30°C, 1000 RCF, brake 6 for acceleration and deceleration, 25 minutes. The centrifuge has different buckets for the two different types of centrifuge tubes (Figure 12). The centrifuge has can accommodate four 50 mL tubes or sixteen 15 mL tubes, allowing the centrifuging of 50 mL and 112 mL of whole blood, respectively.

Once the centrifuge cycle was completed, the tubes were gently removed from the centrifuge to prevent mixing of the separated layers, and placed in a tube holder. After successful centrifugation, the bottom layer (pellet) contained the erythrocytes, a thin intermediate layer with visible white regions contained the leucocytes, and the upper region (supernatant) contained the plasma (Figure 13).

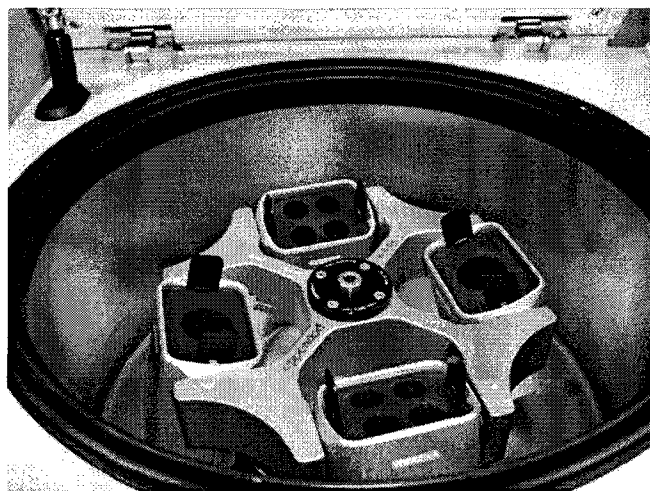


Figure 12 Centrifuge interior showing the two different types of buckets available for the 50 mL tubes (left and right) and the 15 mL tubes (top and bottom)

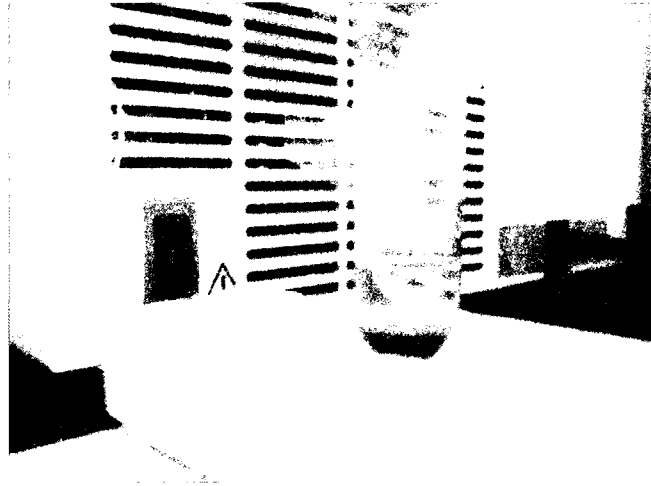


Figure 13 Centrifuged whole blood showing a clear separation into the pellet and plasma

If unsuccessful, the centrifuged blood could take on various appearances. The most common was an almost clear plasma layer with fibrils of the leucocytes concentrated near the central axis of the plasma. Alternatively, there could be an insufficient generation of the erythrocyte pellet. The centrifuge settings described in this section were the result of many different tests and experiments, and produced the best results the highest number of times from anything that was tried. However, after an unsuccessful run the supernatant plasma could be removed and re-centrifuged to rescue the run and not have to wait for another blood collection.

Figure 14 shows an unsuccessful run in a 15 mL tube, with cloudy plasma. Note that the run was an attempt to centrifuge the same 12.5 mL that can be successfully centrifuged in a 50 mL tube (Figure 13). For the 15 mL tubes, 7 mL was found to be the best quantity to use when attempting to centrifuge whole blood.



Figure 14 Centrifuged whole blood an unsuccessful centrifuge run, showing cloudy plasma and a lack of thorough pelleting of the erythrocytes

Successfully centrifuged tubes were removed from the rotor and placed in a holder. A plastic transfer pipette was then used to draw the plasma slowly from the top of the plasma layer. This transfer was continued until the transfer pipette approached the pellet interface. Every effort was made to prevent the pellet surface from breaking. Because backflow from the pipette tended to compromise the pellet surface, it was important to apply suction as one smooth, continuous movement, and then remove the pipette from the plasma column. If the interface surface broke, the plasma in the transfer pipette was put back into the tube, and the pipette discarded.

The collected plasma was put into a 50 mL centrifuge tube. If centrifuging in 50 mL tubes, the contents of four tubes were combined into one 50 mL tube. If centrifuging in 15 mL tubes, the plasma from seven tubes was transferred into one 50 mL tube. This mixing led to a more homogenized mixture of plasma, and set up for the adequate dilution (§3.3.3.4).

Figure 15 shows a single 50 mL tube collection of plasma, presumed to be PRP at this point. This figure shows a typical yield for a good centrifuge run, about 27-30 mL of clear, yellow-tinged PRP for every 50 mL centrifuged.



Figure 15 Separated plasma, presumed to be PRP at this point, and collected into a 50 mL tube

3.3.3.4 *Dilution*

The PRP was then diluted by adding PBS to complete 50 mL in the tube. The diluted PRP (d-PRP) was separated into 15 mL tubes labeled for the individual slides to be tested. For dynamic tests, 15 mL of d-PRP were added to the tubes, for static tests, 7 mL of d-PRP were added to the tubes.

3.3.3.5 *Chemical loading*

The standard experiments consisted of four conditions to be tested: static vs. dynamic flow, and no chemical additive vs. chemical additive. Table 2 shows the amount of 1 mM L-a required in each prepared 15 mL tube of d-PRP.

Table 2 Quantities of adhesion chemical additive, 1 mM L-a solution, to be added to each prepared tube of d-PRP for the two different flow conditions and two different chemical additive conditions

Flow Condition Chemical	Static 7 mL d-PRP	Dynamic 15 mL d-PRP
0 μ M L-a	0 μ L L-a	0 μ L L-a
20 μ M L-a	140 μ L L-a (1 mM)	300 μ L L-a (1 mM)

The tubes were thoroughly mixed by gently rocking back and forth multiple times. Excessive shear stresses could trigger early platelet clotting. The prepared tubes were placed inside the CEC, for the experimental run.

3.3.3.6 *Rinses*

For each tube prepared in (§3.3.3.5), a 15 mL centrifuge tube was prepared with 7 mL PBS to be used during the rinse portion of the platelet adhesion tests (§3.3.4.3).

3.3.4 Use of d-PRP in Platelet Adhesion Tests

The use of d-PRP in static and dynamic flow differed only in the flow conditions. The process of adding d-PRP, rinsing, staining, storage and waste disposal were the same for both of the flow conditions. The individual differences to the flow conditions processes are detailed first.

3.3.4.1 *Flow conditions*

3.3.4.1.1 *Static exposure to PRP condition*

The static exposure to PRP condition was simple. Once the d-PRP was applied, ensuring that the entire slide was covered, the slides and dishes remained undisturbed until time for their rinse, dry, and staining. The static condition served as the control condition for the active transport and shear stress related platelet activation.

3.3.4.1.2 Dynamic flow condition

For the dynamic flow condition, the orbital shaker was set at 1 Hz, to emulate the pulsatile condition at about 60 beats per minute (bpm). Upon the addition of d-PRP, the orbital shaker was turned on, and allowed a couple of seconds to come up to speed before the timer was started. The amount of fluid selected was sufficient to have a permanent coating over the slide during the dynamic motion. Because the oscillatory motion was not axisymmetric, the wave moving around the dish was not symmetrical, as seen in Figure 16 and Figure 17.

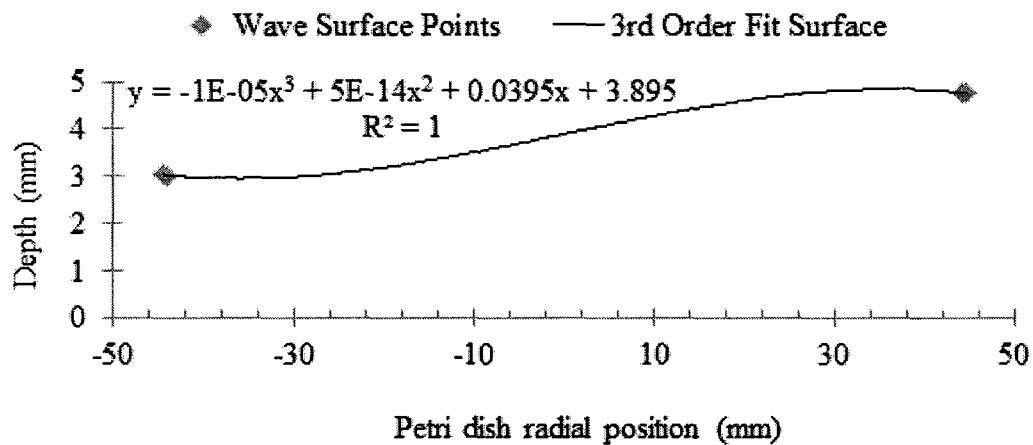


Figure 16 Estimated cross-section of the waveform circulating around the Petri dish during oscillatory motion while over the Petri dish only. Graph shows the third order polynomial best-fit line from measured points at the dish wall, and an estimated point 0.5 mm inside the dish that estimated the slope at the wall

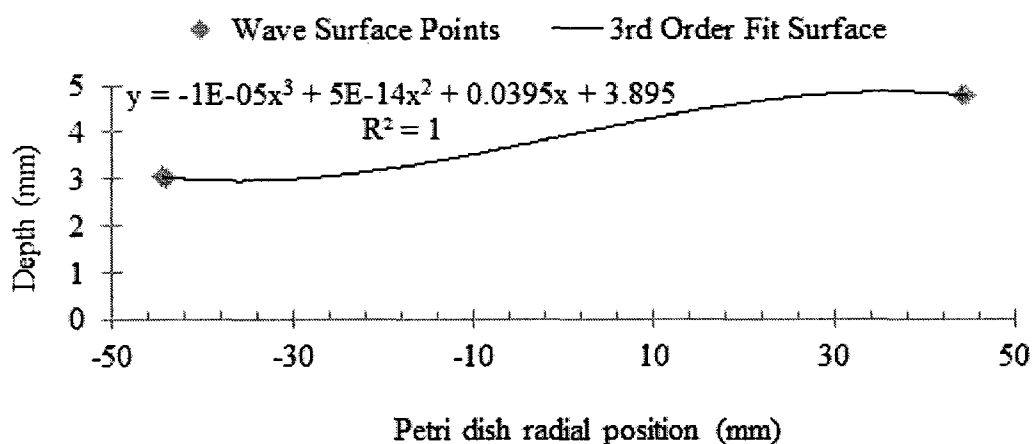


Figure 17 Estimated cross-section of the waveform circulating around the Petri dish during oscillatory motion while over the slide region only. Graph shows the third order polynomial best-fit line from measured points at the dish wall, and an estimated point 0.5 mm inside the dish that estimated the slope at the wall

The height of the wave was estimated from photographs and modeled with a third order polynomial, with wave height as a function of radius, shown in Figure 16. These waveform estimations were used for shear stress calculations in §3.8.3. This condition tested the combination of convective transport and diffusive transport of chemical additives and pd-NO, as well as shear stress activation of platelets.

3.3.4.2 Introduction of d-PRP

The lid for the Petri dish was removed and placed under the base, as a secondary dish, that was used during the drying process.

The 15 mL prepared d-PRP tubes were emptied directly into the Petri dishes. Other methods were investigated, such as transferring the fluid with pipettes and syringes, but were found to be too slow or impose too high a shear stress/velocity during fluid introduction.

Once the d-PRP was added to the first dish in a given run (dynamic or static), a 30-minute timer was set. The rest of the dishes for the given run were then completed.

This way, when the timer would go off the dishes could be drained in the same order, ensuring as close to the same amount of time in d-PRP for each slide as practical without having to do each slide individually.

3.3.4.3 *Rinse*

Once the timer for a given run would go off, the dishes were emptied and then rinsed with PBS. To empty a dish, the Petri dish was lifted, and the slide pressed against the bottom of the dish with the forceps. The dish was then tipped on its side and the d-PRP was emptied into the waste container. The dish was then set returned to its lid-base. After all the dishes for a given run were emptied, the rinses were applied.

The previously prepared rinses (§3.3.3.6) were applied to the individual dishes with the same method as described for the d-PRP (§3.3.4.2). After the first rinse was introduced, a 4-minute timer was set. At the end of the rinse time, the dishes were emptied following the same procedure as for the d-PRP (§3.3.4.2).

3.3.4.4 *Drying*

Once the slides had been rinsed and drained, they were removed from the Petri dish using the forceps from the side of the dish marked with a (+). Sometimes the slide could become detached from the silicone backing during this step, allowing some of the d-PRP to contaminate the back of the slide. Care was taken to avoid this condition, but it was not always accomplished. This possibility of contamination was one reason the slide cleaning during microscopy was introduced (§3.4.3.1), the second reason being the AO staining which could run into the same difficulty.

The slides were then placed on the upturned lids of the Petri dishes from which they were removed, with the side distal from the forceps manipulation side placed up on

the rim of the dish, and the forceps manipulation side down on the inside surface of the lid. This placement left the slide tipped at an angle, and allowed it to dry from both the upper and lower surfaces. If allowed to dry in the CEC with the temperature and humidity controls on, a slide would dry and be ready for staining within a couple of hours. In many cases, however, staining did not occur until several hours later, and as late as the next day, because of the amount of time an entire experimental day could take.

3.3.4.5 *Staining with AO*

An additional set of Petri dishes marked the same as the original set for the experimental run was prepared (§3.3.2.4). The dry slides were transferred into the new set of dishes, with the forceps side aligned relative to the markings on the dish. The dishes were then transferred either to a darkened room or to the CEC. The CEC could be darkened by placing a heavy dark sheet over the entire structure. The darkened room was the office within the laboratory, windowless and lockable to prevent unintended exposure to light. A sign reading: “BIOHAZARD – Bovine Plasma Fluorescence experiments. DO NOT ENTER until this sign is removed,” along with the contact information for the researchers, was placed on either the office door or the drape over the CEC.

In the darkened space, 15 mL tubes, one for each slide, were filled with 7 mL of AO; the PBS tubes from the rinse were refilled and set aside for use. These tubes could be washed and reused, so there was not excessive waste of lab materials. The AO was applied to the slides following the same process described in §3.3.4.3. The slides were stained for 20 minutes, then rinsed and dried following the same procedures described in §3.3.4.3 and 3.3.4.4.

3.3.4.6 *Slide storage*

Prior to storage, all of the slides were marked for identification. On the silicone elastomer backing, at the forceps manipulation end of the slide, the following information was written with a permanent marker: 1) “S” or “D” for static or dynamic flow condition, 2) “0” or “L-a” for the control or the chemical additive condition, 3) The date or run number. 4) “d-LbL” or “s-LbL.” The same storage procedure as described in §3.2.4.5 was followed, with the addition of an aluminum foil lining to the dish to block light and keep the stained slides isolated in darkness.

3.3.4.7 *Waste disposal*

The d-PRP, PBS, and AO were combined into a single waste container, and handled as described in §3.2.4.4.

3.4 Post-Experiment Processing

3.4.1 Overview

To test the various hypotheses, post-experiment processing provided a quantification of platelet adhesion from fluorescence microscopy images. Slides exposed to d-PRP under the various control and experimental conditions were imaged following one set of protocols (§3.4.4, 3.4.4.4.1, and 3.4.4.4.2), while s-LbL and plain slides used in testing the s-LbL AO anomalies (“Red-Green tests”) (§3.4.3.2) were imaged with a different protocol (§3.4.4.4.3).

The microscopy images for both of the principal imaging processes described above were converted from their original high-resolution “tiff” format to a more manageable resolution “jpg” file or fast image processing via a free image processing program, IrfanView© (§3.4.5.3). These preprocessed files were then used with their

respective programs for data processing. s-LbL and d-LbL microscopy image files were processed using a laboratory standard image processing program (§3.4.5.4). A separate program was used to process the Red-Green test images (§3.4.5.5).

3.4.2 Equipment List

The following equipment and supplies were used during fluorescent imaging

- 1 – Forceps
- 2 – KimWipes®: Kimberly-Clark Professional, Kimtech Science – delicate task wipes, 1-ply
- 3 – Microscope: Olympus IX51, serial number 7D01816, FITC and TRITC filters, 10x and 40x magnification
- 4 – Microscope digital camera: Olympus DP71 color camera
- 5 – Fluorescent light source for microscopy: Photonics Solutions, Inc., X-Cite Series 120, Exfo Model #XE120-XL, serial number XE120-XL-0782
- 6 – Computer/microscope software: Dell Workstation Precision 380, Windows XP, Core2Duo processor, Tag: GDR30F1, with DP Controller and DP Manager software programs by Olympus
- 7 – Bio-Rad vortexer (§3.2)
- 8 – Micropipette (§3.2.3.1)

The following reagents were required for fluorescent imaging:

- 1 – IPA, 97%
- 2 – Fibrinogen FITC stain: Thermo Scientific, Fibrinogen, polyclonal FITC labeled, Item #RB-1942-R2, 2 mL
- 3 – PBS (§3.2.3.7)

3.4.3 Preparing Samples for Imaging

Staining platelets prior to the experiments without damage to the platelets themselves is possible, as demonstrated by *in vivo* studies such as the one by Tangelder, et al. [54] However, the process of removing excess stain from the PRP during pre-staining – re-centrifugation to remove the stain/plasma mix and re-suspending the stained platelets in unstained plasma could further damage the platelets.

3.4.3.1 *Glass slides*

The glass slides to be imaged were retrieved from storage and taken to the microscopy room, which remained darkened during the imaging process. All slides to be imaged on a particular day were removed from the storage container and laid out on a wax paper sheet next to the microscope.

Before each slide was imaged, the elastomer backing was removed and the slide was set aside on the wax paper to prevent contamination. IPA was then poured onto a KimWipe®, and used to clean the exposed underside of the slide thoroughly. This cleaning minimized unwanted fluorescent signals from the bottom surface of the slide.

3.4.3.2 *Special preparation to test s-LbL functionality*

Red-Green tests involved marking the fibrinogen surface with a fluorescent tag that emitted light at a different wavelength than the AO red wavelength. Fluorescein isothiocyanate (FITC) tagged anti-fibrinogen antibody was a simple way to test the concentration of fibrinogen on the surface. FITC fluoresces green ($\lambda \approx 521$ nm) given a blue ($\lambda \approx 495$ nm) excitation, which provided a sufficiently different emission for adequate microscopy imaging and later superposition of the images.

3.4.3.2.1 Fibrinogen staining

A dilute 15 mL solution of the FITC-labeled fibrinogen antibody (Thermo Scientific) to stain the surface of six s-LbL slides that were exposed to d-PRP. The solution was pre-diluted from the manufacturer, but is expensive. Tests revealed that this more dilute form worked well enough for the purposes of testing the surface.

The solution was prepared as follows: 15 mL of PBS were placed in a 15 mL centrifuge tube, and 750 μ L of FITC tagged solution (Thermo Scientific) was added. The solution was vortexed with the Bio-Rad vortexer for 30 seconds.

The diluted stain was applied to $\frac{1}{2}$ of each of the slides to be tested, allowed to stain for 20 minutes, then rinsed and dried as described for the AO stain (§3.3.4.5).

The slides that were tested were from a prior set of s-LbL experiments that had been imaged and processed. Because the results from these and other slides had been inconsistent, the validity of the previously used LbL and staining methodology was questioned. The experimental conditions used with these slides are listed in Table 3.

Table 3 The slides stained with fibrinogen-FITC stain, showing the flow condition (static/dynamic) and the concentration chemical additive, L-a

Flow Condition	pd-NO chemical additive L-a μM
Dynamic	0
Dynamic	5
Dynamic	10
Dynamic	20
Dynamic	25
Static	0

3.4.4 Microscopy

3.4.4.1 *Naming convention and directory structure*

In order to speed up the collection of images, the DP Manager program worked in tandem with the DP Controller microscope interface program. The Manager program saved and managed the images generated by the controller program. By setting an auto-capture and auto-naming system, images could be captured quickly and identified uniquely for each experiment. The auto-capture settings were as follows:

Within the main working folder for the laboratory, new folder for the day's experiments was set. The naming convention for the folder was as follows:

MM-DD-YYYY [LbL style] [bioactive surface or flow conditions] [chemicals]
[special modifiers]

An example main directory from the work performed was therefore:

5-28-2010 dLBL S-D 0-20 La Ln ADP

Subfolders within this main folder were be generated for each of the slides and slide regions to be imaged. These folders were named according to the following convention:

[Flow condition] [exposure] [chemical concentration] [chemical] [shear region]

Within the DP Manager program, under the drop-down menu “Capture,” the Auto-save settings were set. These settings were as follows:

Date format: YYYY-MM-DD

Autosave on capture

Prefix: same as the sub-folder name

Auto-numbering starting at 1

For the experiment listed above, a sample file name generated would be:

“Dynamic 666_67 ms 0uM ADP High – 2010-06-4-1.tiff”

It was necessary to set these parameters for each slide/slide region to be imaged.

3.4.4.2 *Microscopy settings file*

The microscope imaging and settings were controlled by the DP Controller program on the Dell computer attached to the Olympus microscope. The computer drove the camera, so the software and then computer were to be shut down after every experimental run. A settings file was saved that contained all of the microscopy settings to make it simple to perform a microscopy experiment. The file was saved to the main working folder for the laboratory “Dr. Jones”, and titled “Jones lab Platelets Acridine Orange 10-19-2009”. The file could be saved and loaded from the final, load settings tab under the DP controller program tabs. The settings details are in APPENDIX G:

3.4.4.3 *Microscope setup*

It was necessary to adjust some of the microscope settings manually. The fluorescence source was the X-Cite Series 120 source. This source was turned on and allowed to warm up for at least a few minutes before collecting images. To extend lamp

life, the source was to remain on if the pauses between experiments were to be less than $\frac{1}{2}$ hour. The steps to setting up the microscope were as follows: The excitation source was turned on. On right hand side of microscope, the shutter was set to camera, and the main light source shutter on the upper portion of the microscope was opened. The fluorescence filters were Tetramethyl Rhodamine Iso-Thiocyanate (TRITC) for AO and FITC for FITC-fibrinogen. On the left hand side of the microscope, the main filter was pushed in. Finally, the stage was wiped down stage with a KimWipe® soaked in IPA.

3.4.4.4 *Imaging process*

The images were collected from three principal regions on a slide (Figure 18). The distinction between low-, medium-, and high-shear regions matters for the dynamic flow condition slides. Although there was no relationship between slide location and shear rate for slides exposed to static exposure to PRP, the locations were referenced in the same way when imaging. It was helpful to have two people work together, with one handling the slide cleaning, microscope stage, and focusing, and the other managing the software programs and file naming conventions.

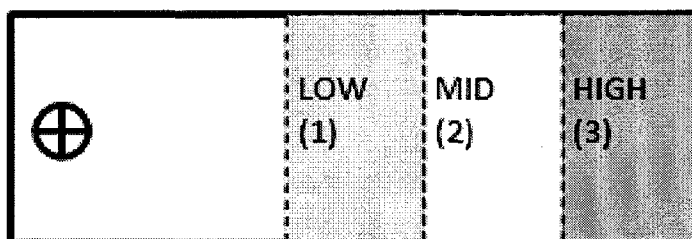


Figure 18 Imaging locations on a slide. Shear regions from which images were captured are highlighted, The mark for the forceps handling edge is indicated on the left side

The slide was placed on the stage with the active surface for imaging (the “top” of the slide) facing down, with the long axis perpendicular parallel to the front edge of the

stage. The images were taken from the far edge relative to the researcher (“top” because of how the images appear on the screen during imaging), and across the slide to the near edge. Images were taken sequentially down the slide to the bottom, over at least one image region, and back up to the top of the slide. 41 images were taken of each region, 123 images per slide. As each new region came into focus, objective criteria were used to determine whether the image was a valid region to collect. If a portion of the image met the exclusion criteria, then the microscope stage was moved enough to exclude just that portion and subsequent imaging continued from the new point. The exclusion criteria and examples from experimental images are shown in the following sections.

3.4.4.4.1 *s-LbL imaging criteria*

For s-LbL, the only feature that led to exclusion was a fibril (Figure 19) or similar contamination. Fibrils were often formed in the layering liquids and deposition of these fibrils in bulk form rather than as a part of the LbL surface were not representative of the adhesion on LbL being evaluated.

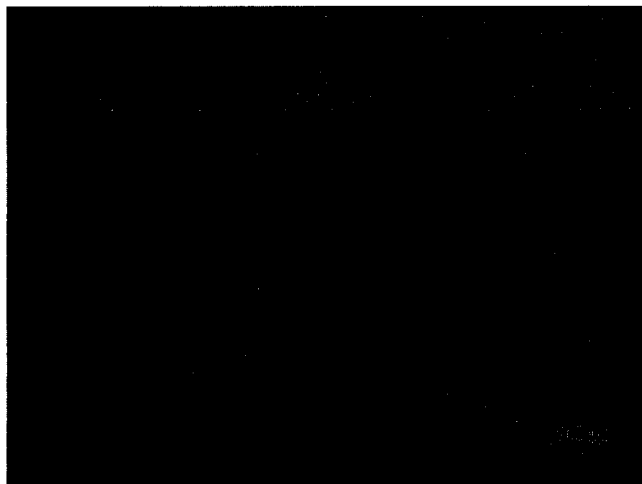


Figure 19 Image in which a fibril is visible on the lower left hand side, used as a criterion for excluding a region from imaging

3.4.4.4.2 d-LbL imaging criteria

For d-LbL images, the fibril criteria, used for s-LbL, was also applied. In addition, areas that were circular drying rings, which suggested a drying artifact or badly formed d-LbL, were excluded (Figure 20).



Figure 20 Example of an image where there is a malformation of the d-LbL or a drying ring area

3.4.4.4.3 FITC-Fibrinogen to AO comparisons

Two sets of tests were run on the s-LbL surface for the Red-Green comparisons. First, a test was performed to establish the link between fibrinogen accumulations and platelet adhesion. It was theorized that the platelet adhesion patterns seen in s-LbL tests could come from inhomogeneously distributed fibrinogen. s-LbL surfaces were tagged with FITC-labeled fibrinogen antibody, and the platelets with AO. By imaging with FITC (Fibrinogen) and TRITC (AO) filters in the microscope on a single area, the superposition of platelet deposits on fibrinogen could be established.

The results of these initial tests (§4.4.2) led to further questions about the s-LbL surfaces. A second test was designed using the static and dynamic flow condition experiments (§3.3.4.1.2 and 3.5.6.3), replacing the d-PRP with the buffer, PBS. These

slides should have had no platelet accumulations, and therefore no AO stain results under fluorescence microscopy. The results (§4.4.3.1) were surprising and unexpected, showing strong stain accumulation and stain levels affected by the presence of the chemical additive L-a and shear region.

A positive control test was performed to determine the general morphology of adhered platelets. To ensure platelet adhesion, d-PRP was exposed to plain glass slides that had been cleaned following the same protocols as the LbL processes (§3.2.4.2). Because glass serves as a platelet activator [49], the LbL surface was removed as a variable (§4.4.3.2). The images obtained from these slides did not match the results from s-LbL, but were later found to be consistent with d-LbL (§4.5).

For the regions to be evaluated by comparing FITC-stained fibrinogen to AO stained platelets (§3.4.3.2), two images were taken at each location, following the criteria listed above. For the first image, with the TRITC source and filter in the microscope were used to capture the red fluorescence, and for the second image the FITC source and filter were used to capture the FITC-stained fibrinogen green fluorescence image. These images were taken in pairs, without moving the microscope stage, to ensure superposition of the images would work during processing (§3.4.5.5). In both cases, the previously described rejection criteria were applied.

3.4.5 Image and Data Processing

3.4.5.1 *Overview*

The standard image processing program processed all images in each folder that was created for a given day. The processing involved: 1) thresholding the images to the same standards as the work in Eshaq [12] , 2) calculating the black and white areas

generated after thresholding, again following the standards in Eshaq's work, 3) Calculating the percent surface area above the threshold for each image, 4) Collecting the results from each individual imaging folder (image set) into a single file, 5) Calculating the mean and standard deviation for each image set, 6) Establishing outliers based on the standard deviations and saving a file with outliers removed, and 7) saving all of the processed images and a montage of original and processed images for each image set. Percent surface area coverage was the principal metric for this type of processing.

The Red-Green processing program thresholded the data in the same way as the standard image processing program. The thresholded data were then assigned pseudocolor based on the type of fluorescence. TRITC microscopy was colored RGB Red, and FITC microscopy was colored RGB Green. These red and green images were placed in montages for each image set. The red-green image pairs were added together to form an RGB Yellow where thresholded areas overlapped. The percent surface area was estimated from the thresholded data and the overlap between the red and green threshold areas was inspected qualitatively. Overlap was expected, because FITC-stained fibrinogen and AO-stained platelets have different emission spectra, but platelets were expected to accumulate over fibrinogen regions. However, s-LbL surfaces that were never exposed to d-PRP should fluoresce, or should fluoresce little, under AO stain. Percent surface areas of no-PRP slides were expected to be negligible. Significant AO stain accumulation on no-PRP slides would indicate that AO fluorescence microscopy of s-LbL surfaces does not reliably quantify platelet adhesion.

3.4.5.2 *Software used*

Quantitative data were extracted from the images with the following software:

IrfanView© Version 4.27 [55]

improcess_FINAL.m

falseColor_FINAL.m

The MATLAB script *improcess_FINAL.m* was developed in-house and was used to calculate percent area coverage of suspected platelet aggregation from AO stained regions. The MATLAB script *falseColor_FINAL.m* was developed in-house and was used to calculate percent area covered by FITC-labeled fibrinogen and AO, to assess the overlap between fibrinogen and AO staining. *IrfanView* was used to process microscope images into images formatted for the MATLAB scripts. Details of both MATLAB scripts are provided in APPENDIX A.

3.4.5.3 *Pre-processing using IrfanView*©

IrfanView was used to transform the collected microscope images into JPG files, a smaller, more manageable image and file format, as follows:

- a) Entering “B” within the program or File >> Batch Conversion/Rename from the drop down menus opened the batch conversion window.
- b) Work As: Batch conversion – Rename result files
- c) Batch conversion settings: JPG-JPG/JPEG format, standard options
- d) Batch rename settings: Name Pattern: image###
- e) Look in: ([day’s microscopy images]\[individual slide region images]) to select the folder containing the microscopy images for a given slide region.
- f) Add All

- g) Output directory results files: Use current ('look in') directory. This saved the output files in the same principal directory, required for processing with the *improcess_FINAL.m* program.
- h) Start Batch
- i) Repeat for each of the region subfolders in a given day's main folder.

3.4.5.4 *Standard image processing program to calculate surface coverage*

The *improcess_FINAL.m* program was developed for this dissertation, expanded from the image processing methods described by Eshaq [12]. This code calculates percent surface area coverage by converting color images to grayscale, thresholding to generate binary (black and white) images, and calculating the white area as a percent of total image area. A full description can be found in APPENDIX A. A flowchart of this program is shown in Figure 21.

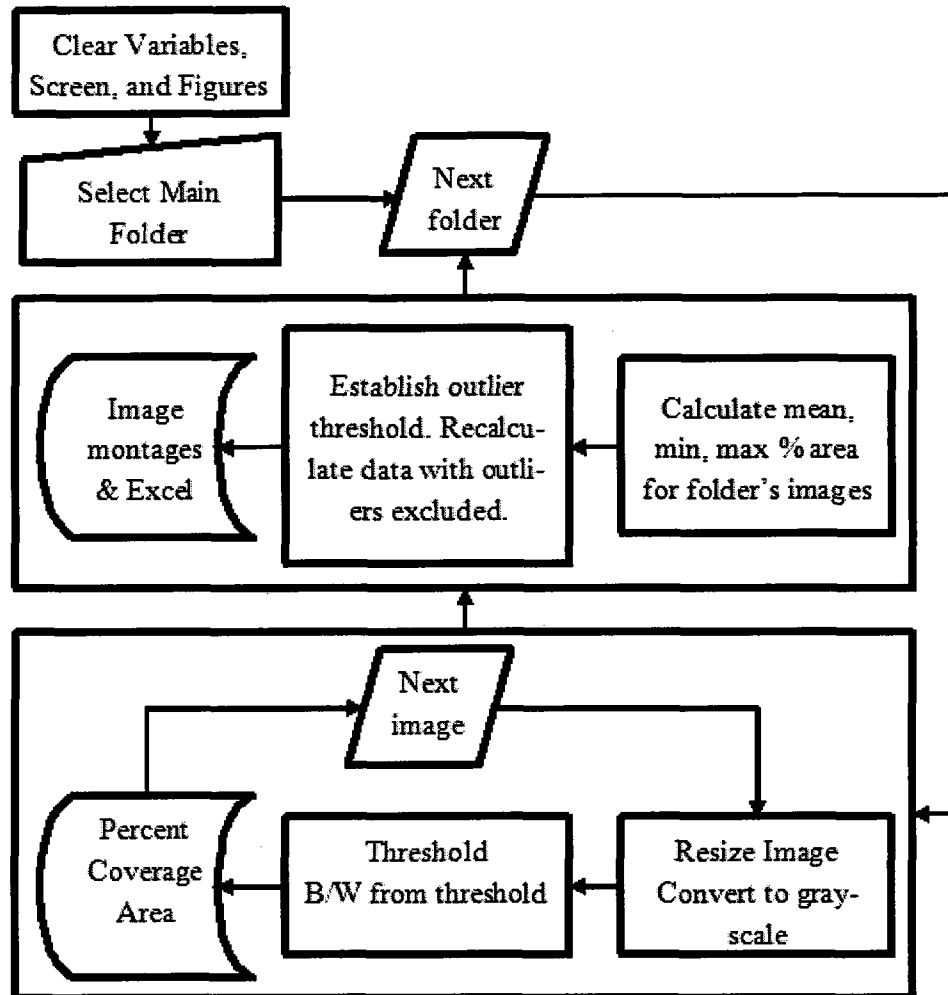


Figure 21 Flowchart for standard image processing program, *improcess_FINAL.m*

3.4.5.5 Image processing program for analysis of stained fibrinogen

To evaluate the platelet accumulation via AO staining as a function of the fibrinogen substrate, a program, *falseColor_FINAL.m* (APPENDIX A) was created. The images from microscopy were arranged in pairs, AO platelet stained and FITC fibrinogen stained, which had been taken from the same location by simply changing filters. These paired images were processed with IrfanView as described in §3.4.5.3.

falseColor_FINAL.m processed these pairs of AO and FITC images, with a modification to the thresholding process from the standard imaging program. The threshold value

remained the same, but instead of black and white images, pseudocolor images were generated. For the AO platelet images, the thresholded images were converted to RGB Red, [1 0 0], while the fibrinogen images were thresholded to RGB Green [0, 1, 0]. These images were then superimposed, generating an RGB yellow [1, 1, 0] in regions where they overlapped. The flowchart for the program is in Figure 22.

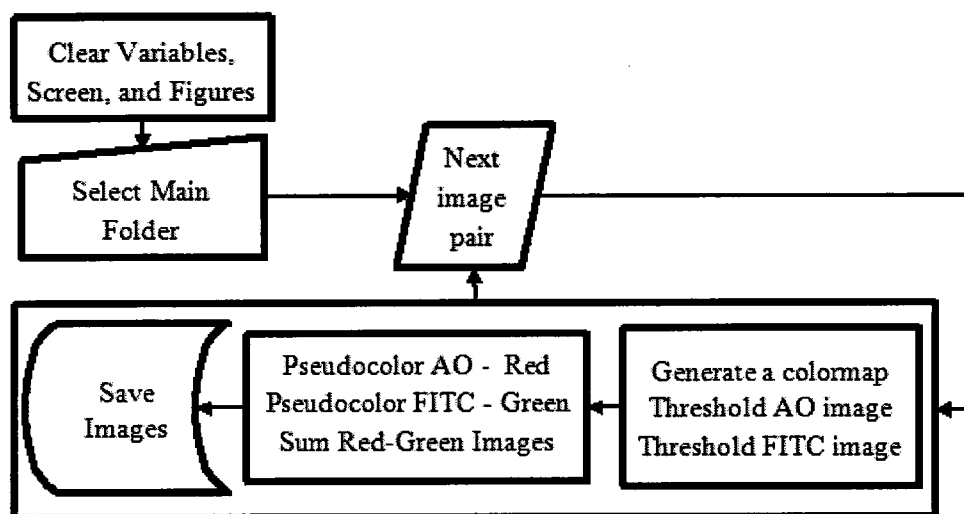


Figure 22 Flowchart for standard image processing program, *improcess_FINAL.m*

3.5 d-LBL Biointerfaces for Platelet Adhesion Studies

3.5.1 Overview

The results from analyzing the red-green superposition (§3.4.5.5 and 4.4.2) indicated a need for a new approach to generating an LbL surface that would not include surface anomalies that could retain the AO stain without the presence of cellular material. Other researchers have demonstrated an improvement in various self-assembled types structures can be obtained when self-assembly is performed under flow, as opposed to static conditions (§2.2).

The approach delineated in this section was proposed, tested, and refined over a series of experiments. The basic premises of the proposed new approach did not change, but the specific items such as the speed of oscillation during layering (1 Hz vs. 1.33 Hz), the substrate to be used (glass slides vs. whole Petri dishes), and specific handling during the drying process of LbL (laying on wax paper or racking vertically) were refined and updated to their final protocol shown here. All four hypotheses were tested with the surfaces generated by d-LbL. By subjecting d-LbL surfaces to static and dynamic flow conditions with and without platelet chemical additive, and then processing the resulting slides, statistical tests were performed to answer the principal questions related to each hypothesis (§1.5).

3.5.2 Equipment and Reagents List

In addition to the equipment and supplies required for s-LbL (§3.2.4.1), the following were used:

- 1 – Orbital shaker, §3.2.4.6
- 2 – pH Meter, §3.1
- 3 – NaOH, §3.1
- 4 – 50 mL centrifuge tubes, §3.1
- 5 – 50 mL tube racks
- 6 – Square plastic container to hold 15-tube rack on orbital shaker.

The following reagents were also required:

- 1 – Collagen: Type I, from calf skin, Sigma Item #C9791-100MG, Stored at -4°C.

Acid soluble

- 2 – Acetic Acid: Glacial, laboratory stock, molarity 17.4

3 – DIW, §3.2.4.6

4 – 97% Isopropyl alcohol (IPA)

3.5.3 Solutions Preparations

3.5.3.1 *Polyions and fibrinogen*

The polyions and fibrinogen were prepared following the same procedures as described for s-LbL, in §3.2

3.5.3.2 *Acetic acid – Collagen solution buffer*

The acetic acid needed to be diluted to a point where it could be used as an acid buffer to generate the collagen coating solution. A 0.1 M acetic acid solution was prepared as follows: 5.75 mL glacial acetic acid was placed in a 1000 mL flask. DIW was added to the flask to complete 1000 mL of solution. The solution was stirred thoroughly, labeled, and stored in the vent hood.

3.5.3.3 *Collagen*

Sigma recommends $10 \mu\text{g}/\text{cm}^2$ of collagen to cover a surface adequately. To cover eight slides would require 1.55 mg of collagen in solution, which means that as a minimum 0.194 mg of collagen per slide to be covered was needed. A 0.083 mg/mL collagen was prepared as follows: 50 mg collagen (Sigma) was dissolved into 50 mL of 0.1 M acetic acid in a 50 mL centrifuge tube. The solution was allowed to dissolve overnight, and then placed on the orbital shaker for at least 2 hours to reduce the number of fibrils to a minimum. The solution would never become fully dissolved, however. Vitrogen liquid collagen is recommended for future experiments. The acetic acid/collagen solution was added to a 500 mL flask, and DIW was added to complete 375 mL of dilute collagen solution. This process yielded a solution of 0.133 mg/mL collagen

solution. A centrifuge tube for d-LbL (§3.5.4.1) would contain 5 mg collagen, roughly 25.8 times the collagen required for adequate coating. The solution was balanced for pH using NaOH, and 0.1 M acetic acid (in lieu of HCl). Final solution was much more dilute after balancing, resulting in a solution of 0.083 mg/mL collagen, or roughly 12 times the collagen required for adequate coating in a 50 mL tube for d-LbL.

3.5.4 Surface Preparation

The surfaces for s-LbL were prepared in a bulk, static process, with multiple slides being layered in the same solution bath. The d-LbL process dealt with slides individually, immersed in LbL solutions in 50 mL centrifuge tubes, in a dynamic environment that kept the immersion solution constantly moving over the slide surface.

3.5.4.1 *Centrifuge tubes*

A maximum of 15 slides could be processed at one time, compared to the 14 that would be processed if two researchers were working simultaneously on the s-LbL process. The 15 slides still required two researchers in order to minimize the possibility of errors inherent to trying to do too much at one time.

It was necessary to prepare 15 tubes of each of the solutions ahead of time. On the day when collagen was run, eight collagen tubes were prepared and seven fibrinogen tubes. On all other days, 15 fibrinogen tubes were prepared. In addition to the polyions, biointerfaces, and rinses, a set of 15 tubes of IPA were prepared to allow for the cleaning of the slides. The tubes were labeled with their individual solutions on both the tube and the lid, so that when washed the tubes could be kept together adequately.

3.5.4.2 *Orbital shaker and CEC*

The orbital shaker did not need to be placed into the CEC for this process, as the d-LbL process occurred at ambient temperature like the s-LbL process, and required the CEC to be left available for drying the slides. The CEC settings remained the same as for the s-LbL process (§3.2.4.6).

3.5.4.3 *Cleaning slides*

Individual slides were selected and placed, one per 50 mL tube, in isopropyl alcohol. The tubes were capped tightly, and placed in the 15-tube rack. The rack was then turned horizontally and placed in the rectangular container. This orientation placed the slides horizontally and allowed the liquid to wash over the slides as the orbital shaker oscillated.

The slides were cleaned at 2 Hz on the orbital shaker for 7 minutes, then transferred into a set of rinse tubes and rinsed for 7 minutes. The slides were left in the rinse as they were extracted individually for drying. They were dried with the nitrogen supply and placed in the CEC. The CEC was set to 15% relative humidity and 35°C for at least 10 minutes.

3.5.4.4 *Layering*

With the first layer of polyion, the slides were placed in the same configuration each time. The end of the slides on the cap end of the centrifuge tube was treated in the same way as the slides for s-LbL (Figure 5) – ensuring that the slide was always handled from the same end with forceps, and keeping one surface consistently on top as the upper surface.

3.5.4.4.1 Layering technique – polyions

To layer the polyions dynamically, the same steps as for s-LbL (§3.2.4.3.1) were followed, except that the slides were placed in the individual tubes with solution, tightly capped, and placed horizontally on the orbital shaker as described in §3.5.4.3. The orbital shaker was set to 1 Hz.

3.5.4.4.2 Layering technique – rinsing

To rinse the slides dynamically, the same steps as s-LbL were followed (§3.2.4.3.2), with the changes described in §3.5.4.4.1. The rinses were changed after every full bilayer cycle.

3.5.4.4.3 Layering technique – bioactive surface

To layer the bioactive surface dynamically, the same steps as for s-LbL were followed (§3.2.4.3.2), with the changes described in §3.5.4.4.1. For the fibrinogen surface, the polyion was PDDA (§3.2.3.6), and the orbital shaker was set to 1 Hz. For the collagen surface, the polyion was PSS (§3.2.3.5), and the orbital shaker was set to 1 Hz. The polyions were run for 10 minutes, and the bioactive surfaces for 20 minutes.

3.5.4.4.4 Layering technique – drying

The same steps as s-LbL (§3.2.4.3.4) were followed to dry the dynamically labeled slides.

3.5.4.4.5 Waste disposal

To dispose of the waste products during the d-LbL process, the same steps as for s-LbL were followed (§3.2.4.4). However, the fibrinogen and collagen tubes were disposed of in the laboratory's biohazard waste bag, and their contents were not added to the general waste container described for s-LbL. The rest of the tubes were emptied into

the waste container, and then washed, rinsed in reverse osmosis water (on tap in the laboratory), and dried in the CEC after the experiment day was completed.

3.5.5 Storage

Slides were stored according to the same steps as s-LbL (§3.2.4.5).

3.5.6 Platelet Adhesion Studies with d-LbL

3.5.6.1 *Experiment preparation*

See §3.3.2, the procedures remained the same.

3.5.6.2 *Blood collection*

See §3.3.3, the procedures remained the same. One change to the protocol was the setting aside of a small quantity of d-PRP for flow cytometry, described in §3.8.4.

3.5.6.3 *Use of d-PRP in platelet adhesion tests*

See §3.3.4, the procedures remained the same.

3.5.6.4 *Post-experiment processing*

See §3.4, the procedures remained the same, except the FITC-fibrinogen tests were not repeated for d-LbL.

3.5.6.5 *Data processing*

See §3.4.5, the procedures remained the same.

3.6 **Bioanalyzer Flow Cytometry**

3.6.1 Overview

The Bioanalyzer® (Agilent) system was used to quantify the relative cell densities between samples taken on different days. Agilent technologies technical support was contacted and they had no recommendations for how to count platelets with the flow cytometry option of the Bioanalyzer. While there was no indication that it would not

work, it was an option they had never attempted or documented. The Bioanalyzer works with LoC technology. The flow cytometry chips provide six 10 μ L wells for test samples. A well for focusing dye provides an automated way for the system to focus before each individual chip experiment. When inserted into the Bioanalyzer, the system uses a pressure cartridge to move the samples and cell buffers through a series of microchannels into a laser counting area, where lasers and detectors excite the samples and detect red and green fluorescence, and count the individual events from each of six wells. In theory, since AO can fluoresce red or green depending on which part of the platelet it is adhered to [52], the laser and detector setup should have been able to detect stained platelets, so it was attempted, and worked, though not to the degree expected, see discussion, §5.2.

All of these procedures took place in a darkened, windowless room with ultraviolet “black light” illumination until the final step of loading the prepared chip into the Bioanalyzer.

3.6.2 Equipment and Reagents List

The following equipment was required to perform flow cytometry:

1 – Bioanalyzer: Agilent 2100 Bioanalyzer®, serial number DE72904734

2 – Vortexer: Bio-Rad (§3.1)

3 – Micropipettes (§3.1)

4 – 2.0 mL tubes

5 – Bioanalyzer computer: HP Compaq, Pentium Duo, Microsoft Windows XP,
serial number CZC7283LWT

6 – Bioanalyzer software: Agilent technologies, Waldbrown Analytical Division
B4, System #G1030AX, System Serial #DE01742445

7 – Bioanalyzer vortexer: IKA Works, MS2S9 Minishaker, 03.266671

8 – Bioanalyzer cell chips: Agilent technologies, 2100 Bioanalyzer,

Lot#ME11BL01, Kit#5067-1519-25Cell Assay

9 – 1 mL centrifuge tubes

In addition, the following reagents were required for flow cytometry:

1– Bioanalyzer reagents: Lot #0933, Kit#5067-1519, Contents: Priming solution,

2xCell buffer, Focusing Dye, Cell Buffer

2 – AO stain (§3.3.2.7)

3.6.3 Sample Preparation

1 mL d-PRP from an experimental day (§3.3.4 and 3.5.6.3) was set aside for flow cytometry.

3.6.3.1 *Platelet staining*

The d-PRP was stained on a 1:1 ratio with AO, producing 2 mL of stained mixture. This mixture was vortexed for 15 seconds, and allowed to stain for 20 minutes. At the end of the 20 minutes, the mixture was vortexed for 15 seconds.

3.6.3.2 *Sample dilution*

The stained, homogenized mixture was then diluted as follows into each of two 1 mL centrifuge tubes:

First tube: 300 μ L Agilent Cell Buffer, 3 μ L stained d-PRP

Second tube: 600 μ L Agilent Cell Buffer, 3 μ L stained d-PRP

3.6.4 Chip Preparation

The equipment for chip preparation is shown in Figure 23. A chip was removed from its sealed envelope, and prepared as follows, per the Agilent protocols found on p.

13 and 14 of the Agilent handbook located with the machine in the general laboratory. To prime the chip, 10 μL of priming solution (white cap) was added into the primer (P) well, allowing at least 60 seconds before putting any of the other solutions in the chip. 10 μL of focusing dye (yellow cap) were added into the focusing (FD) well. 30 μL of cell buffer solution were loaded into each of the cell buffer (CB) wells, then the diluted stained d-PRP samples were vortexed (Bio-Rad) for at least 5 seconds. To load the samples: 10 μL of diluted stained d-PRP were added into each of the test wells. Wells 1, 2, and 3 were loaded with the high concentration cell suspension, while wells 4, 5, and 6 were loaded with the low concentration cell suspension.



Figure 23 Equipment used to prepare for a Bioanalyzer run. Shown from left to right, 10 μL and 200 μL pipette tips, a new cell chip, the reagents box, a 1 mL centrifuge tube, and the two micropipettes

3.6.5 Sample Loading

The Bioanalyzer machine was turned on, the computer turned on, and the software loaded before bringing the sample chip, covered to protect from excessive light exposure, from the darkened room to the general laboratory.

The chip vortexer (IKA Works) was used to vortex the chips at 1000 s^{-1} for five seconds before the chip was loaded into the Bioanalyzer. No visible bubbles should have remained in any of the wells by this point. If bubbles were visible, the well was drained with the micropipette and reloaded. Bubbles in the wells were the primary reasons for failed runs, and focusing dye problems were the second most common. The prepared chip was then loaded into the machine, and the lid was closed.

3.6.6 Agilent Software

Once the chip was loaded and detected by the software, the various settings could be made to run a cell assay.

3.6.6.1 *Cell assay*

The following settings were fixed for a given run:

COM port: 2 for communicating with the Bioanalyzer.

Assay Selection: Generic Series II

Assay Details: Generic, Version 2.0, Modified May 8, 2006, Copyright © 2002-2006 Agilent technologies

Destination: Custom [set the destination folder for the day's run]

File Prefix: [Stat Dyn w-o L-a], indicated the experiment running on a day when static and dynamic flow conditions with and without the chemical additive L-a. On the three days that this test was performed, the prefix was as indicated here.

Data Acquisition Parameters: Default

Once the on-screen run checklist had all green checks, the run was started. The run was monitored for a few minutes to ensure it did not fail.

3.6.6.2 *Results generation and storage*

The program automatically generated histograms for each of the six test wells. These histograms included the number of red events and the number of blue events detected in each well. These would be the total number of events detected from a given well. The software also generated scatter plots showing the two types of fluorescence on a single plot. These results were saved automatically, per the naming convention defined in the previous section.

3.7 **SEM Imaging of Surfaces**

3.7.1 Overview

Field-emission scanning electron microscope (FE-SEM) images were taken to use as a qualitative basis to support the conclusions drawn on s-LbL, including potential reasons for AO retention on the s-LbL surface in the absence of platelets.

3.7.2 Equipment List

1 – Field Effect Scanning Electron Microscope (FE-SEM): Hitachi S-4800

Scanning Electron Microscope in the IfM Metrology Laboratory.

2 – An s-LbL slide

3 – A fibrinogen d-LbL slide

4 – A collagen d-LbL slide

3.7.3 SEM Imaging Process

FE-SEM images were taken in the metrology lab of the Institute for Micromanufacturing (IfM) at Louisiana Tech. Dr. Alfred Gunasekaran operated the FE-SEM and took all of the images. To preserve surface fidelity as much as possible, especially since the structures of interest were the nano-scale surface produced by LbL,

gold sputtering was avoided. Avoiding the sputtering did not permit the highest magnifications possible, but did allow images down to the 500 nm scale. At this highest magnification, only a few seconds were available to focus the image and take the image before the area became charged and impossible to image.

The samples to be imaged were prepared from s-LbL and d-LbL slides, with no PRP. Slides were cut to 1" square, marked for top surface, and given to Dr. Gunasekaran for imaging. He placed the slides on a stage, adjusted the stage height to get the appropriate sample elevation for coarse focusing in the system, and placed them into the microscope via the electronically interlocked airlock system. Once the sample was in the imaging zone within the FE-SEM, the image was coarsely focused at the 30 μm scale. Areas of interest were identified, and images in the 500 nm to 5 μm scales were taken. The clearest images were then selected for inclusion in this work.

3.8 Particle Tracking

To provide an estimate of the localized dynamic flow conditions, including mass transport phenomena for pd-NO, particle tracking experiments were performed. The results for particle tracking were used to test Hypotheses 2, 3, and 4 (§1.5.2, 1.5.3, and 1.5.4). To test Hypothesis 2, the particle tracking software provided an estimate of local shear stresses as a function of radial distance from the center of a Petri dish. For Hypotheses 3 and 4, the particle tracking software provided an estimate of velocity means and standard deviations a function of radial position. The velocities at any given point were used to estimate localized transport phenomena for pd-NO. Transport phenomena, velocity means and standards of deviation, and shear stresses were used to explain the shear-dependent results for Hypothesis 2. Hypotheses 3 and 4 were tested by analyzing

the statistics on the means and standard deviations of the calculated percent surface areas for each of the test slides. However, the particle tracking software provided an additional metric for explaining the observed results.

3.8.1 Experimental Setup

To replicate the experimental conditions (dynamic flow condition) a glass slide with elastomer backing was placed in a Petri dish, with the back of the slide painted black before being covered by the elastomer. The surface of the orbital shaker was a corrugated black elastomer, and did not provide a reflective surface. The hole-punch was used to create 3 mm discs from the white wax-covered paper, and these discs were used as the particles for tracking.

3.8.2 Equipment and Software List

1 – Orbital shaker (§3.3.2.2)

2 – Disposable Petri dish

3 – Glass slide

4 – White wax-covered paper, obtained by disassembling a typical fast-food-type drinking cup.

5 – Hole puncher

6 – Fujifilm Finepix 12.0 megapixel digital camera

7 – Red food coloring

The following third-party software components [56] were combined into the final program, *ParticleTrack_FINAL.m* (APPENDIX A):

bpass.m

cntrd.m

lentrck.m

parse_noran.m

pkfnd.m

read_gdf.m

read_noran.m

track.m

dsxy2figxy.m

3.8.2.1 *Printed template and Petri dish*

The particle tracking software needed constant reference points from which to establish a size scale, an axis orientation, and the center of the Petri dish. To provide these, a template was generated to place on the surface of the orbital shaker (APPENDIX F). This template had four sets of identifying marks the software used to set the horizontal (X) axis, and the vertical (Y) axis. The distance between two axis markers was used to establish a length-to-pixel scale when processing the data for velocity calculations. The intersection of the two axis lines was used to identify the center of the Petri dish for polar coordinate calculations.

The Petri dish was set in the center of the template, and the slide placed in the dish aligned along the Y-axis, as shown in Figure 24. 15 mL of dark red-dyed water were added to replicate the fluid quantity used during the dynamic condition experiments. The center surface of the fluid was covered with seven of the 3-mm discs. The discs were placed in the center to allow particles to be imaged across all the radii of the dish, as the particles had a tendency to spread to the outer rim of the dish when placed under the dynamic flow conditions.



Figure 24 Slide with blackened back placed in the Petri dish aligned with the vertical axis markers. The template and its two horizontal axis markers and lower vertical axis marker can be seen in the image

3.8.2.2 *Camera setup on orbital shaker*

A hole was cut out of the top of a large plastic container. The container was translucent to allow the ambient light to penetrate and reflect off the white particles. The particles could then stand out from the background and be identified as particles via image thresholding during data processing. The container over the dish and template is shown in Figure 25.

The camera was placed with the lens in the hole, which was cut exactly large enough to have the lens base fit snugly in the hole and prevented the camera from moving with respect to the container and therefore the Petri dish. The camera and container were placed over the template on the orbital shaker. The video recording was started; the orbital shaker was then turned on and set to 1 Hz and 35-55 seconds of particle movement were recorded for each of four runs.

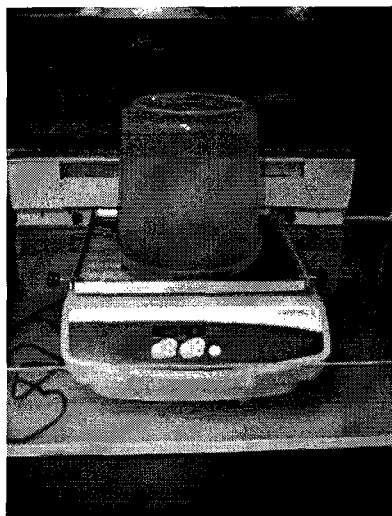


Figure 25 Container with a hole cut in the bottom, set over the template and Petri dish. This setup allowed for filming of the fluid in the dynamic flow condition with no relative motion between the camera and the Petri dish

3.8.3 Data Processing

The collected videos were processed using a suite of programs, details of which are located in APPENDIX A. A main program, *ParticleTrack_FINAL.m*, was developed for this dissertation. This program performed all of the pre-processing of the videos, called the third party programs for particle identification across the frames of the videos, processed the resulting data and statistics, and generated and saved the images and spreadsheets detailing these results. The flow patterns drove most particles to the outside edge of the Petri dish for a large percentage of the filmed time. The flowchart for this program is found in Figure 26 and Figure 27.

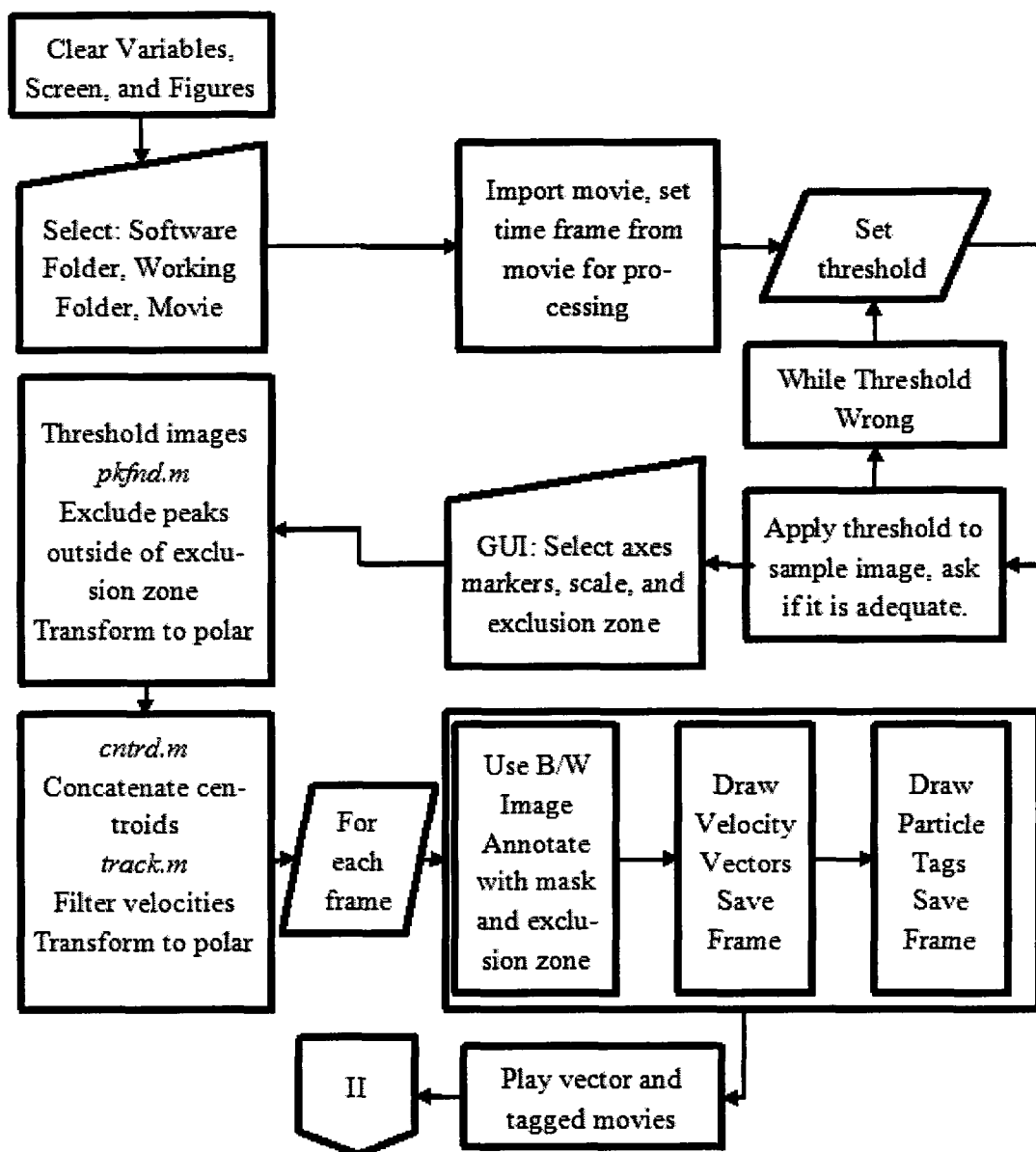


Figure 26 Flowchart 1 of 2 for particle tracking program, *ParticleTrack_FINAL.m*

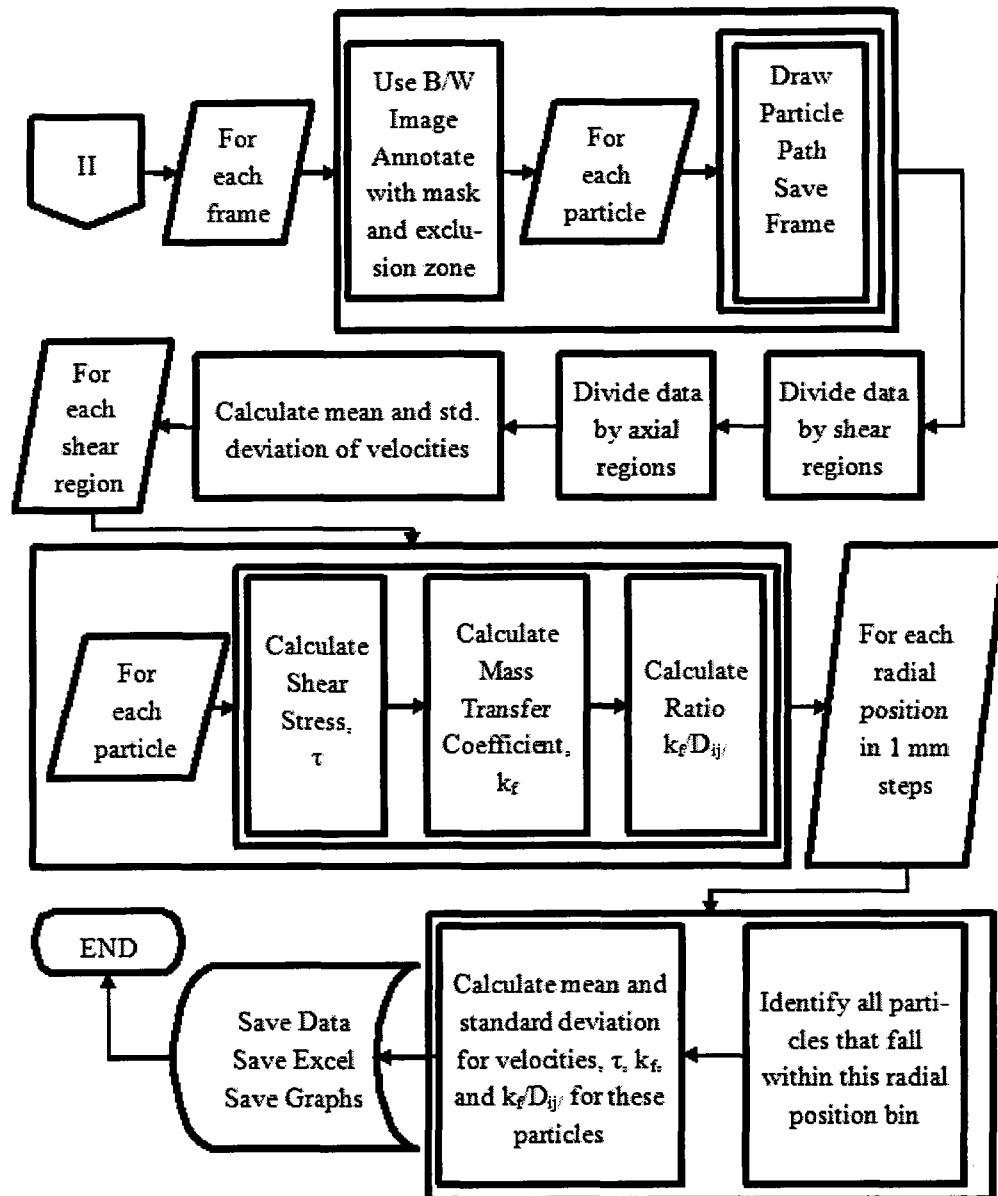


Figure 27 Flowchart 2 of 2 for particle tracking program, *ParticleTrack_FINAL.m*

3.8.4 Transport Model

The transport model employed in the *ParticleTrack_FINAL.m* program (§3.8.3, and APPENDIX A) was based on the concept of localized transport over a flat plate.

Because the flow was more complex than even a Von Karman flow with axisymmetric boundary movements [57], a generalized transport model was not within the scope of the

work presented here. This model was developed to provide localized data that could later be validated by a more complex and in-depth CFD or similar numerical model.

The static exposure of surfaces to PRP has been studied by others [58] [59], and there are published values for the diffusion coefficient of NO in blood [60] [61]. The object of the transport model presented here was to provide a way to compare the localized convection-enhanced transport to the numbers provided by these previous works.

The flow over a flat plate model was selected because on a localized scale, it more adequately represented what was occurring in transport. Plata et al. have modeled the diffusion and convection of NO produced by the endothelium in a microchannel flow, claiming that at the time of publication it was one of only two models in the literature that accounted for convective flow of NO in a physiological condition. [62]

The model is shown here in Figure 28 and Figure 29. The inputs to this model were: 1) The top surface profiles as a function of radial position along the dish, for profiles located over the slide (Eq. 3-1 and Figure 16), and profiles located over the Petri dish (Eq. 3-2 and Figure 17). 2) Velocities calculated by the particle tracking software, 3) Kinematic and dynamic viscosities, μ and ν , of the liquid, in this case warm water, 4) The diffusion coefficient for NO, D_{ij} , and 5) The wall concentration of NO, $C = C_0$, which was assumed to be a unit concentration, as this model was intended to give an idea of the relative transport efficiency at the various shear conditions, while specific values of NO transport would be of little use without experiments to estimate the potential for local pd-NO based on adhered platelets.

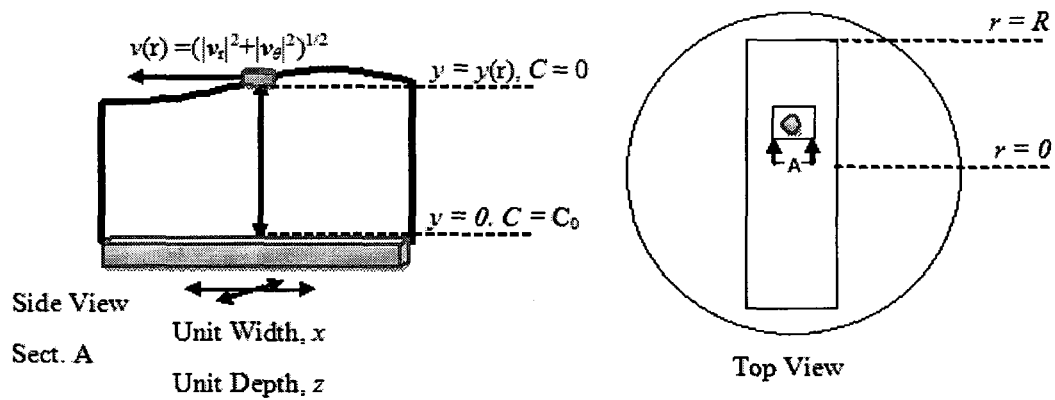


Figure 28 Local flat-plate transport model boundary conditions, calculated for a unit width and depth (into page). The top view shows one of the localized areas calculated for transport given a particle location, with the detail view shown from a side view for section A

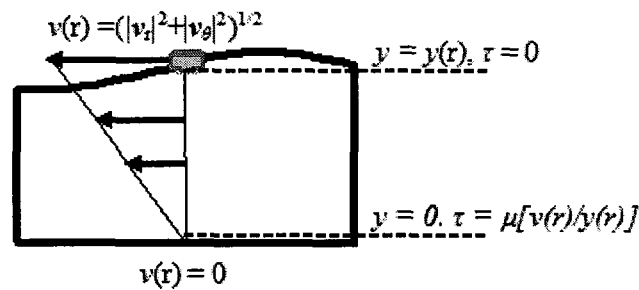


Figure 29 Local transport model, shear stress definition, linear shear stress model

The surface profiles, obtained empirically from measurements of the upper and lower boundaries of the wave (Figure 16) are as follows:

$$y_{slide}(r) = -(1 \times 10^{-5})r^3 + (2 \times 10^{-14})r^2 + 0.0395r + 2.895 \quad \text{Eq. 3-1}$$

$$y_{dish}(r) = -(1 \times 10^{-5})r^3 + (5 \times 10^{-14})r^2 + 0.0395r + 3.895 \quad \text{Eq. 3-2}$$

Thus, for any particle's radial position, the estimated local liquid column height could be estimated. The simplified localized shear stress, τ_{loc} , could therefore be approximated as follows:

$$\tau = \mu \frac{dv(r)}{dy} \rightarrow \tau_{loc} = \mu \frac{\Delta v(r)}{\Delta y(r)} = \mu \frac{v(r) - 0}{y(r) - 0} = \mu \frac{v(r)}{y(r)} \quad \text{Eq. 3-3}$$

Where μ was the kinematic viscosity, $v(r)$ was the localized velocity magnitude, and $y(r)$ was the localized profile elevation. $v(r)$ was obtained from the particle tracking data, and $y(r)$ was calculated from Eq. 3-1 or Eq. 3-2, depending on the location of the particle. The values for μ and ν were obtained for water at 30°C, an approximation for the d-PRP [63]. All values were transformed to length units of mm for consistency with the measurement data. These two viscosity values were:

$$\mu = 7.98 \times 10^{-10} \text{ N s mm}^{-2} \quad \text{Eq. 3-4}$$

$$\nu = 0.801 \text{ mm}^2 \text{ s}^{-1} \quad \text{Eq. 3-5}$$

The equation for calculating the localized mass transfer parameter of fluid moving over a flat plate, k_f , is expressed in Eq. 3-6 [64].

$$k_f = 0.646 \frac{D_{ij}}{L} Re^{\frac{1}{2}} Sc^{\frac{1}{3}} \quad \text{Eq. 3-6}$$

Where D_{ij} is the diffusion coefficient for the substance in question, in this case NO, L is the characteristic dimension, $y(r)$, Re is the local Reynolds number, and Sc is the Schmidt number. These values are given in the following equations.

$$D_{ij} = 0.0045 \text{ mm}^2 \text{ s}^{-1} \quad \text{Eq. 3-7}$$

$$Sc = \frac{\nu}{D_{ij}} = \frac{0.801 \text{ mm}^2 \text{ s}^{-1}}{0.0045 \text{ mm}^2 \text{ s}^{-1}} = 178 \quad \text{Eq. 3-8}$$

$$Re = \frac{\nu L}{\nu} = \frac{\nu(r)y(r)}{\nu} \quad \text{Eq. 3-9}$$

Eq. 3-6 can therefore be rewritten as:

$$\begin{aligned} k_f &= 0.646 \frac{0.0045 \text{ mm}^2 \text{ s}^{-1}}{y(r)} Re^{\frac{1}{2}} (178)^{\frac{1}{3}} \\ &= \frac{3.63 \text{ mm}^2 \text{ s}^{-1}}{y(r)} Re^{\frac{1}{2}} \end{aligned} \quad \text{Eq. 3-10}$$

Reducing the localized transport coefficient to a simplified function of $\nu(r)$ and $y(r)$. Dimensional analysis of Eq. 3-10 shows that k_f is in units of mm s^{-1} . The diffusion coefficient is in units of $\text{mm}^2 \text{ s}^{-1}$. The localized mass transfer coefficient was used in conjunction with a local concentration, C_{loc} , whereas the diffusion coefficient D_{ij} was used in conjunction with the concentration gradient, $\frac{\partial C}{\partial y}$. The comparison done here must consider this usage difference. The ratio shown in Eq. 3-11 quantifies the relative mass transport in convective (dynamic flow condition) versus diffusive (static exposure to PRP condition) states.

$$\frac{k_f C_0}{D_{ij} \frac{dC_0}{dy}} = \frac{k_f C_0}{D_{ij} \frac{C_0 - 0}{y(r) - 0}} = \frac{k_f C_0}{D_{ij} \frac{C_0}{y(r)}} = \frac{k_f y(r)}{D_{ij}} \quad \text{Eq. 3-11}$$

3.9 Statistical Analysis

3.9.1 Overview

The collected percent surface area coverage results were evaluated for both means and variances. A Welch's t-test was used to test means, where the samples in two data sets were unpaired or independent with the assumption that the variances were unequal.

The null hypothesis was that the means of the two compared samples had a difference of zero [65]. An F-test was used to compare variances, with the null hypothesis being that no differences in variances existed for the two compared sample sets [66].

For both the t-test and the F-test, the significance level was set to $p < 0.05$. The built-in statistical functions in the Data Analysis add-on for Excel® were used to perform this statistical analysis. Tests on sample data were performed to validate the methods. The validation for the t-test is described in APPENDIX D and the validation for the F-tests is described in APPENDIX E.

Statistical tests were performed on paired sets of data, from which conclusions could be drawn. The tests compared the control conditions against other conditions. The paired comparison types are delineated in Table 4, Table 5 and Table 6. The specific hypotheses that were tested are described in the following sections.

3.9.2 Hypothesis 1

Statistical tests were not sufficient to provide the full answer to Hypothesis 1. Evaluation of fluorescence images provided the principal indicators that s-LbL surfaces retained anomalous AO stain, often resembling an expected d-PRP test even when the surfaces had never been exposed to d-PRP: These fluorescence images were: 1) s-LbL surfaces exposed to d-PRP (§4.4.3.3), 2) s-LbL surfaces exposed to buffer PBS only (§4.4.3.1), and 3) plain glass slides exposed to d-PRP (§4.4.3.2). However, the statistical tests also served to validate the statistically significant differences between d-LbL and s-LbL at each of the tested conditions. These statistical tests are listed in Table 4.

Table 4 Pairings for statistical testing of results used to compare s-LbL and d-LbL percent surface coverage by AO stain

Pair #	Flow Cond.	LbL Type	Region	L-a μ M	Pair #	Flow Cond.	LbL Type	Region	L-a μ M
1	Dyn.	d-LbL	Low	0	5	Dyn.	d-LbL	Low	20
	Dyn.	s-LbL	Low	0		Dyn.	s-LbL	Low	20
2	Dyn.	d-LbL	Mid	0	6	Dyn.	d-LbL	Mid	20
	Dyn.	s-LbL	Mid	0		Dyn.	s-LbL	Mid	20
3	Dyn.	d-LbL	High	0	7	Dyn.	d-LbL	High	20
	Dyn.	s-LbL	High	0		Dyn.	s-LbL	High	20
4	Static	d-LbL	N/A	0	8	Static	d-LbL	N/A	20
	Static	s-LbL	N/A	0		Static	s-LbL	N/A	20

Supporting evidence for the functionality of d-LbL surfaces was the test of the process on a collagen biointerface and a fibrinogen biointerface. It was expected that if the process was valid, the patterns in collagen adhesion would remain consistent with the patterns in fibrinogen adhesion. This test would also strengthen the case for using fibrinogen as a biointerface, if adequately comparable to collagen. The statistical tests in Table 5 were used to test these comparisons across each shear region, flow condition, and chemical additive condition.

Table 5 Pairings of statistical tests used to compare d-LbL Fibrinogen and d-LbL Collagen for percent surface coverage

Pair #	Flow Cond.	Bio-Interface	Region	L-a μ M	Pair #	Flow Cond.	Bio-Interface	Region	L-a μ M
9	Dyn.	Fib.	Low	0	14	Dyn.	Fib.	Low	20
	Dyn.	Coll.	Low	0		Dyn.	Coll.	Low	20
10	Dyn.	Fib.	Mid	0	15	Dyn.	Fib.	Mid	20
	Dyn.	Coll.	Mid	0		Dyn.	Coll.	Mid	20
11	Dyn.	Fib.	High	0	16	Dyn.	Fib.	High	20
	Dyn.	Coll.	High	0		Dyn.	Coll.	High	20
12	Static	Fib.	N/A	0	17	Static	Fib.	N/A	20
	Static	Coll.	N/A	0		Static	Coll.	N/A	20
13	Static	Coll.	N/A	0					
	Static	Coll.	N/A	20					

3.9.3 Hypothesis 2

To test whether platelet adhesion, indicated by fluorescent percent surface coverage, depended on shear stress, statistical tests were performed to compare the fluorescent percent surface coverage on d-LbL surfaces within the three shear regions in the dynamic tests. These comparisons were performed for both 0 μ M added L-a and 20 μ M added L-a. Table 6, test pairs 18-20, were the statistical tests that provided the statistical significance of these differences. A successful experimental result would be statistically significant increases in adhesion with increased shear rates.

Table 6 Pairings of statistical tests used to examine d-LbL surfaces under different flow and chemical additive conditions

Pair #	Flow Cond.	LbL Type	Region	L-a μ M	Pair #	Flow Cond.	LbL Type	Region	L-a μ M
18	Dyn.	d-LbL	Low	0	26	Dyn.	d-LbL	Mid	0
	Dyn.	d-LbL	Mid	0		Dyn.	d-LbL	Mid	20
19	Dyn.	d-LbL	Low	0	27	Dyn.	d-LbL	High	0
	Dyn.	d-LbL	High	0		Dyn.	d-LbL	High	20
20	Dyn.	d-LbL	Mid	0	28	Static	d-LbL	N/A	20
	Dyn.	d-LbL	High	0		Dyn.	d-LbL	Low	20
21	Static	d-LbL	N/A	0	29	Static	d-LbL	N/A	20
	Dyn.	d-LbL	Low	0		Dyn.	d-LbL	Mid	20
22	Static	d-LbL	N/A	0	30	Static	d-LbL	N/A	20
	Dyn.	d-LbL	Mid	0		Dyn.	d-LbL	High	20
23	Static	d-LbL	N/A	0	31	Fib-Stat.	d-LbL	N/A	0
	Dyn.	d-LbL	High	0		Fib-Stat.	d-LbL	N/A	20
24	Static	d-LbL	N/A	0	32	Static	d-LbL	N/A	0-20
	Static	d-LbL	N/A	20		Dyn.	d-LbL	All	0-20
25	Dyn.	d-LbL	Low	0					
	Dyn.	d-LbL	Low	20					

3.9.4 Hypothesis 3

To test whether the addition of L-a decreased observed platelet adhesion indicated by fluorescent percent surface area coverage, the d-LbL surfaces were tested according to the test pairs 25-30 described in Table 6. Validation of this hypothesis would be indicated by statistically significant decreases in platelet adhesion across each of the listed test pairs, as well as a statistically significant difference between the static exposure to PRP condition and all dynamic flow condition cases.

3.9.5 Hypothesis 4

To test whether the addition of L-a affected platelet adhesion in static exposure to PRP, the fluorescent percent surface coverages on d-LbL surfaces were compared between test pair 13 from Table 5, and test pair 24 from Table 6. The reduction in

fluorescent coverage with the addition of L-a in static and dynamic conditions was compared between test pair 32 from Table 6. The change in fluorescence percent surface coverage (FPSC) for each test day and flow condition was calculated as follows:

$$\Delta_{La} = (FPSC)_{20\mu M L-a} - (FPSC)_{0\mu M L-a} \quad \text{Eq. 3-12}$$

The results for each test day were then averaged, and tested for significant differences with a t-test. Validation of this hypothesis would be indicated by a statistically significant difference between the 0 and the 20 μM L-a chemical additive conditions in both collagen and fibrinogen tests, with greater differences in the dynamic conditions than in the static conditions.

CHAPTER 4

RESULTS

4.1 Overview

For the various chemical and dynamic flow conditions reported in the s-LbL (§4.4) and d-LbL (§4.5) sections, a sample of the total images taken are shown. The locations of all data files on the supplemental digital media are listed in APPENDIX B.

The measure of platelet adhesion used in this section is the percentage of surface coverage obtained when fluorescent images were processed with the MATLAB image processing program. For simplicity, this measure will be referred to as “platelet adhesion.” However, true platelet adhesion quantification will not be confirmed by the work presented here, but rather is strongly suggested by the results, and is left to future work for final confirmation.

Because one of the principal variables being tested for Hypotheses 2 and 3 (and to a small extent, Hypothesis 1) was the dependence of adhesion on shear stress, particle tracking was used to quantify the shear rates and transport phenomena at different regions of the slides. The particle tracking results (§4.2) and the flow cytometry that quantified the available platelets for adhesion are presented first, laying the foundation for the results of the platelet adhesion tests in the subsequent sections. (§4.3, 4.4, 4.5, and 4.6)

4.2 Particle Tracking

4.2.1 Overview

Because the particle paths depended strongly on the initial particle positions, not every video segment had particles that in each of the three shear regions along a Petri dish. The most useful exemplars were those that contain data from all three shear regions, and are the ones shown in this results section. The full videos and results set can be found in the files detailed in APPENDIX B.

Particle tracking was used for two primary purposes: 1) to establish localized velocities and shear stresses to verify the existence of a shear gradient on a single slide (Hypothesis 2, §1.5.2), and 2) estimate local transport phenomena to help explain platelet adhesion behavior in a shear gradient from the diffusion of pd-NO. Means and variances of both the velocities and transport coefficients were examined as a function of distance from the center of the dish. The variances in these values were compared to measured variances in adhesion.

Each particle tracking run video was split into different evaluation time blocks of seven seconds. Not all blocks had particles distributed well across all three shear regions. Because of the difficulties in synchronizing data for wave position or phase around the dish, an additive or ensemble average of the different results might have resulted in losing data. For example, if data from the peak of the wave were averaged with data from the low point of the wave, the true averages would be filtered or attenuated. Therefore, only time blocks that had a good distribution of particles across the shear regions were selected, and the best example shown in the results section.

4.2.2 Images Containing the Particles

Raw and processed video frames are shown in Figure 30 and Figure 31, respectively.

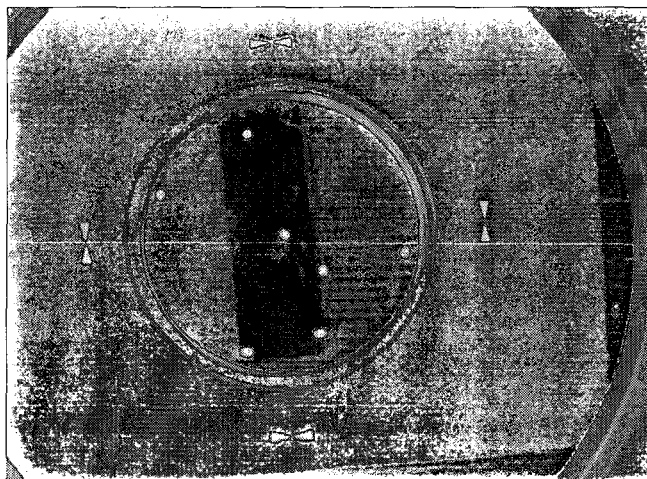


Figure 30 Still frame from the “Run 1” video for particle tracking. The Petri dish, slide with blackened silicone backing, template with position and sizing markers, and particles can be seen

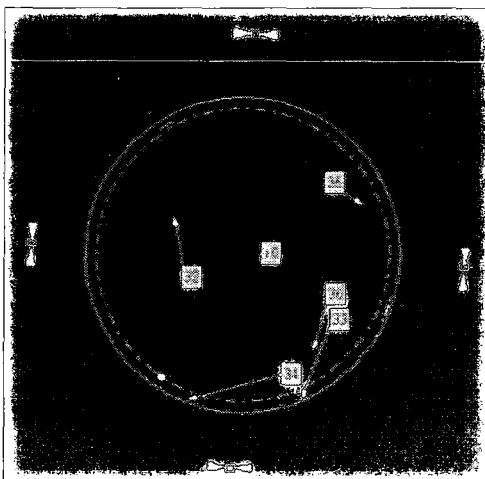


Figure 31 Still frame from the “Run 1” Tagged Vector video for particle tracking. Particles are tagged with identifying numbers, and velocity vectors are extended from the particle centroids. The alignment markers, Petri dish outline, and exclusion zone can also be seen

4.2.2.1 *Particle path lines*

The paths followed by tracked particles were collected into videos for each analyzed time block. These paths videos helped corroborate the assumption that certain time blocks of videos had better distributions of particles tracked throughout the analyzed video segment. Figure 32 shows the particle paths from the 21 s-28 s segment of the video from Run 1, showing a lack of paths crossing the low-shear region of the slide, making the data available from that time block incomplete. Figure 33 shows the paths for the segment selected for the results in the previous sections.

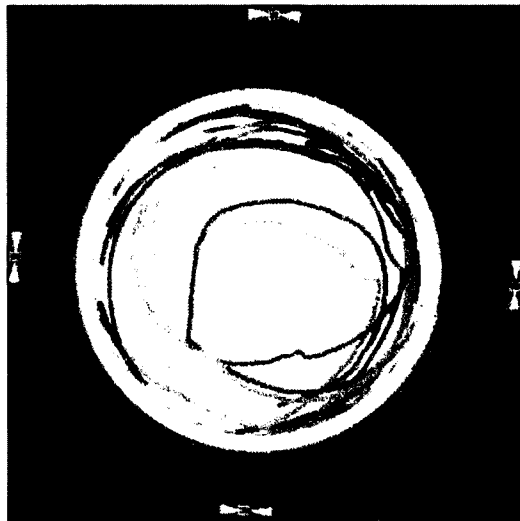


Figure 32 Sample frame showing paths for all tracked particles, from 21s-28s of the original video, "Run 1"

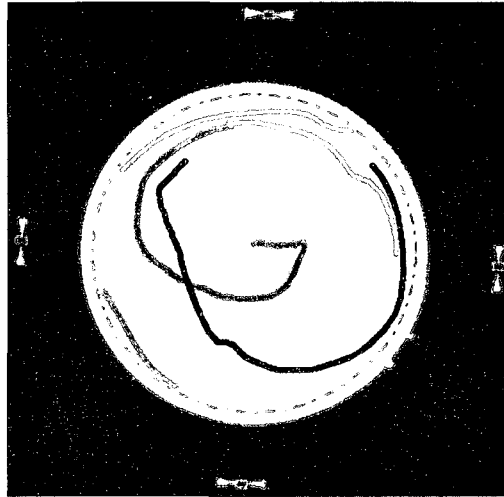


Figure 33 Sample frame showing paths for all tracked particles, from 7s-14s of the original video, "Run 1"

4.2.2.2 *Velocity magnitudes in different regions over the slide*

The velocities for each particle tracked in a given segment of the video were divided into shear regions. Particles that fell within a 1" wide band straddling the X-axis, the axis aligned with the slide, were isolated, and the magnitudes of their velocities are shown as a function of time in Figure 34. There was a good distribution of velocity data points for all three shear regions through the observed time. The velocity data were oscillatory, which matches the periodic nature of the dynamic flow, with a wave moving around the dish at 1 Hz.

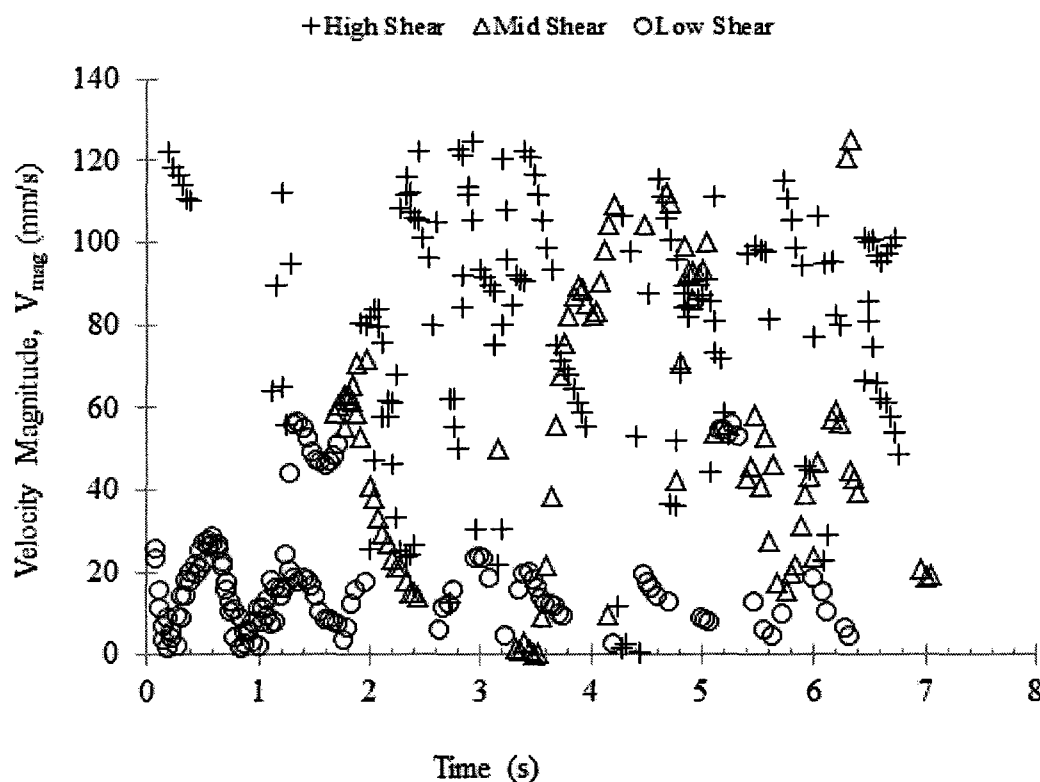


Figure 34 Velocities over each slide region as a function of time, from 7s-14s of the original video, “Run 1”

4.2.2.3 Velocity magnitudes in different positions over the dish

The velocities for each particle tracked in a given segment of the video were divided into shear regions. Particles that fell within a 1” band straddling the Y-axis, aligned with the non-slide axis (over the Petri dish only), were isolated and their velocity magnitudes are shown as a function of time in Figure 35. The oscillatory pattern and the velocity magnitudes were similar to those over the slide (Figure 34). This similarity was unsurprising, as the slide was only 1 mm thick. The low shear region consists of data points that are nearly completely shared with the slide velocities in Figure 34. The mid shear region shares fewer data points, and the high shear region is nearly independent.

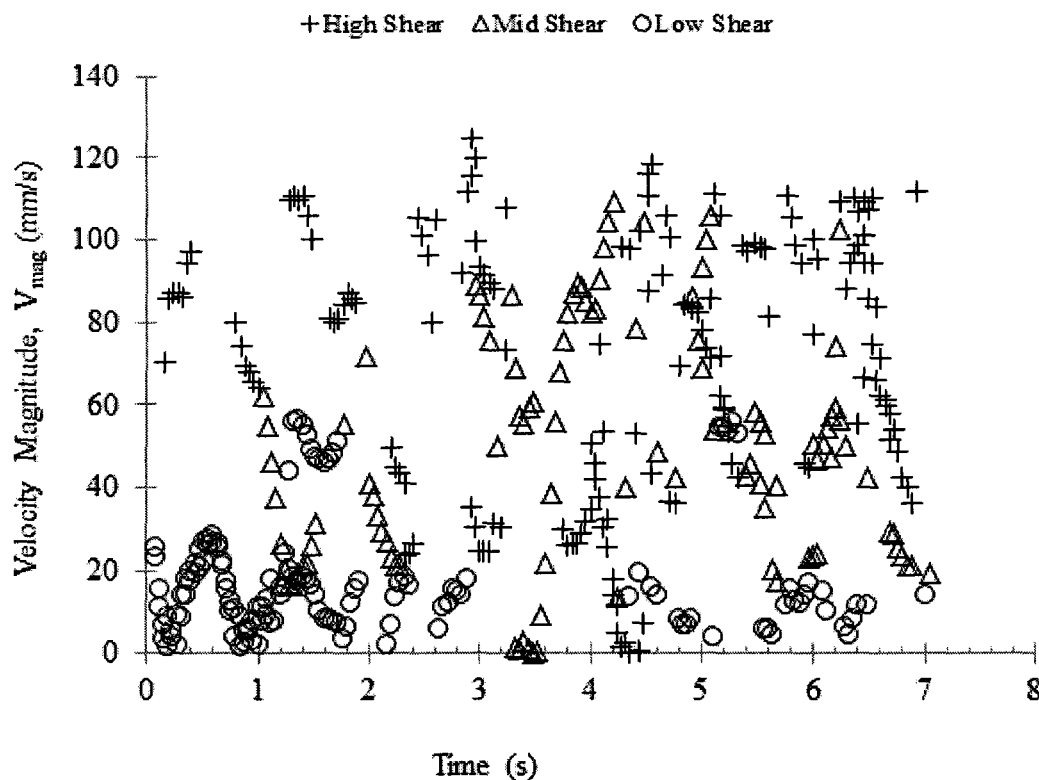


Figure 35 Velocities over each Petri dish region as a function of time, from 7s-14s of the original video, “Run 1”

4.2.2.4 Radial angular and combined velocities over the slide

All particles in a given segment of one of the particle tracking videos were binned into 1 mm radial bins from the center (0 mm) to the outside edge of the slide (44 mm). The angular and radial velocities in each bin were averaged to provide radial and angular velocities, averaged over time and angular position (θ) as a function of radius $V_r(r)$ (Figure 36), and $V_\theta(r)$ (Figure 37), respectively. The two components were then added vectorially to provide a combined velocity, $V_{mag}(r)$ (Figure 38). In all cases, the velocity is relatively flat over the first 1/3 of the slide region, begins to rise in the second 1/3 of the slide, and continues to increase through the final third of the slide. The velocity variance generally increases with the mean value. The angular velocity increases more

rapidly than the radial velocity at the beginning of the second 1/3 of the slide.

Surprisingly, the maximum value is slightly higher for the radial velocity than the angular velocity. This averaging method may have contributed to this result, with the absolute values of the velocities being summed rather than the signed velocities. This method was used because the localized transport phenomena depended on the velocity magnitude at the given radial location, and not on the direction.

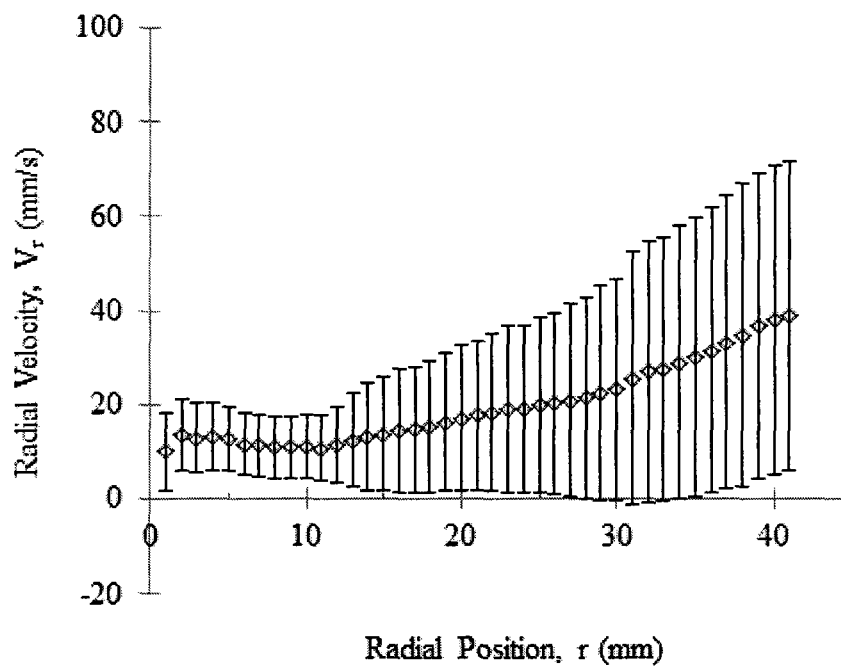


Figure 36 Radial velocities averaged over time and angular position, from 7s-14s of the original video, "Run 1"

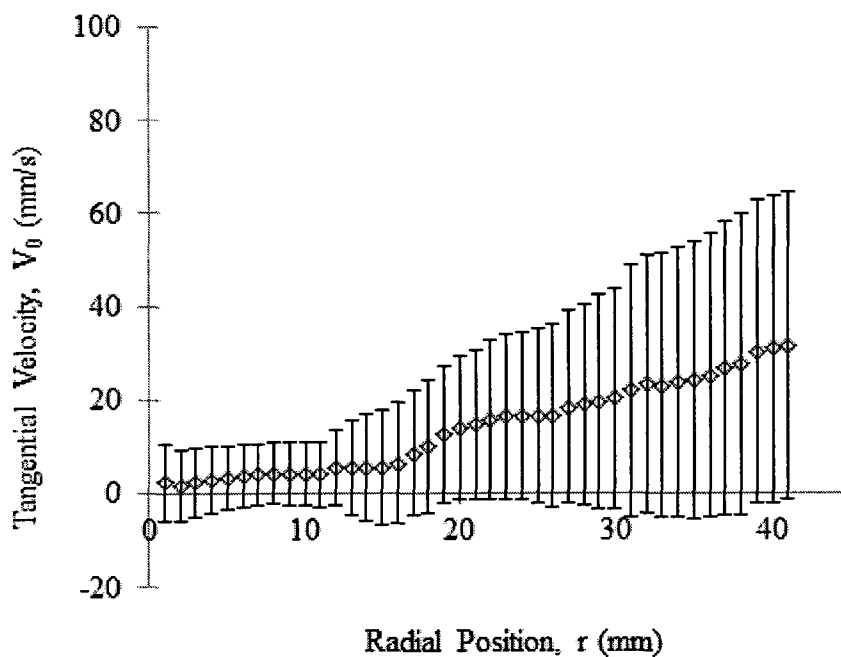


Figure 37 Angular velocities averaged over time and angular position, from 7s-14s of the original video, "Run 1"

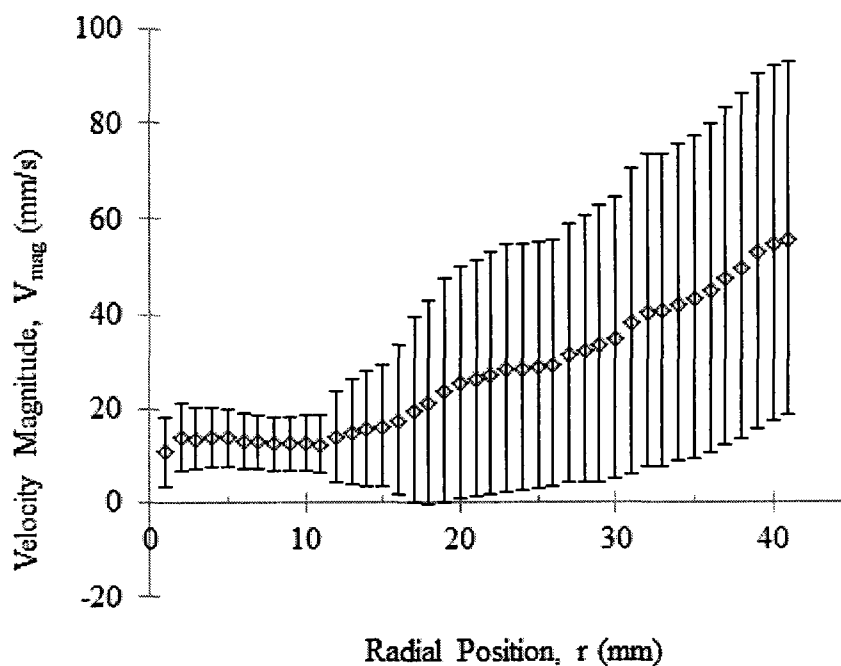


Figure 38 Velocity magnitudes averaged over time and angular position, from 7s-14s of the original video, "Run 1"

4.2.2.5 Shear stress

The calculated shear stresses in a given segment of one of the particle tracking videos were binned into 1 mm radial bins from the center (0 mm) to the outside edge of the slide (44 mm). These data were averaged, producing a shear stress, τ , that was representative of angular position, θ , and time-averaged localized shear stress (Figure 39). Hypothesis 2 was supported by these results, as a shear stress gradient was demonstrated. However, the magnitude of shear stress was low. Physiological shear stresses are $\sim 15 \text{ dynes-cm}^{-2}$, or roughly 1000 times the magnitude of stress shown.

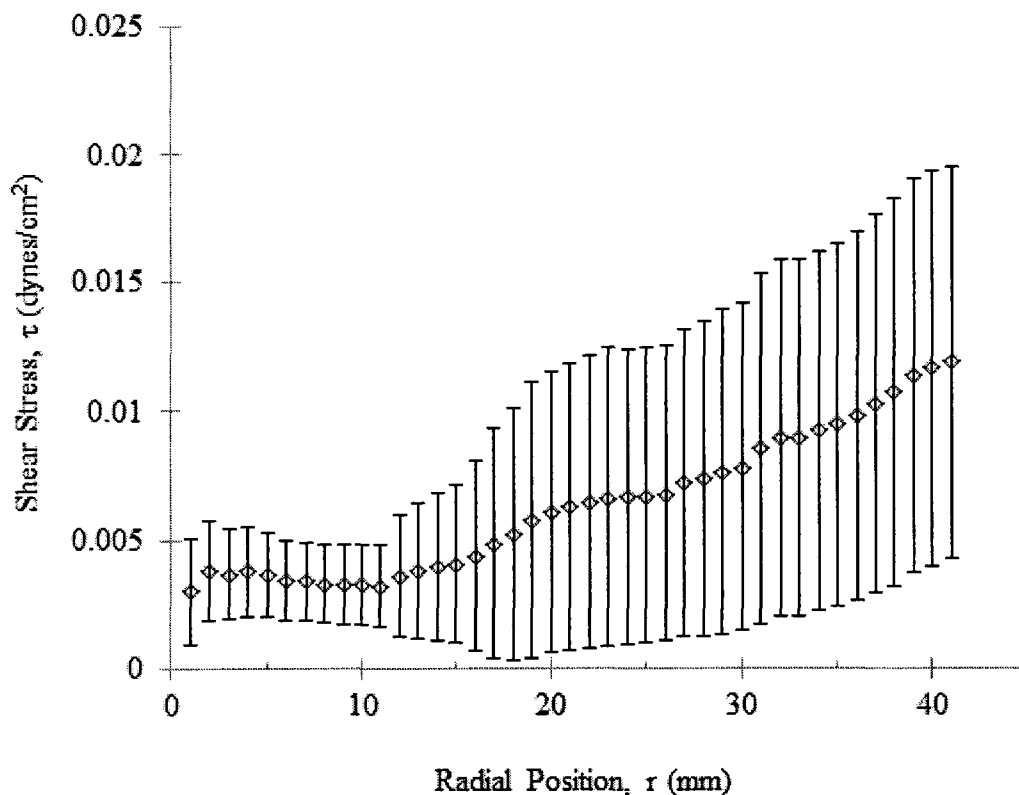


Figure 39 Shear stress magnitudes averaged over time and angular position, from 7s-14s of the original video, "Run 1"

4.2.2.6 Transport coefficient

Localized mass transport coefficients were calculated at each tracked particle point. These calculated coefficients in a given segment of one of the particle tracking videos were binned into 1 mm radial bins from the center (0 mm) to the outside edge of the slide (44 mm). These data were then averaged, producing a localized mass transport coefficient, k_f , which was representative of angular position, θ , and time-averaged localized mass transport (Figure 40). The transport coefficient curve shape and variances was driven by the velocity curve shape and variances.

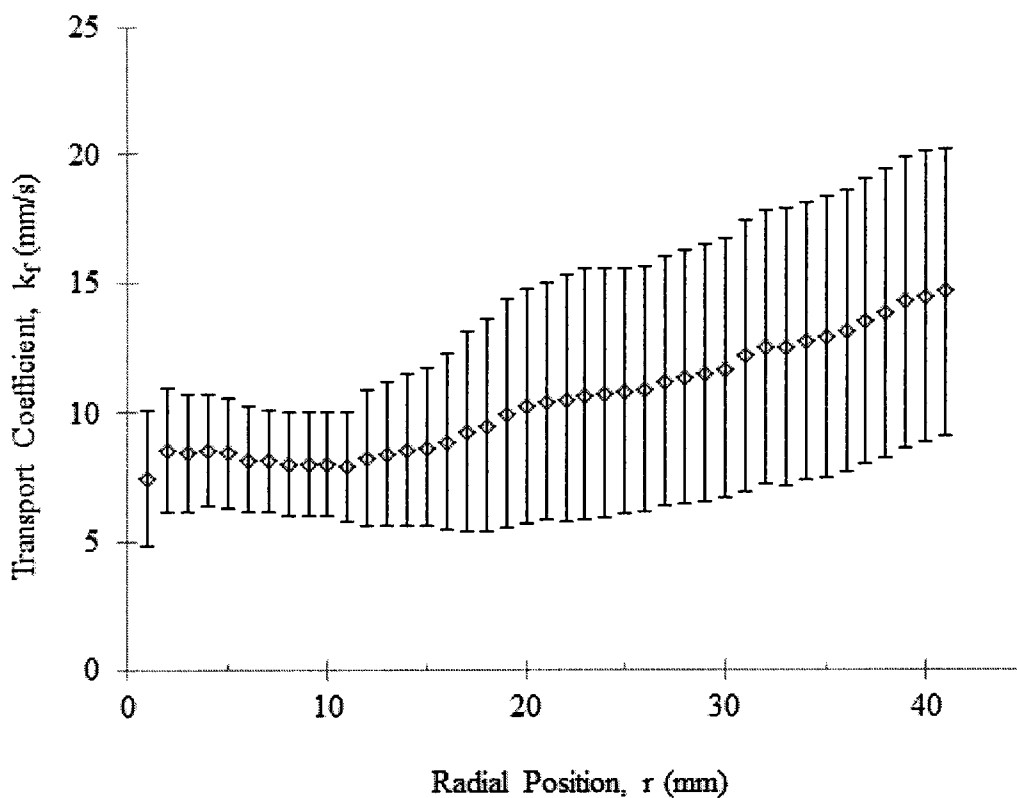


Figure 40 Localized mass transport coefficient averaged over time and angular position, from 7s-14s of the original video, “Run 1”

An important comparison was the relative efficiency of transport between active, convective transport (k_f), and pure diffusion (D_{ij}) for NO. To estimate the ratio between

the localized mass transport coefficients and the diffusion coefficient, Eq. 3-11 was used.

The results can be seen in Figure 41. The transport of NO was enhanced between 7000 and 15000 times that of pure diffusion according to these results.

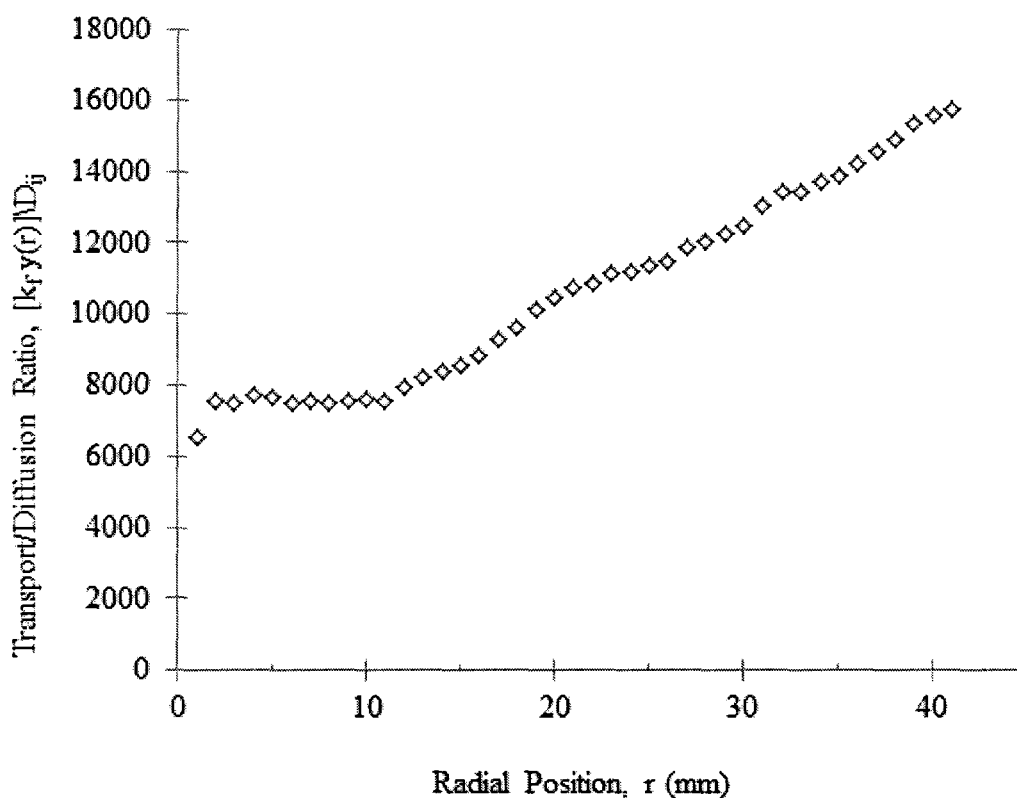


Figure 41 Ratio of localized mass transport of NO to NO diffusion constant, from 7s-14s of the original video, “Run 1”

The enhanced mass transport from convective forces was another potential difference between the swirl experiments and previously performed microchannel experiments. In one such experiment, the centerline velocity of the microchannel was about $100 \text{ mm}\cdot\text{s}^{-1}$. Taking a microchannel height of about $100 \mu\text{m}$ and assuming perfectly parabolic flow, the same localized shear stress calculations can be applied to get an estimate for transport in the microchannel using the transport model used in this

dissertation (3.8.4). The shear stress was calculated from Eq. 3-3, with viscosity values from Eq. 3-4 and Eq. 3-5, and the Schmidt number was calculated from Eq. 3-8.

$$\begin{aligned}\tau_{loc} &= \mu \frac{v(r)}{y(r)} = (7.98 \times 10^{-10} \text{ N s mm}^{-2}) \frac{100 \text{ mm s}^{-1}}{0.05 \text{ mm}} \\ &= 15.96 \text{ dynes cm}^{-2}\end{aligned}\quad \text{Eq. 4-1}$$

$$Re = \frac{v(r)y(r)}{\nu} = \frac{(100 \text{ mm s}^{-1})(0.05 \text{ mm})}{0.801 \text{ mm}^2 \text{ s}^{-1}} = 6.24 \quad \text{Eq. 4-2}$$

$$\begin{aligned}k_{f\text{microch}} &= \frac{3.63 \text{ mm}^2 \text{ s}^{-1}}{y(r)} Re^{\frac{1}{2}} = \frac{3.63 \text{ mm}^2 \text{ s}^{-1}}{0.05 \text{ mm}} (6.24)^{\frac{1}{2}} \\ &= 181.4 \text{ mm s}^{-1}\end{aligned}\quad \text{Eq. 4-3}$$

The shear stress from Eq. 4-1 matches the physiological condition of 15 dynes cm^{-2} well. The Reynolds number was low, again matching the laminar, low velocity conditions in the microchannels. Applying the same assumptions for the microchannel model as for the local transport model in the swirl flow generates a local transport about 10 times greater in the microchannels than in the swirl flow.

4.3 Flow Cytometry

4.3.1 Overview

Flow cytometry results are shown for PRP samples from two of the experimental days. The complete data can be found in the supplemental digital materials, detailed in APPENDIX B.

The results are shown for each of six test wells, along green and red excitation fluorescence. The platelets were stained with AO. The high counts in blue-excited fluorescence serve as a further indicator that FITC-fibrinogen staining cannot be used as a way of establishing background distribution relative to platelets, as platelets can interact

with AO in such a way that the binding can provide green emission spectra [52] In fact, the flow cytometry results consistently show much higher event counts under blue excitation fluorescence than under green excitation fluorescence, about 4-5 times the blue excitation events than the green excitation events. This result was contrary to what was unexpected, but does serve to invalidate the use of FITC-fibrinogen staining in conjunction with AO-stained platelets.

For all the flow cytometry results shown, wells 1, 2, and 3 (Figure 43 and Figure 45) show the low dilution condition, and wells 4, 5, and 6 (Figure 44 and Figure 46) show the high dilution condition. The high dilution condition was twice as dilute as the low-dilution case. The total events in the high dilution cases were roughly double those from the low dilution case, as shown in Figure 42.

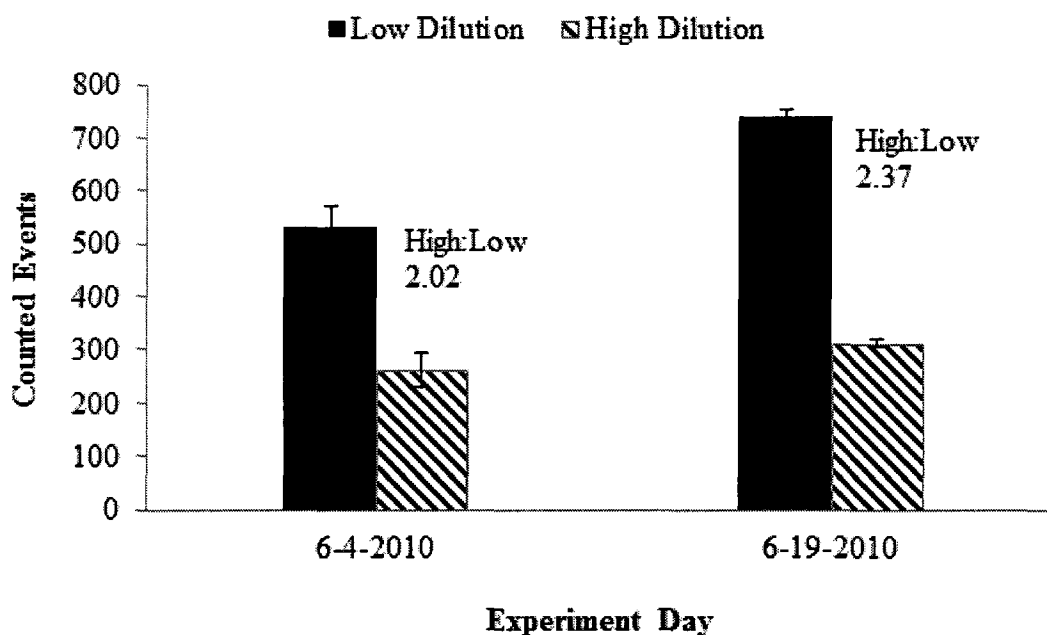


Figure 42 Flow cytometry results summary on the two reported days, showing the total number of reported events for high and low dilution, and the ratio between the two dilutions for each day

The Bioanalyzer may have a limited ability to count platelets. The manufacturer, Agilent, does not have protocols established for platelet cytometry, so these tests were an initial measure of functionality. d-PRP was approximately 22 mL PBS to 28 mL PRP. Normal bovine platelet counts can range from 200,000-550,000/ μL [67]. The expected platelet counts from the dilutions were calculated from the description in (§3.6.3) as follows, for a sample platelet count of 240,000:

After dilution of PRP into d-PRP, the new platelet concentration was:

$$240,000 \mu\text{L}^{-1} \times \frac{28 \text{ mL}}{50 \text{ mL}} = 134,400 \mu\text{L}^{-1} \quad \text{Eq. 4-4}$$

After the d-PRP was mixed with AO in a 1:1 ratio, the platelet concentration became:

$$134,400 \mu\text{L}^{-1} \times 0.5 = 67,200 \mu\text{L}^{-1} \quad \text{Eq. 4-5}$$

This stained mixture was added to two concentrations of cell buffer, at a ratio of 3 μL d-PRP to 300 μL cell buffer for the high concentration and 3 μL d-PRP to 600 μL cell buffer for the low concentration. The expected counts were therefore:

$$67,200 \mu\text{L}^{-1} \times \frac{3}{300} = 672 \mu\text{L}^{-1} \quad \text{Eq. 4-6}$$

$$\text{and } 67,200 \mu\text{L}^{-1} \times \frac{3}{600} = 336 \mu\text{L}^{-1}$$

The limiting cases were 560/ μL -1540/ μL for the 200,000-550,000/ μL normal platelet counts reported above. At first glance, these platelet counts seem to agree with the flow cytometry results. However, because the flow cytometer count was for all events in a 10 μL well, they represent platelet counts that were an order of magnitude smaller than normal bovine platelet counts.

4.3.2 Histograms of Platelet Count vs. Fluorescent Intensity

The individual sample well histograms for the two test days are shown in the following figures. The summary graph in Figure 42 was a combination of all fluorescence events detected by the Bioanalyzer for a single test well, while the histograms represent the number of events counted in each test well (“Samples”, rows), separated by blue fluorescence (left column) and red fluorescence (right column).

Figure 43 and Figure 44 show the six test wells for the PRP processed for the “6-4-2010 d-LbL” experiment. The histograms show peak values that roughly match the expected 2:1 blue:red ratio seen in Figure 42. Figure 43 shows the histograms for the high concentration PRP wells, and Figure 44 shows the low concentration PRP wells.

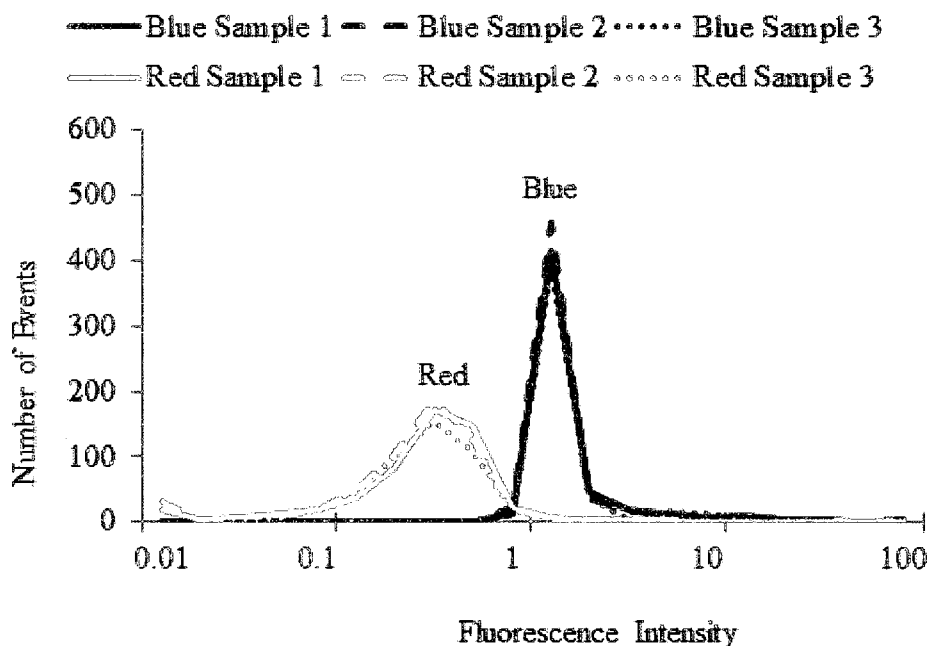


Figure 43 Sample wells 1-3 for the high-concentration stained PRP suspension, 2X the diluted concentration in wells 4-6, 6-2-2010 experiment

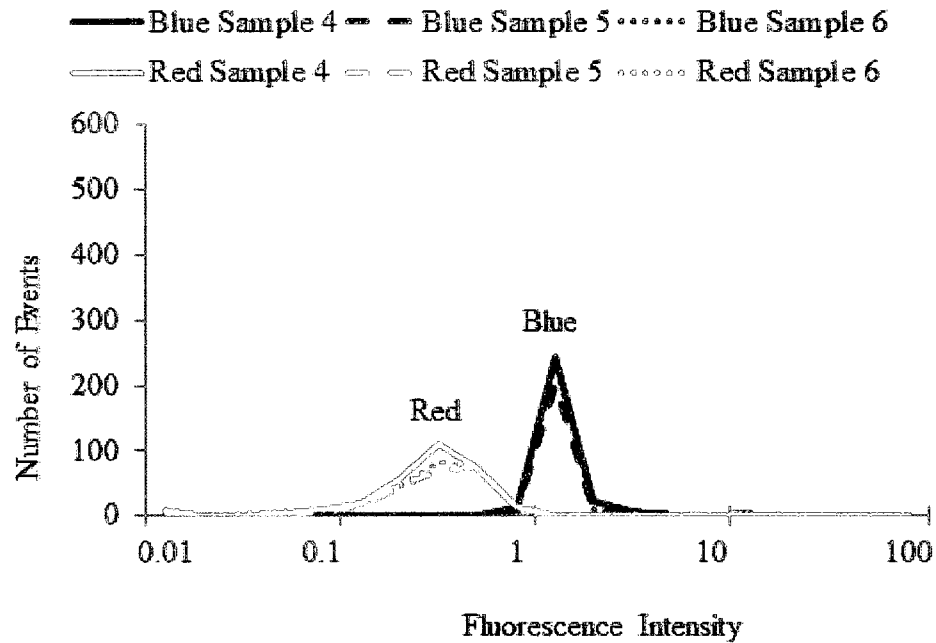


Figure 44 Sample wells 4-6 for the low-concentration stained PRP suspension, 0.5X the diluted concentration in wells 1-3, 6-2-2010 experiment

Figure 45 and Figure 46 show the six test wells for the PRP processed for the “6-19-2010 and 6-21-2010 d-LbL” experiments. The histograms show peak values that roughly match the expected 2:1 blue:red ratio seen in Figure 42. Figure 45 shows the histograms for the high concentration PRP wells, and Figure 46 shows the low concentration PRP wells.

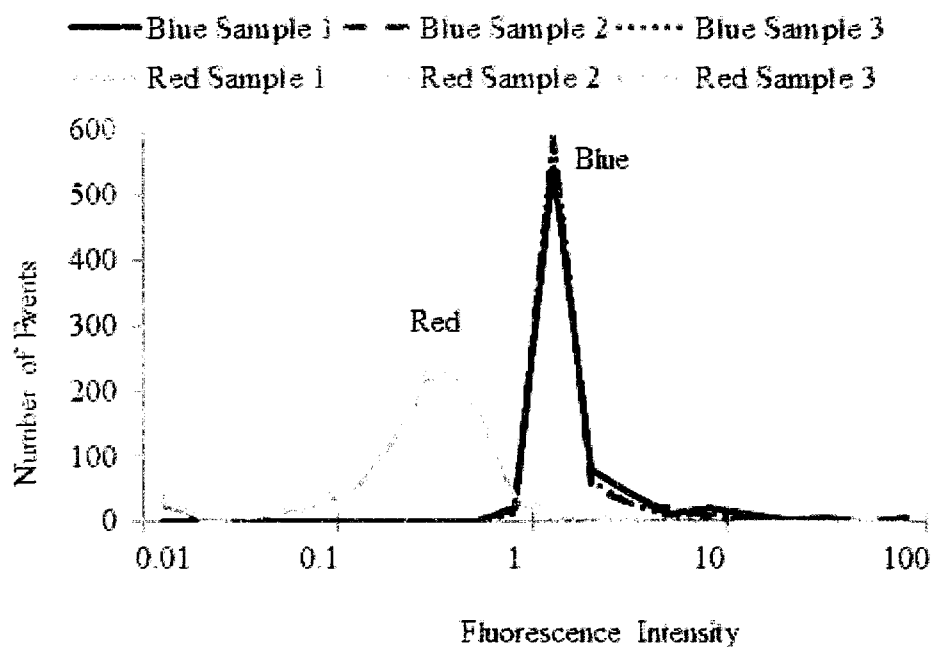


Figure 45 Sample wells 1-3 for the high-concentration stained PRP suspension, 2X the diluted concentration in wells 4-6, 6-16-2010 experiment

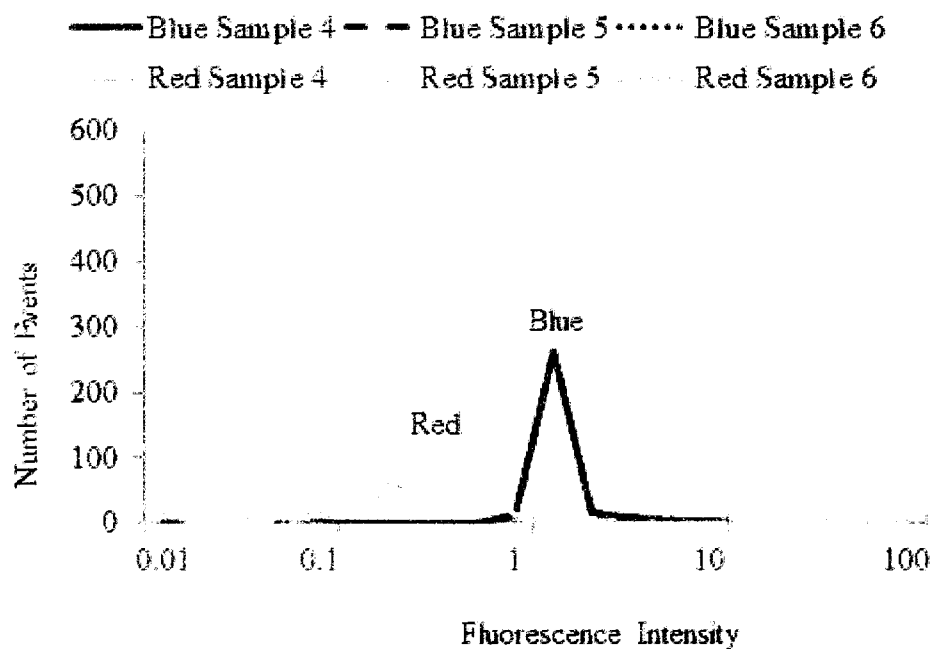


Figure 46 Sample wells 4-6 for the low-concentration stained PRP suspension, 0.5X the diluted concentration in wells 1-3, 6-16-2010 experiment

4.4 s-LbL Results

To test whether d-LbL surfaces provided an unambiguous identification of stained cellular material (Hypothesis 1, §1.5.1), a negative control had to be established. s-LbL surfaces were tested, and found to retain AO on the surface, even in the absence of platelets (§4.4.3.1). Because s-LbL surfaces were the previous standard biointerface for platelet adhesion studies in our laboratory, a set of control experiments was performed following the same conditions as the subsequent d-LbL experiments. These surfaces were then compared against the d-LbL surfaces to complete testing of Hypothesis 1.

The most common form of processed image results was the image montages. The image processing program generated these montages automatically at the end of set of images processed. A montage allows for a rapid visualization of every image that comprised a set, making qualitative examinations easier.

Figure 47 shows one of these montages, generated from the original TRITC fluorescence microscopy of AO stained surfaces/platelets. Once image processing occurred, the images had black and white thresholded counterparts, seen in Figure 48. Only the areas that were considered good candidates for platelet accumulation as indicated by AO fluorescence concentrations were highlighted as data in the black-and-white (B/W) image. To make these images easier to print and copy, a negative of the black-and-white images (W/B) was generated, shown in Figure 49. For all of the results, the negative image (Figure 49) is the one displayed. One limitation of the MATLAB montage function was that the B/W and original color montages were not necessarily arranged in the same order. While the montages accurately include each of the images for a given microscopy set, they do not necessarily do so in the same grid layout on the

montage. This limitation was merely cosmetic, as the statistics and percent area calculations were performed on an image-by-image basis, and not on the montages. The montage images should be considered data summaries with respect to imaging data. The W/B images directly match their B/W counterparts because this negative image process was performed outside of the MATLAB program using IrfanView to generate the cosmetic “printable” W/B form of the images.



Figure 47 A sample montage image, in original color. AO fluorescence of adhered platelets on a d-LbL fibrinogen surface, with no L-a under high-shear dynamic flow



Figure 48 The black and white (B/W) of the color montage in Figure 47

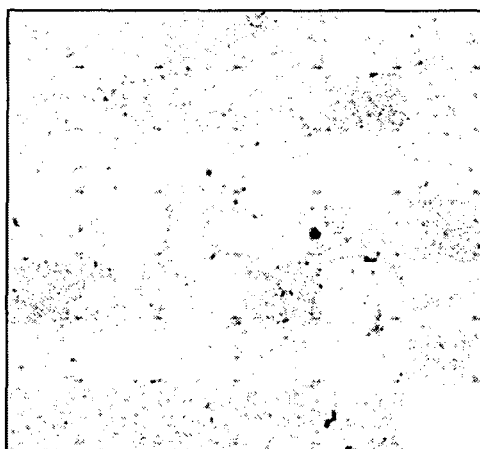


Figure 49 The negative black and white (W/B) montage of Figure 47

4.4.1 Static and Dynamic Flow Conditions

Experiments were performed in which s-LbL surfaces were exposed to PRP without flow (static exposure to PRP condition). The montages of the FM images for the static exposure to PRP condition are shown in Figure 50. The sub-figures A and B represent the adhesion results without and with 20 μM L-a, respectively. The 20 μM L-a condition appears to show visibly lower adhesion. However, this trend was not supported

by the means and standard deviations calculated by the MATLAB program for both the static slides averaged together for that experiment day.

The numbers on each figure indicate the mean coverage \pm standard deviation in percent of total surface area, excluding outlier images. Image outliers were automatically excluded by the image processing program. An outlier was defined as an image whose percent coverage mean value was more than three standard deviations away from the mean for the folder's entire image set. The same numbering convention was followed for all subsequent montage images.

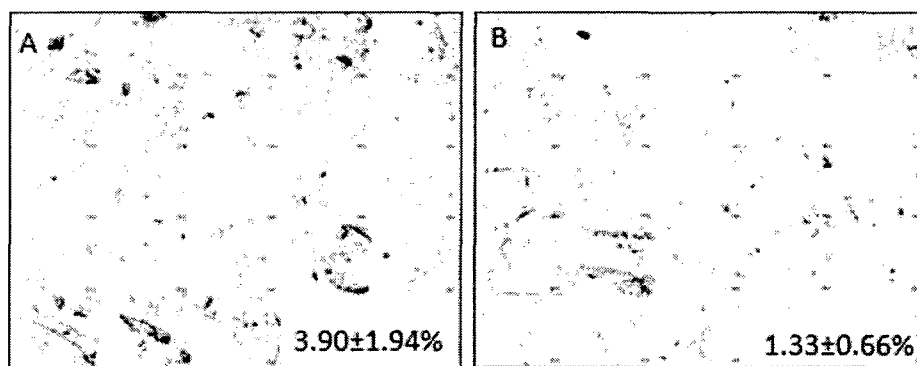


Figure 50 s-LbL static exposure to PRP condition, montage of all thresholded negative black and white (W/B) images for experiment “3-31-2010 Static-Dynamic”.
A: no chemical additive, B: chemical additive, 20 μ M L-a

Experiments were performed in which the s-LbL surfaces were exposed to PRP under dynamic flow conditions. These montages are shown in Figure 51, with increasing shear from top to bottom, no chemical additive on the left column and chemical additive, 20 μ M L-a, on the right column. A visual inspection suggests that the percent surface coverage increases with increased shear rate for both chemical additive conditions, while the addition of chemical additive appears to reduce coverage with respect to the no chemical additive condition only at the high shear region.

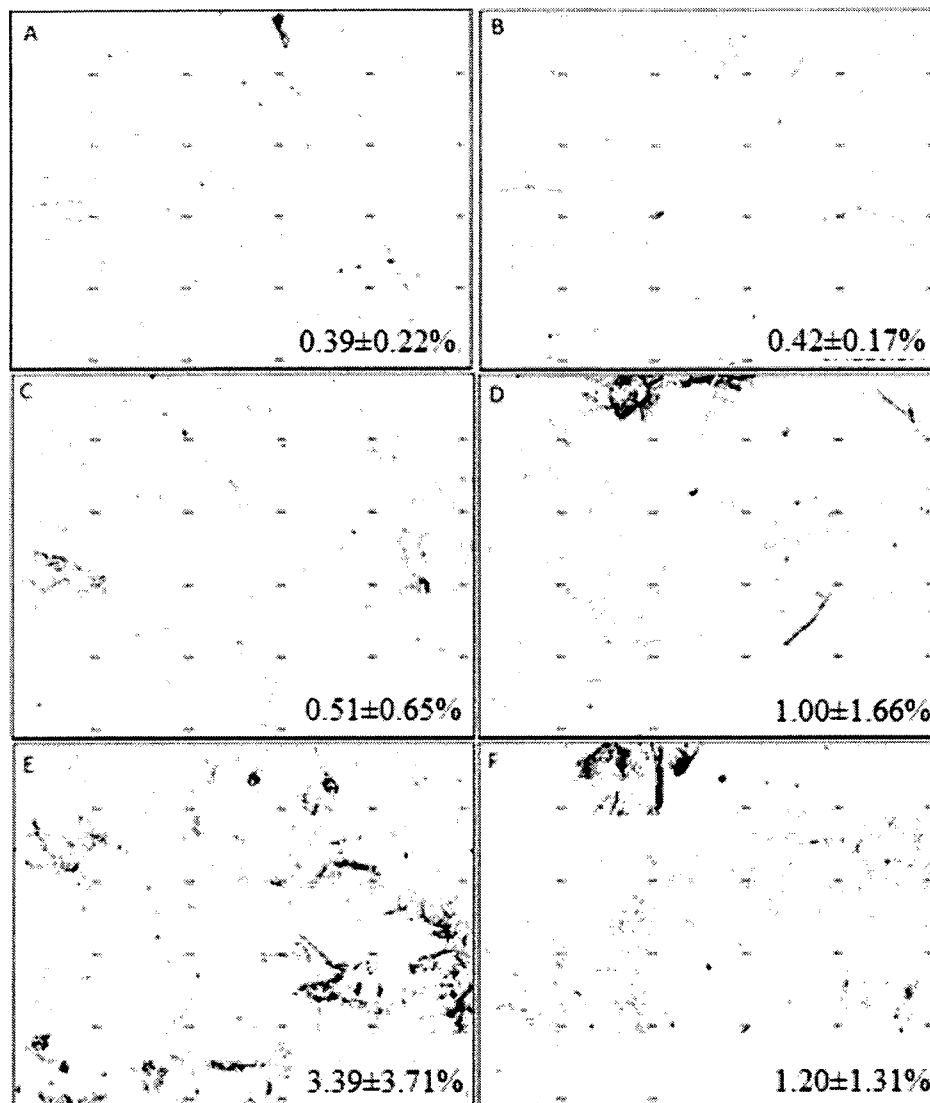


Figure 51 s-LbL dynamic flow condition, montages of all thresholded negative black and white (W/B) images for experiment “3-31-2010 Static-Dynamic”. A, C, and E: no chemical additive; B, D, and F: 20 μ M L-a. A, B: low shear; C, D: mid shear; E, F: high shear

4.4.2 s-LbL Percent Surface Area Coverage Summary

The image processing program was used to calculate the percent surface area coverage on s-LbL for each of the constituent images for the data set (§3.4.5.4). The program automatically excluded results where the value of an individual image was greater than three standard deviations outside of the mean for the whole sub-group

(outliers). “Sub-groups” are the subdivisions such as “Dynamic 0 μ M Low” for Figure 52. The montages of the images that the image processing software used to generate Figure 52 are found in §4.4.1.

While this graph shows the expected trends, namely increased adhesion with increased shear stress, lower adhesion with the presence of L-a, and no difference between the chemical additive and no chemical additive condition for static exposure to PRP, further tests showed these results to be unreliable (Red-Green tests, §4.4.3).

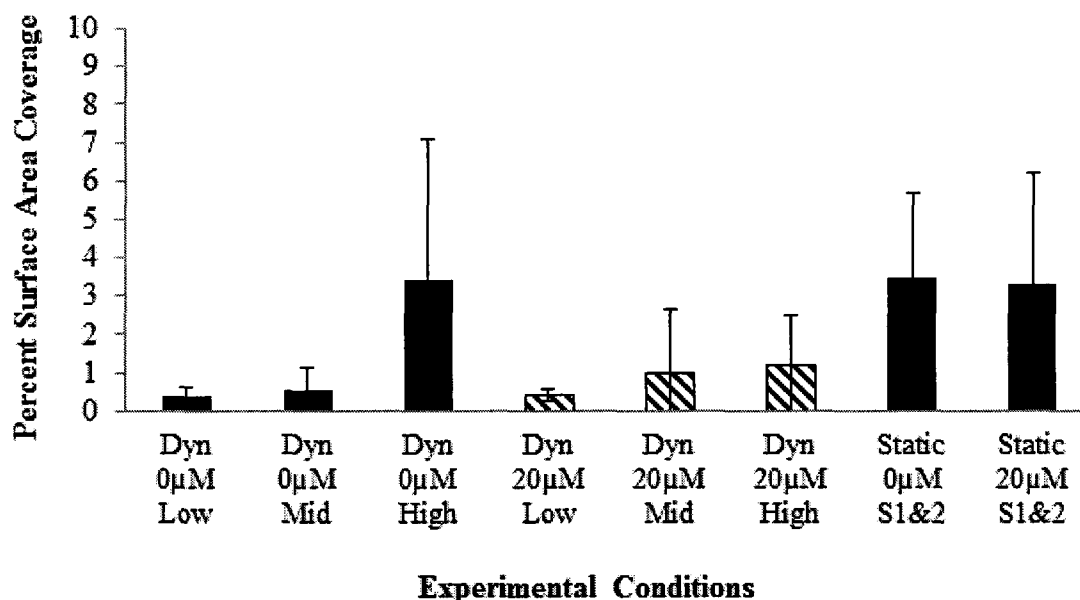


Figure 52 s-LbL experiment results for the “3-31-2010” experiment set

4.4.3 Red-Green Comparisons

The experiments in this section provided the control case against which Hypothesis 1 was tested (§1.5.1). These tests explored the following control conditions, all stained with AO and imaged with FM: 1) s-LbL slides not exposed to PRP (§4.4.3.1), to test for anomalous retaining of AO by the surface – AO stain not associated with platelet adhesion, 2) plain glass slides exposed to d-PRP (§4.4.3.2), to establish a baseline

for platelet accumulation morphology independent of the biointerface, and 3) s-LbL slides exposed to the same test conditions as d-LbL (§3.3.4), to serve as a negative control.

4.4.3.1 *s-LbL no PRP*

Figure 53 is a sample image of an s-LbL surface stained with AO. A large quantity of AO was retained by the surface, though no cellular material was present. This image, and others collected in the same manner, indicated that s-LbL was unreliable for platelet adhesion studies when using FM images as the quantifying assay.

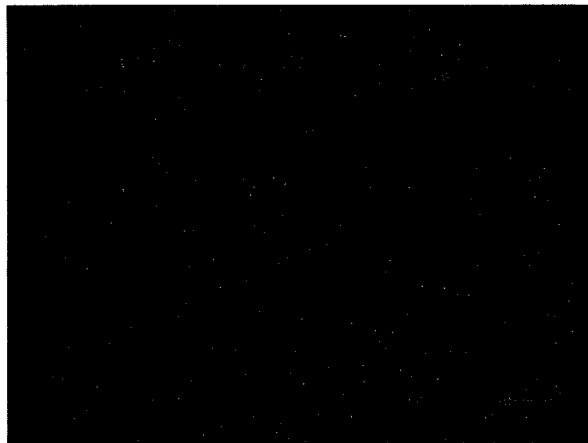


Figure 53 s-LbL static exposure to PRP condition, PBS with no d-PRP, stained with AO. Result shown from the “3-19-2010 Static-Dynamic” experiment data set. There was retention of AO stain on the LbL surface in the absence of platelets

Figure 54 shows the montage of processed images for the s-LbL, no d-PRP, and static exposure to PRP condition. The area that the processing identifies as surface coverage through thresholding was comparable to the surface coverage identified from s-LbL surfaces exposed to PRP under static exposure to PRP conditions in §4.4.1. For all montage images, the lower right-hand corner number of each montage is the calculated percent surface coverage.

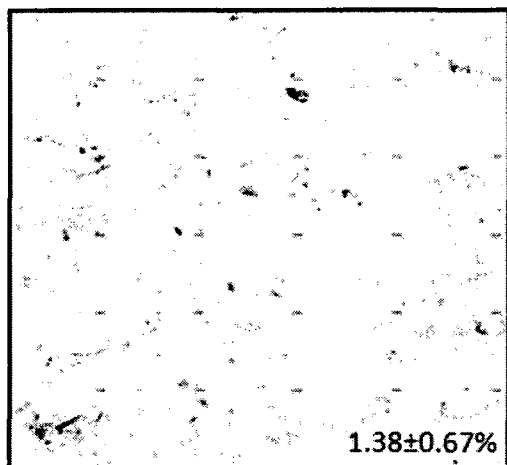


Figure 54 s-LbL static exposure to PRP condition, PBS with no d-PRP, stained with AO, montage of all W/B images for the “3-19-2010 Static-Dynamic” data set

Figure 55 shows montages from experiments in which the s-LbL surfaces were exposed to PBS, without PRP, under dynamic flow conditions. Shear rate increases from the top row to the bottom row. The left column of images is from experiments with no chemical additive, and the right column is from experiments with 20 μM L-a. A visual inspection suggests that the presumed percent surface coverage, though high, does not necessarily increase with increasing shear, while the addition of chemical additive appears to reduce coverage with respect to the no chemical additive condition.

The results were further indication that anomalous retention of AO by the s-LbL surface provides false positives for platelet adhesion, which renders s-LbL platelet percent area coverage unreliable from FM images and indicates the need for an improved surface for platelet adhesion studies.

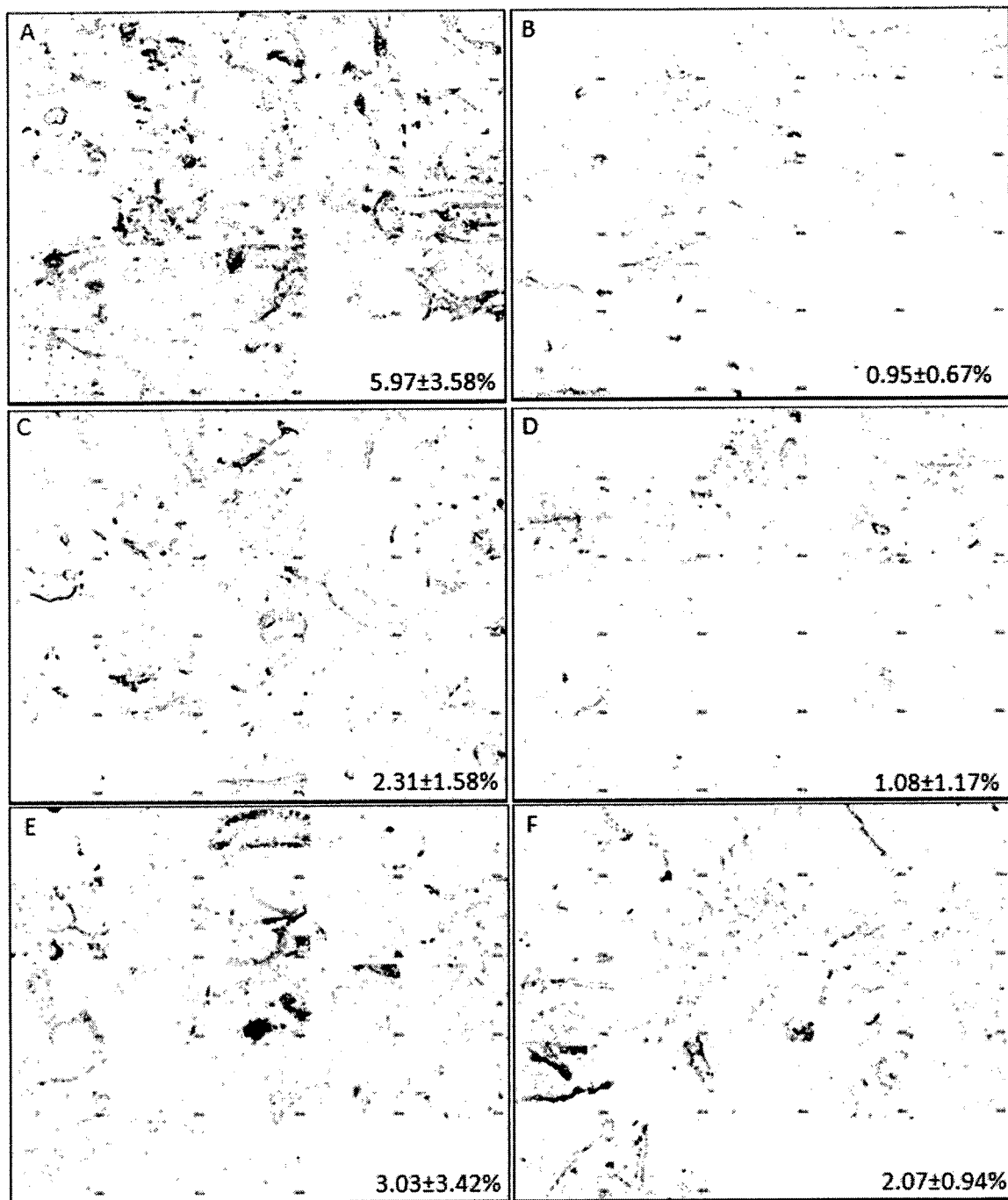


Figure 55 s-LbL Dynamic flow condition, PBS with no d-PRP, stained with AO, montage of all images for the “3-19-2010 Static-Dynamic” experiment data set. A, C, and E: no chemical additive; B, D, and F: chemical additive, 20 μ M L-a. A, B: low shear; C, D: mid shear; E, F: high shear.

The calculated percent surface coverage for these PBS studies is summarized in Figure 56. The percentages are similar to values obtained in experiments for which the surface was exposed to PRP. Furthermore, trends exist, such as the increase in surface coverage with shear for the L-a case and the decrease in percent surface coverage with added L-a in all of the dynamic TRITC cases. These trends could be incorrectly interpreted as shear-dependent and L-a dependent platelet adhesion.

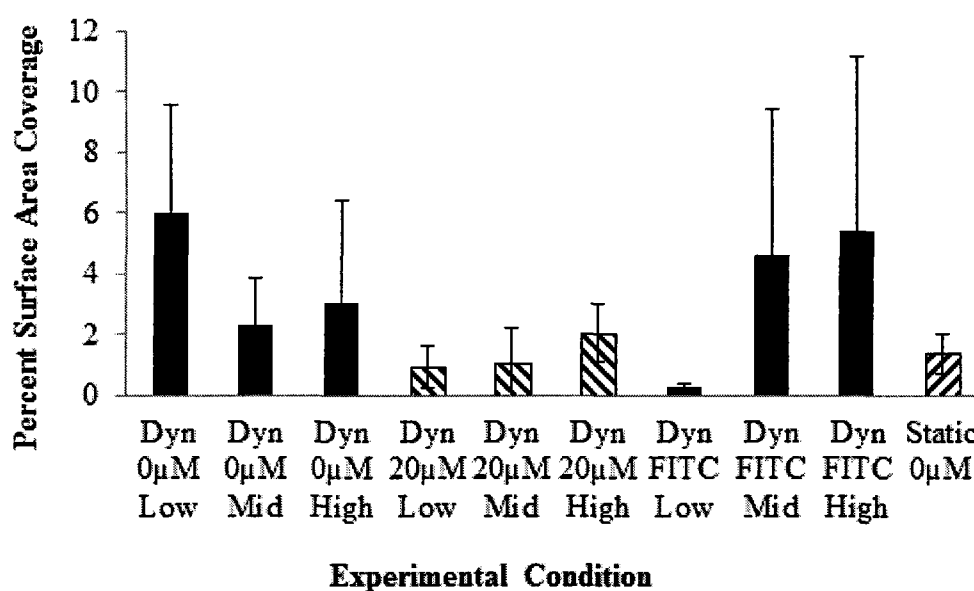


Figure 56 s-LbL with PBS (no d-PRP) percent surface area coverage in static and dynamic flow conditions, with and without chemical additive in the dynamic condition, stained with AO and imaged in both FITC and TRITC

4.4.3.2 Plain glass slides with PRP

Figure 57 shows the montage for d-PRP exposed to plain glass slides. The glass served as a platelet activator, with a smooth surface free of the LbL surface morphology characteristics.



Figure 57 d-PRP on plain glass slide from the “3-31-2010 Static-Dynamic” experimental set, montage of set “Static Plain 0uM...”

Figure 58 shows A: the AO-stained aggregation image from one of the d-LbL experiments, and B: a result from Tsai et al. [68] which shows platelet aggregation in a microfluidic environment on the microfluidic tubing walls. The morphology of the bright AO fluorescence areas from d-LbL was much closer to that shown from the plain glass slides (Figure 57) and the Tsai et al. work than the morphology shown in s-LbL results. It is important to note that in the Tsai et al. work the globules shown are about 2-5 μm , likely representing individual platelets, while the results from the PBS experiments show globules that are around 5-20 μm , likely representing both individual platelets and platelet accumulations.

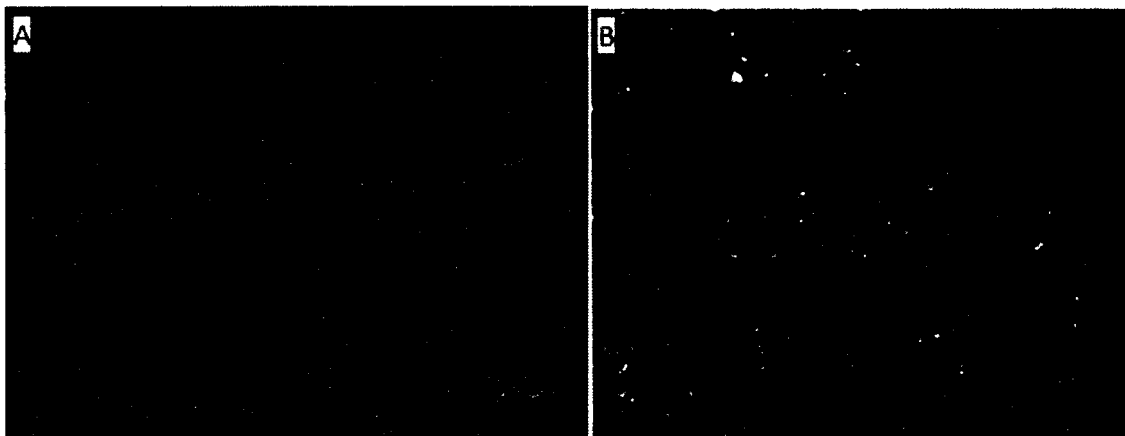


Figure 58 A: Sample d-LbL microscopy result for the high-shear, no chemical additive condition in the “6-4-2010” set. B: Sample platelet adhesion from a microfluidics device as reported by Tsai, et al. [68], with a morphology of small, mostly circular areas of adhesion

4.4.3.3 *s-LbL with PRP*

The fibrinogen surface was tagged with a FITC stain was tested as a way of correlating the distribution of fibrinogen to the distribution of platelet adhesion. The theory was that platelet adhesion might be influenced by inhomogeneity in the biointerface. Results from *s-LbL* surfaces exposed to PRP initially appeared to support this theory, with the “platelet” adhesion (red false color images) correlating well with the “fibrinogen” background (green false color images). However, further research and imaging showed that platelets themselves could fluoresce green from AO’s dual excitation/emission bands. Figure 59 is a sample montage from the static exposure to PRP condition for the experiments in this section. The images were paired, FITC and TRITC imaging, and the similarities in patterns are readily seen.



Figure 59 s-LbL static exposure to PRP condition, FITC-fibrinogen and AO-platelet staining, images taken in FITC/TRITC filter pairs

A sample image pair is shown in Figure 60. The *falseColor_FINAL.m* program (APPENDIX A) was used to turn these images into false-color red and green images, and then superimpose them to a composite. A sample composite image can be found in Figure 61, made by summing the images in Figure 60. The areas in yellow indicate regions where the two false color images have overlapping regions.

4.4.3.3.1 Static condition

Sample red/green pseudocolor images from the static condition are shown in Figure 60, along with their superposition composite of the red/green pseudocolor images in Figure 61.

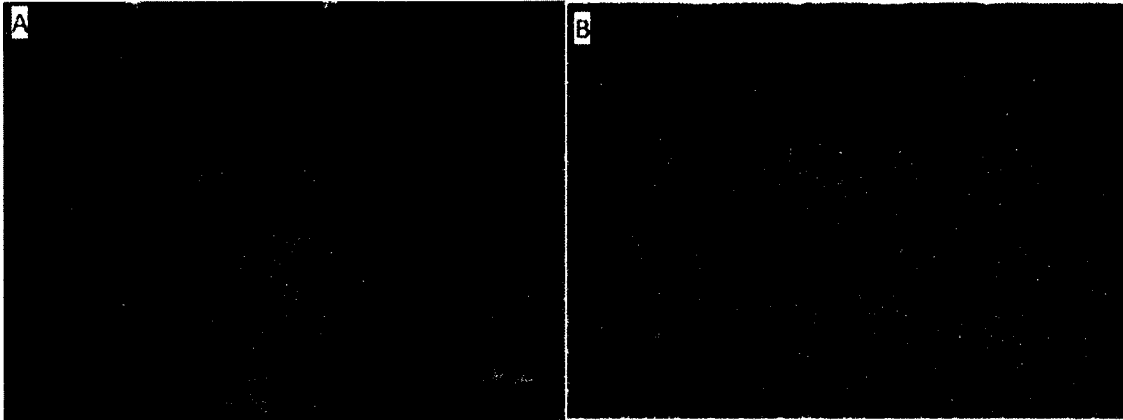


Figure 60 A: One false-color red image (fc-red-image008) generated by thresholding the TRITC filtered AO fluorescence results, and then mapping the thresholded areas to the RGB Red [1,0,0]. B: Corresponding false-color green image (fc-green-image007) generated by thresholding the FITC filtered FITC-fibrinogen fluorescence results, and then mapping the thresholded areas to the RGB Green [01,0]

The superposition, shown in Figure 61, was adequately aligned because the scale bar and text are yellow. The rest of the images show similar patterns of overlap.

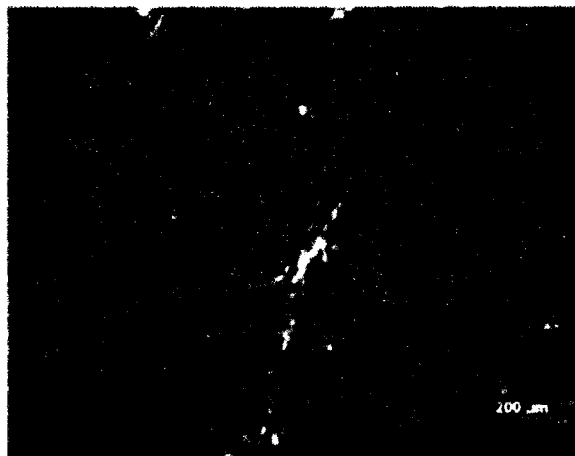


Figure 61 The superposition of the two false color images in Figure 60. The summed image produces RGB Yellow [1,1,0] in areas where the thresholded areas overlap

4.4.3.3.2 Dynamic condition

The tests described in the previous section were repeated on a dynamic condition. At the time of these experiments, the unreliability of the s-LbL processes had not been established yet, so the additional supplementary data shown in APPENDIX B were performed when still attempting to validate the previously used protocols.

Figure 62, A, B, and C each show a sample composite image from the three shear regions Low-1, Mid-2, and High-3 of a dynamic test, with no chemical additive, in the “3-24-2010 FITC-AO” experiment. As with the static condition experiments, these images show strong overlap of red (presumed platelets) on green (presumed fibrinogen). This overlap was expected, and was intended as a further morphology metric during future tests. However, the ability of AO to fluoresce green alongside the FITC-tagged fibrinogen, prevented unambiguous AO-FITC discrimination, and the tests were not made standard.

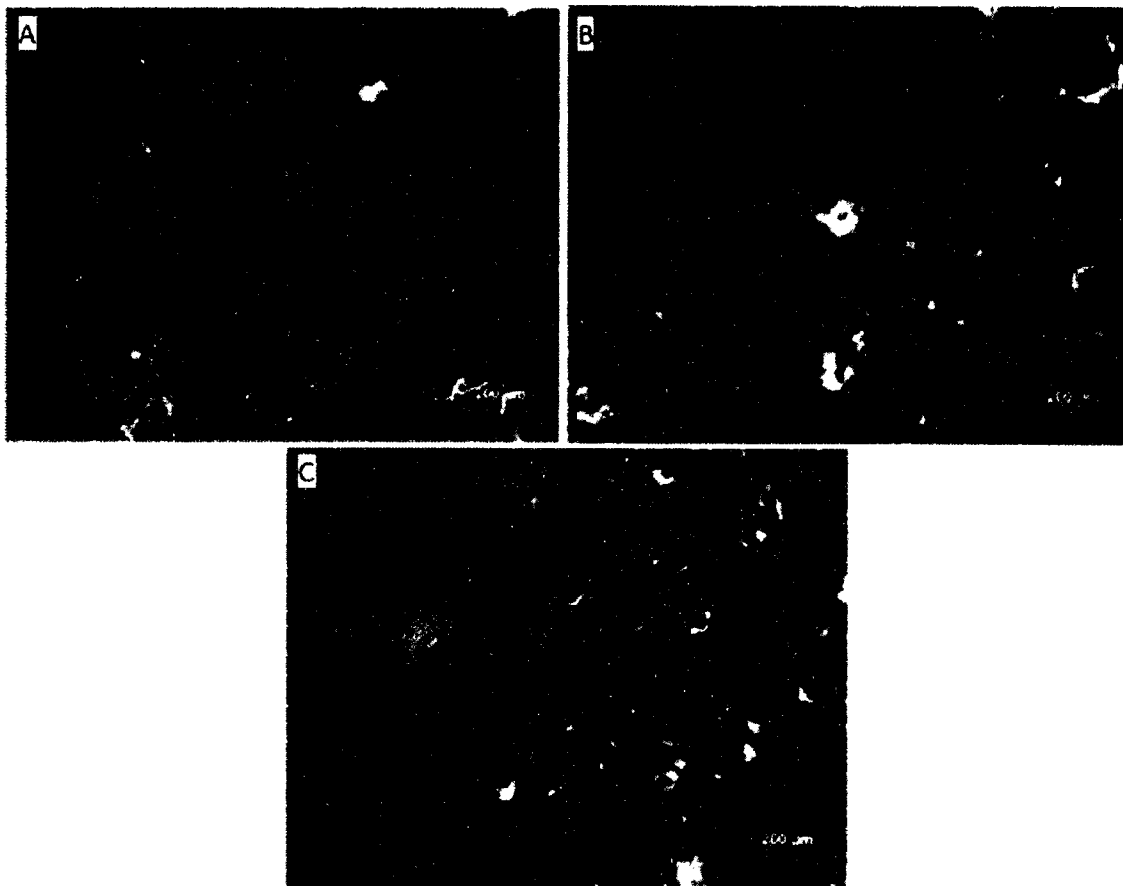


Figure 62 The superposition of the two false color images from the dynamic, no chemical additive condition. A: Low-shear region, B: Mid-shear region, C: High shear region

4.5 d-LbL Results

The new d-LbL surface was tested with fibrinogen in multiple experiments (§4.5.1), and collagen in a control experiment (§4.5.2). The d-LbL results were used to test all four hypotheses. The dynamic flow condition, when imaged across three shear regions on the slides, tested whether platelet adhesion depended on shear stress, as addressed by Hypothesis 2 (§1.5.2). Additional dynamic flow condition experiments with added L-a at a concentration of 20 μM tested whether platelet adhesion depended on this NO precursor under dynamic conditions, as addressed by Hypothesis 3 (§1.5.3). Lower

platelet adhesion was expected with the chemical additive condition, with an increasing percent change as a function of increase shear. Finally, additional static exposure to PRP experiments, with and without the platelet chemical additive L-a, tested whether potential platelet adhesion, indicated by fluorescence surface coverage, depended on this NO precursor under static conditions, as addressed by Hypothesis 4 (§1.5.4). If L-a activity was significant under static conditions, it should reduce the amount of platelet adhesion in a manner similar to dynamic flow conditions.

4.5.1 PRP Exposure to d-LbL Fibrinogen

Experiments were performed in which d-LbL surfaces with fibrinogen biointerfaces were exposed to PRP without flow (static exposure to PRP condition). The montages of the FM images for the static exposure to PRP condition are shown in Figure 63. The sub-figures A and B represent the adhesion results without and with 20 μM L-a, respectively. The 20 μM L-a condition showed visibly higher adhesion; this was supported by the means and standard deviations calculated by the MATLAB program.

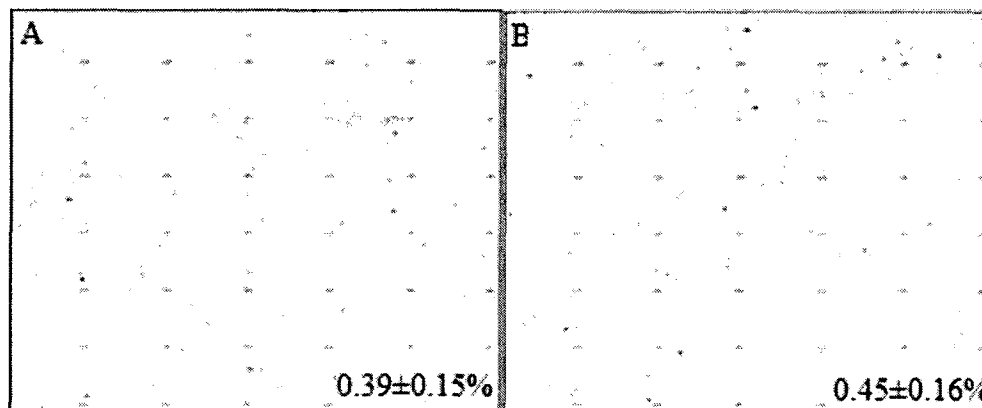


Figure 63 Montages of d-LbL surfaces exposed to d-PRP under static conditions, and stained with AO. A: no chemical additive; B: 20 μM L-a. “5-17-2010 dLbL” data

Figure 64 shows montages for the dynamic flow condition, with rows representing different shear rates (Low/Mid/High) and columns representing no L-a and 20 μ M L-a. Visual inspection and calculated percent surface coverage indicate that adhesion increased with increasing shear rate and decreased with added L-a.

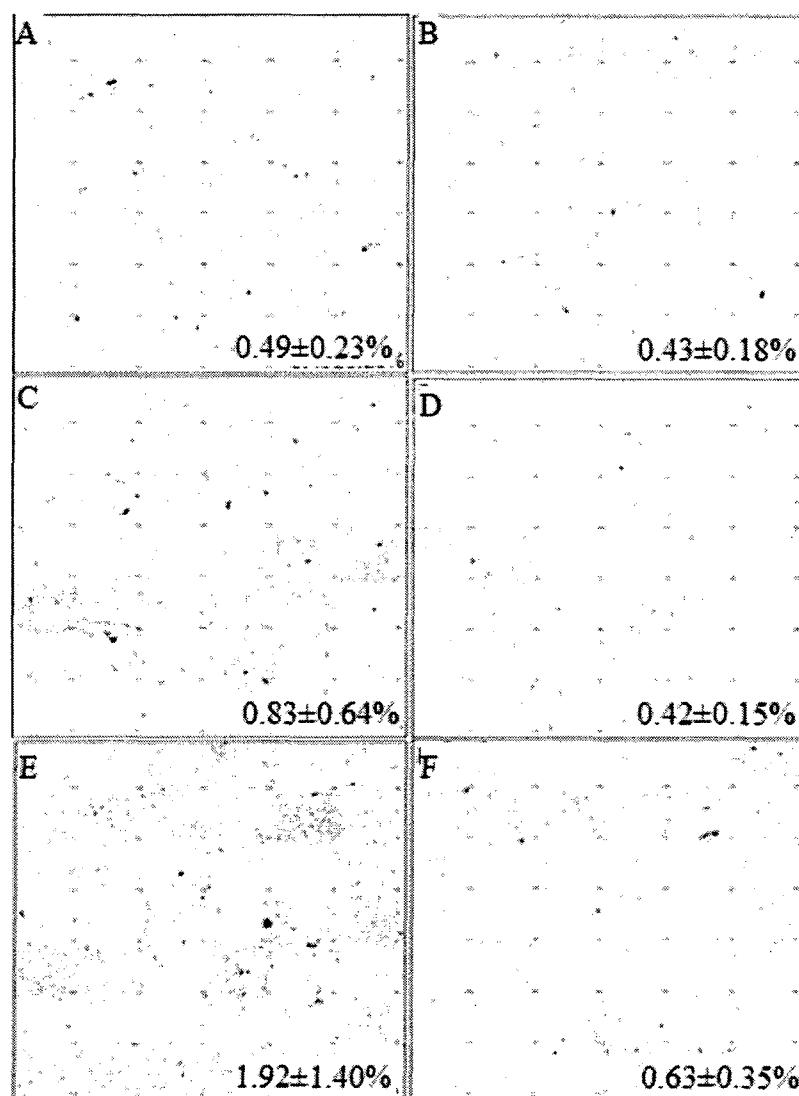


Figure 64 Montages of d-LbL surfaces exposed to d-PRP under dynamic flow conditions, and stained with AO. A, C, and E: no chemical additive; B, D, and F: chemical additive, 20 μ M L-a. A, B: low shear; C, D: mid shear; E, F: high shear. "5-17-2010 dLbL" data

4.5.2 PRP Exposure to d-LbL Collagen

Tests in which d-LbL collagen was used as the biointerface were performed as a positive control for the d-LbL fibrinogen experiments (§4.5.1). Frilot's work was performed on collagen [11], so the comparison was important to validate Hypothesis 4 (§1.5.4). For the standard deviations, collagen was limited to one control experiment, so the deviations come from the variances in the individual images.

PRP was exposed to d-LbL collagen biointerfaces. The montages of the FM images are shown in Figure 65. The left hand image was obtained with no added L-a and the right hand image was obtained with 20 μM L-a. The 20 μM L-a condition appears to show higher adhesion, but the differences between the means and standard deviations were not statistically significant. Montages of the images obtained from d-LbL collagen exposed to PRP with flow are shown in Figure 66. Images in the left column were obtained with no added L-a, and those in the right column were obtained with 20 μM L-a. Shear rate increases from the top row to the bottom row. There is a tendency for surface coverage to increase with increased shear and to decrease with added L-a.

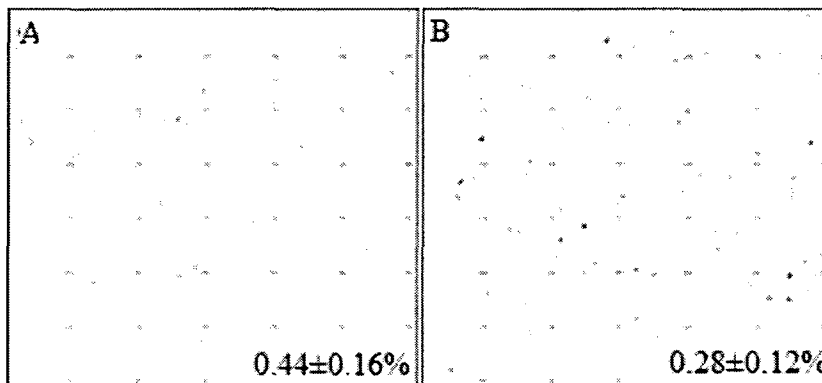


Figure 65 Montages of d-LbL surfaces exposed to d-PRP under static conditions, and stained with AO. A: no chemical additive; B: 20 μM L-a. “6-19-2010 dLbL” data

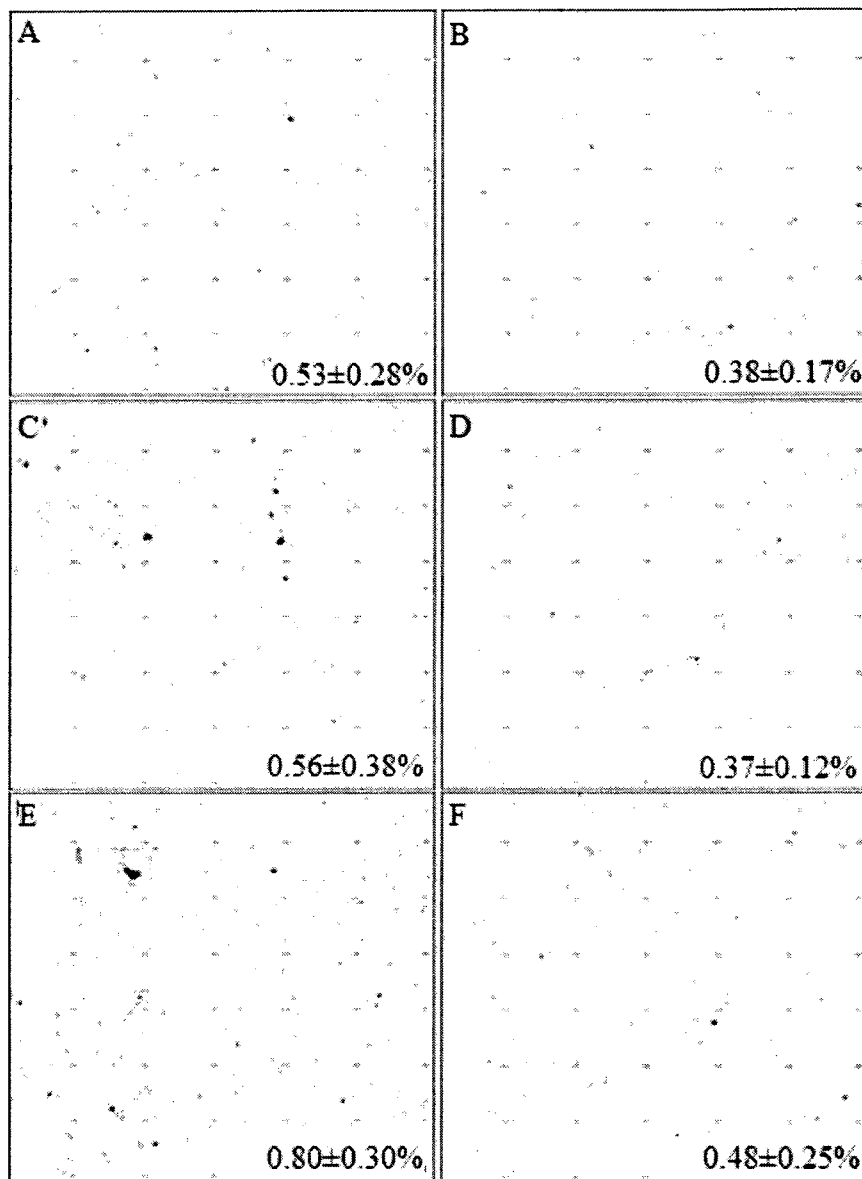


Figure 66 Montages of d-LbL surfaces exposed to d-PRP under dynamic flow conditions, and stained with AO. A, C, and E: no chemical additive; B, D, and F: chemical additive, 20 μ M L-a. A, B: low shear; C, D: mid shear; E, F: high shear. “6-21-2010 dLbL” data

4.5.3 d-LbL Percent Surface Area Coverage

The means and standard deviations of percent surface coverage on d-LbL surfaces are summarized for fibrinogen and collagen combined in Figure 67. The mean values increased with increasing shear, both with and without L-a (Hypothesis 2), they decrease

with the addition of L-a under dynamic conditions (Hypothesis 3), and they decrease with the addition of L-a under static conditions (Hypothesis 4). All of the expected results for the hypotheses appear to be met, though statistics tests (§4.6.3) were required to make final determinations.

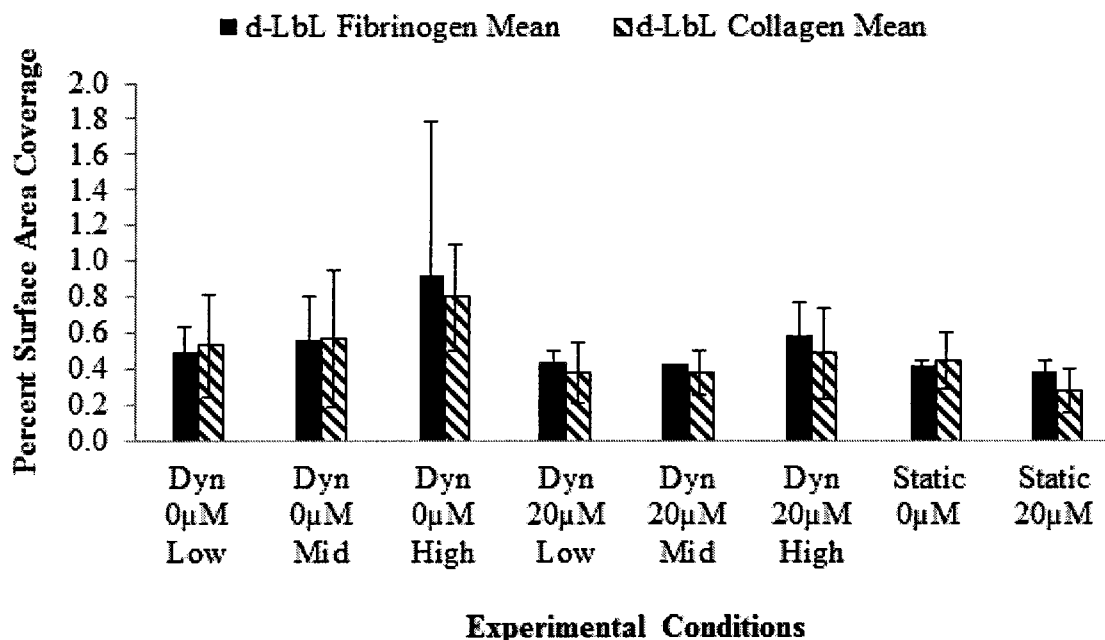


Figure 67 Percent surface area coverage data in each condition category-for the “5-17...”, “6-4...”, “6-19...”, and “6-21...” fibrinogen compared to collagen experiment results

The percent differences shown in Figure 68 further support Hypothesis 3 by showing an increasing difference in platelet adhesion with increasing shear region. The percent difference tends to increase with increasing shear rate. Only one comparison was made for the main results, so no standard deviations exist.

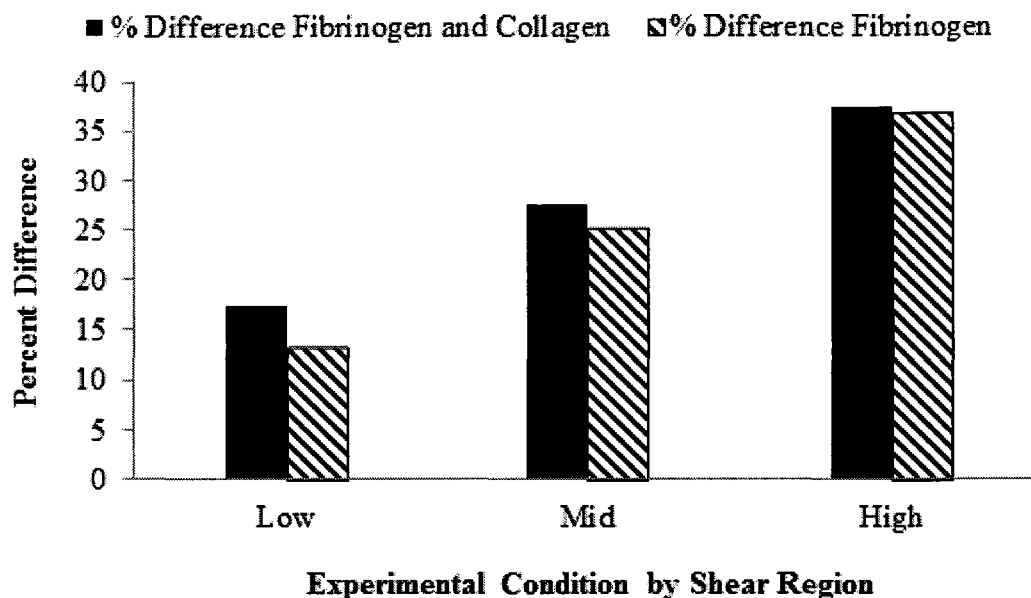


Figure 68 Percent differences between the control (0 μM L-a) and the experimental (20 μM L-a) chemical additive conditions at different shear rates

4.6 s-LbL and d-LbL: Comparisons and Statistics

4.6.1 FE-SEM Surface Comparisons

Representative FE-SEM images of the three studied surfaces are shown. s-LbL fibrinogen (Figure 69), d-LbL fibrinogen (Figure 70) and d-LbL Collagen (Figure 71). The structures shown in Figure 69 for s-LbL are representative of widespread structures found throughout the surface. It was possible that this rough, porous surface provided many pockets for the AO stain to be retained, even after the rinsing process. The other two surfaces, d-LbL, show a mixture of regions, with smoother areas and areas with larger structures. The d-LbL fibrinogen (Figure 70) image shows an accumulation, possibly related to a malformed LbL region that would have retained stain and been ignored in fluorescence microscopy (Figure 20). The collagen surface (Figure 71) shows evidence of fibrils that would be expected from the collagen solution preparation.

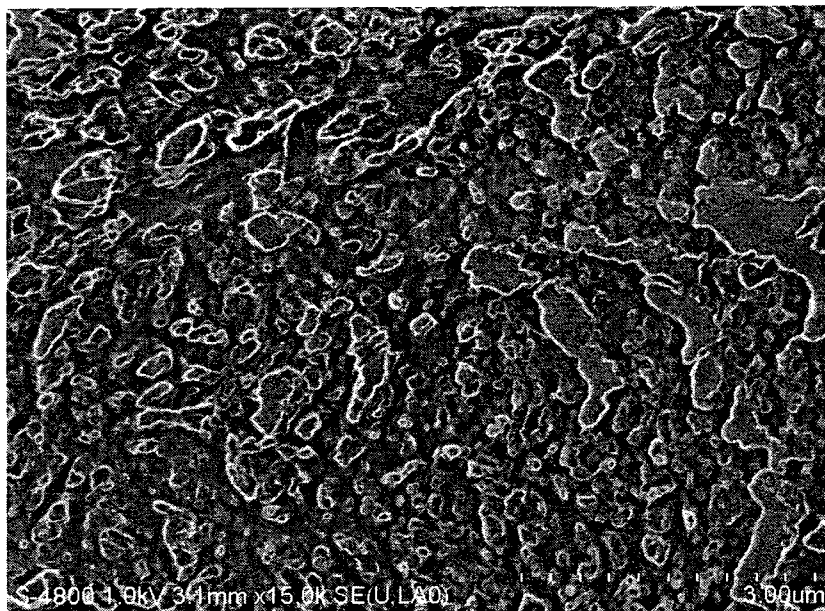


Figure 69 s-LbL, fibrinogen surface, FE-SEM image, 15.0K magnification, scale marks 3.00 μm

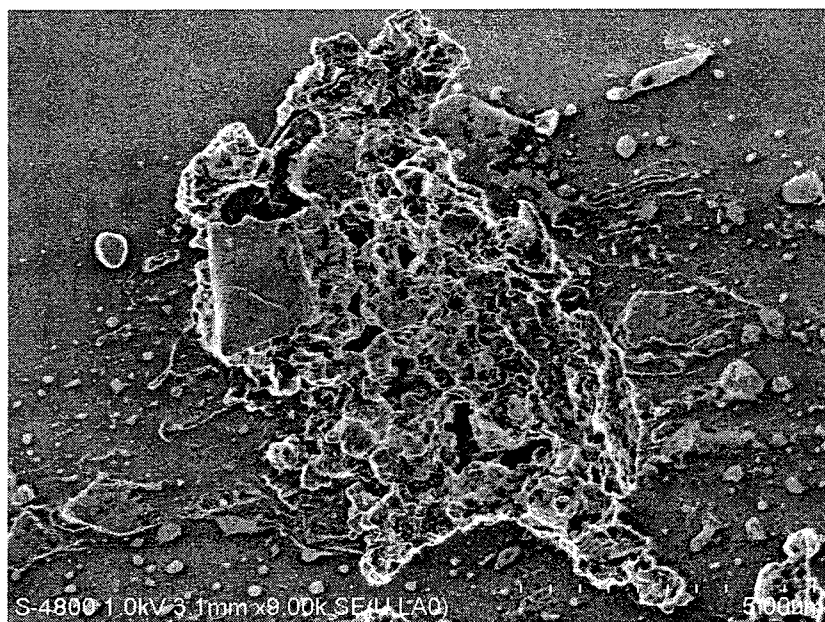


Figure 70 d-LbL, fibrinogen surface, FE-SEM image, 9.0K magnification, scale marks 5.00 μm

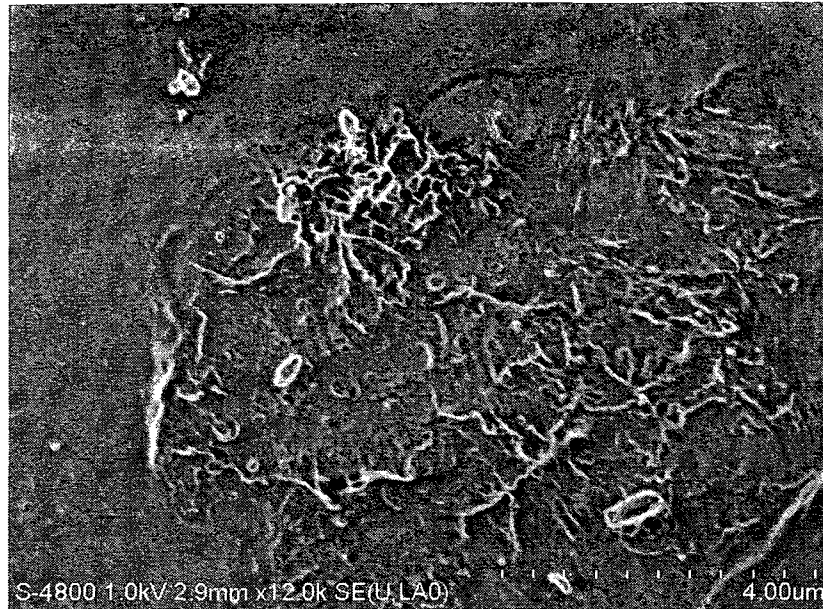


Figure 71 d-LbL, collagen surface, FE-SEM image, 12.0K magnification, , scale marks 4.00 μm

4.6.2 s-LbL to d-LbL Comparison

s-LbL and d-LbL percent surface area coverage comparisons are shown here in Figure 72. The dynamic data are the averaged results of each of the d-LbL experiments, both fibrinogen and collagen. The static data are the results of the s-LbL experiments, with the static exposure to PRP condition being the average of each of two slides from that experiment day. The standard deviations shown are the variance from experiment to experiment for the d-LbL experiments. Because s-LbL was a control day, there was only one day involved, and the variances are the variances from the individual images for that day. For the dynamic flow conditions, the differences between s-LbL and d-LbL were larger at higher shear rates. For no flow, the differences were similar to those seen with flow at the highest shear rates. The surface retention of AO by the s-LbL process was suspected to be the strongest cause of the differences between s-LbL and d-LbL.

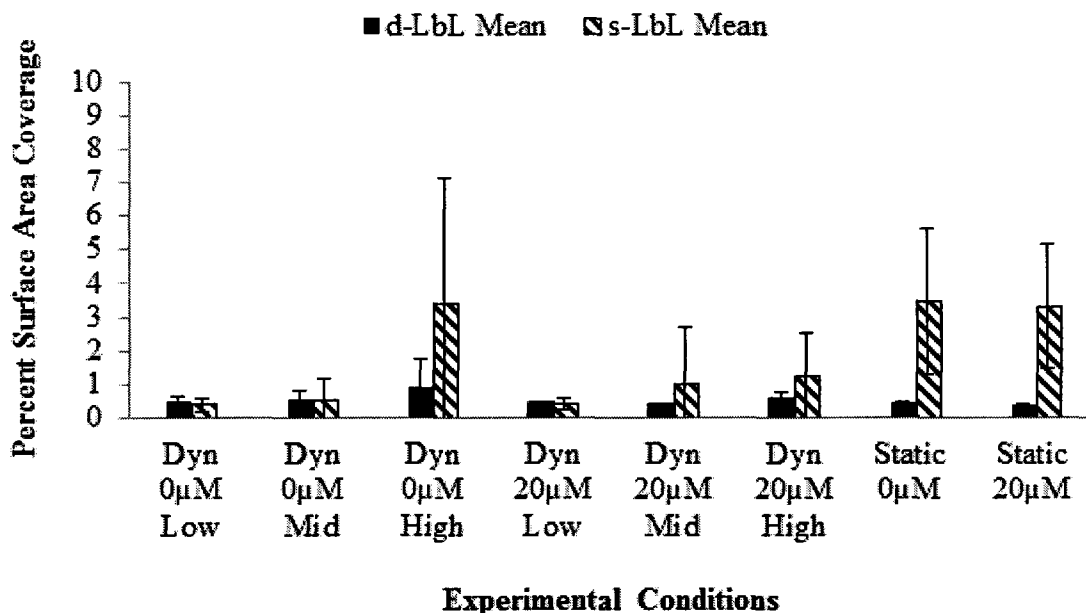


Figure 72 Percent surface area coverage in each condition category-for the “5-17...”, “6-4...”, “6-19...”, and “6-21...” fibrinogen experiment data sets only, averaged over each day’s results

4.6.3 Statistics

The statistical tests described in Table 4, Table 5, and Table 6 are shown in this section. For the t-Tests (two-tailed) and F-tests, significance was assumed for $p < 0.05$. The digital record of these tests is contained in a file, listed with the imaging files in APPENDIX B.

The statistical tests in Table 4 were used to help validate Hypothesis 1 by testing whether s-LbL and d-LbL surfaces have statistically validated differences in both mean adhesion and variance. In all test conditions, the low and mid shear regions tended to be low adhesion and harder to distinguish from one another, and it was not surprising that the s-LbL and d-LbL show no statistical differences in either mean (t-Test), variance (F-test), or both for the low and mid shear conditions (pairs 1, 2, 5, and 6). For the high shear and static conditions, the means were different from each other with a statistical

significance of 0.05. These differences, combined with the results of the s-LbL with no platelets (§4.4.3.1), and the d-PRP on plain glass slides (§4.4.3.2), lead us to conclude that d-LbL demonstrates different adhesion characteristics than s-LbL under high shear conditions, and that the observed platelet adhesion more closely resembles that of platelet accumulations on plain glass slides than on s-LbL. The p-values marked 0.00E+00 were so small that the standard statistics program did not register their actual value.

Table 7 t-Test comparisons for means and F-test comparisons for variances. Items above the 0.05 threshold are in bold

Pair #	Flow Cond.	LbL Type	Region	L-a μM	t-Test P-value	F-test P-Value
1	Dyn. Dyn.	d-LbL s-LbL	Low Low	0 0	2.30E-02	1.52E-01
2	Dyn. Dyn.	d-LbL s-LbL	Mid Mid	0 0	7.43E-01	2.14E-03
3	Dyn. Dyn.	d-LbL s-LbL	High High	0 0	3.91E-03	0.00E+00
4	Static Static	d-LbL s-LbL	N/A N/A	0 0	2.91E-12	0.00E+00
5	Dyn. Dyn.	d-LbL s-LbL	Low Low	20 20	9.67E-01	3.82E-01
6	Dyn. Dyn.	d-LbL s-LbL	Mid Mid	20 20	1.18E-01	0.00E+00
7	Dyn. Dyn.	d-LbL s-LbL	High High	20 20	3.69E-02	0.00E+00
8	Static Static	d-LbL s-LbL	N/A N/A	20 20	1.13E-08	0.00E+00

A second test of s-LbL functionality further supporting Hypothesis 1 was obtained by comparing the function of d-LbL fibrinogen biointerfaces to d-LbL collagen biointerfaces. The results for the statistical tests on the pairs listed in Table 5 are listed in Table 8.

Table 8 t-Test comparisons for means and F-test comparisons for variances. Items above the 0.05 threshold are in bold

Pair #	Flow Cond.	Bio-Interface	Region	L-a μ M	t-Test P-value	F-test P-Value
9	Dyn.	Fib.	Low	0	5.46E-01	2.14E-01
	Dyn.	Coll.	Low	0		
10	Dyn.	Fib.	Mid	0	9.46E-01	1.26E-01
	Dyn.	Coll.	Mid	0		
11	Dyn.	Fib.	High	0	2.73E-01	6.72E-15
	Dyn.	Coll.	High	0		
12	Static	Fib.	N/A	0	3.34E-01	1.48E-01
	Static	Coll.	N/A	0		
13	Static	Coll.	N/A	0	1.65E-06	3.25E-02
	Static	Coll.	N/A	20		
14	Dyn.	Fib.	Low	20	7.42E-02	3.54E-01
	Dyn.	Coll.	Low	20		
15	Dyn.	Fib.	Mid	20	5.07E-02	2.13E-02
	Dyn.	Coll.	Mid	20		
16	Dyn.	Fib.	High	20	5.17E-02	4.08E-02
	Dyn.	Coll.	High	20		
17	Static	Fib.	N/A	20	1.29E-05	1.27E-01
	Static	Coll.	N/A	20		

For all comparisons except pair 13 from, the results were found to be statistically similar in means, variances, or both. Pair 13 was comparing collagen s-LbL at the no chemical additive (control) and chemical additive (experimental) condition. For all other surfaces tested (s-LbL, and d-LbL fibrinogen), the null hypothesis for Hypothesis 4 could not be rejected. On collagen, the differences in both means and variances were statistically significant, supporting Hypothesis 4. From Figure 67, the collagen evidences a reduction in adhesion as a result adding L-a. Though this result contradicts the results by Frilot [11], strong conclusions cannot be drawn, as the collagen tests were a single control experiment. The statistical similarities between the d-LbL collagen and fibrinogen

results, however, remain strong and support the concept that d-LbL was a viable surface for platelet adhesion experiments.

The rest of the Hypotheses (2, 3, and 4) were evaluated by the statistical test pairs described in Table 6, with the results in Table 9. The means for all test pairs except pair 18 showed statistically significant differences. Test pair 18 was the comparison of d-LbL dynamic flow condition, low and mid shear. This result was again unsurprising, supported by the graphical results (Figure 67), and velocity (Figure 38) and shear stress results (Figure 39) from particle tracking (§4.2). The differences in shear stresses and velocities were less pronounced along the first 1/3 and second 1/3 of the slide radius, but grow more quickly along the final 1/3 of the slide radius.

These results support Hypothesis 2, by showing differences between lower and higher shear regions (Pairs 18-20). Hypothesis 3 was supported by the test pairs comparing a given flow condition no chemical additive control to its chemical additive experimental counterpart (Pairs 23-26). Again, the static condition (pair 24) appears to have statistically significant differences between the no chemical additive and chemical additive conditions. However, this pair included the collagen results with the fibrinogen as a lumped d-LbL set of results. When looking at just the fibrinogen results (pair 31), the statistical test provides the expected result across multiple combined experiment days.

Hypothesis 4 appears to be supported by the results in Figure 73, with the mean percent difference in fluorescent percent surface coverage greater in the dynamic flow condition than the static condition. However, the statistical results shown for test pair 32 in Table 9 do not show a statistically significant difference in the means.

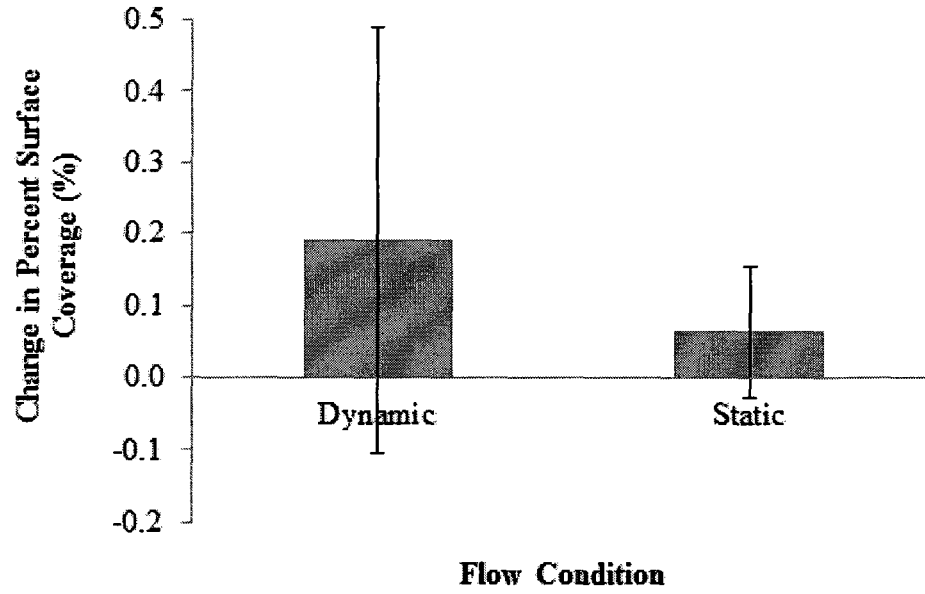


Figure 73 The total change, Δ_{La} , in fluorescent percent surface coverage for the static exposure to PRP and the dynamic flow condition, for the d-LbL fibrinogen and collagen experiments

Table 9 t-Test comparisons for means and F-test comparisons for variances. Items above the 0.05 threshold are in bold

Pair #	Flow Cond.	LbL Type	Region	L-a μM	t-Test P-value	F-test P-Value
18	Dyn. Dyn.	d-LbL d-LbL	Low Mid	0 0	1.57E-01	3.70E-10
19	Dyn. Dyn.	d-LbL d-LbL	Low High	0 0	1.89E-06	0.00E+00
20	Dyn. Dyn.	d-LbL d-LbL	Mid High	0 0	9.51E-05	0.00E+00
21	Static Dyn.	d-LbL d-LbL	N/A Low	0 0	7.68E-04	2.21E-06
22	Static Dyn.	d-LbL d-LbL	N/A Mid	0 0	1.68E-04	0.00E+00
23	Static Dyn.	d-LbL d-LbL	N/A High	0 0	6.47E-09	0.00E+00
24	Static Static	d-LbL d-LbL	N/A N/A	0 20	6.21E-04	1.52E-03
25	Dyn. Dyn.	d-LbL d-LbL	Low Low	0 L-a	4.82E-04	6.87E-07
26	Dyn. Dyn.	d-LbL d-LbL	Mid Mid	0 L-a	3.66E-05	9.90E-33
27	Dyn. Dyn.	d-LbL d-LbL	High High	0 L-a	4.21E-05	1.01E-38
28	Static Dyn.	d-LbL d-LbL	N/A Low	L-a L-a	8.37E-04	2.89E-03
29	Static Dyn.	d-LbL d-LbL	N/A Mid	L-a L-a	2.24E-03	1.34E-01
30	Static Dyn.	d-LbL d-LbL	N/A High	L-a L-a	2.49E-12	0.00E+00
31	Fib-Stat. Fib-Stat.	d-LbL d-LbL	N/A N/A	0 L-A	1.69E-01	9.24E-04
32	Static Dyn.	d-LbL d-LbL	N/A All	0-20 0-20	4.57E-01	4.10E-02

CHAPTER 5

DISCUSSION

5.1 Particle Tracking

5.1.1 Overview

Particle tracking was an efficient and simple tool for calculating the localized dynamic flow conditions and transport phenomena. The results provided by the particle tracking software helped to explain some of the adhesion patterns in the platelet adhesion experiments. Evaluation of Hypothesis 2 required a way to quantify the shear stresses as a function of radial position, while the ability to use shear stress estimates to quantify the diffusive and convective transport of NO allowed a more complete interpretation of Hypothesis 3.

Velocity was averaged across angular position and time. This average characterizes the velocity at any given radius, but as the wave moved around the Petri dish velocity varied in a manner that was only quasi-periodic. The increased variance with increased radial position may explain the similar variance changes in platelet adhesion.

The most interesting results from particle tracking were: 1) estimated shear stress, 2) localized transport phenomena, and 3) ratio between diffusive transport and localized convective transport. Shear stress was three orders of magnitude lower than the physiological shear previously used in microchannel work [12]. At the same time, the

ratio of convective transport to diffusive transport for NO was only one order of magnitude lower in the swirl flow configuration than in a microchannel configuration. Testing in both configurations could help distinguish the shear stress effects from the transport effects in future work with L-a and other platelet chemical additives.

5.1.2 Comparison of Flow Field to Other Sources

The flow configuration used for these experiments, while likely not unique, was not found in the literature review for this work. Some of the most similar analogues to this work were swirl flows such as von Karman flows [57] [69] [70], or other flows based on external oscillatory impulses to open-top tanks [71]. However, these representations were axisymmetric, while the flow in our dynamic flow condition was not. A CFD model, validated against the collected data, would be required to provide a better comparison against the observed platelet adhesion results.

5.1.3 Limitations and Sources of Error

The particle tracking program provided results over only a few discrete points of the swirl flow for any given frame. Without a good way of averaging multiple processed periods together, it took several videos to provide one with sufficient particle distribution across all the shear regions of interest. Without a CFD model, the surface velocities of relatively large particles were the only information available to estimate the shear stresses and transport phenomena. The more complex aspects of the flow, such as recirculation and secondary vortices such as those that arise in axisymmetric von Karman flows were not accounted for, leading to a potential underestimation of shear stress and transport phenomena.

5.1.4 New Questions Raised

The results of the particle tracking experiments raised a few new questions. First, can the swirl flow configuration used in these experiments be combined with microchannel experiments to distinguish chemical additive effects on platelets due to shear stress from those due to the convective transport of pd-NO and the chemical additive? This question remains unresolved because the microchannel tests were not repeated for the d-LbL process. Integrating the Eshaq microchannel experiments and the improvements reported here could help answer this question. Because of the great differences in shear stress (3 orders of magnitude) and NO transport (1 order of magnitude) between the swirl flow and expected microchannel flows, differences in adhesion indicated by fluorescence could indicate whether shear stress or NO transport has the greatest influence on adhesion reduction.

Will a CFD analysis of the swirl flow validate the estimates for surface shear stresses and transport phenomena presented here? A CFD analysis was not within the scope of this study; in addition, any CFD analysis needs physical data against which portions of the model can be validated. By validating velocity results in a CFD given the dynamic input conditions, the shear stress results could be compared against the localized model used here. It was expected that the model for this dissertation, operating on discrete locations and integrative in its derivation, could not account for more complex shear responses. It is likely a CFD result may broadly match the shear results produced here, but show peaks and valleys in shear stress not found by the current approach.

Can the particle tracking program be modified to include phase so multiple results can be adequately averaged together? There was no computationally reliable way to

identify the phase, or wave location around the dish, for the swirling fluid. Without this, sections from different parts of a video cannot be combined to produce data with greater statistical power. Given the current methods employed in particle tracking, the best approach would be to manually identify when the wave crest passes a fixed point, and set this as a phase identifier. This solution was not completely satisfactory, however, because there were no guarantees that the wave would sweep through all angular positions in a reliably periodic fashion.

5.2 Flow Cytometry

5.2.1 Overview

The principal discussion points on flow cytometry have already been explored with the results presented in §4.3. The most interesting aspect of the flow cytometry was the much greater (4-5 times) response to the blue excitation than the red excitation for particles counted by the cytometer. It has been reported that platelets that take up AO can respond to these two excitation spectra, depending on their viability and age [52]. It is possible that these cytometry results indicate that a large percentage of the platelets extracted during centrifuging were damaged by the process, young, or affected in another way that would allow them to uptake the AO in an alternate manner. The most consistent part of the results was the high dilution case, with the event counts close to the same for each experiment day. In contrast, the low dilution case showed larger counts on the second day. The first day showed a near perfect ratio between high- and low-dilution counts, with the expected ratio being 2.0, and the observed ratio, 2.02. On the second day, the experiment results showed a higher ratio, at 2.37.

5.2.2 Comparison of Platelet Counts to the Literature

The comparison of results from Eq. 4-6 with the literature bovine platelet counts [67] and the flow cytometry event counts is initially misleading. The numerical results appear to match well. The flow cytometer counts events over 10 μL of solution, though, rendering the expected:observed ratio to be $\sim 10:1$.

5.2.3 Limitations and Sources of Error for Platelet Counts

Agilent has no established protocol for measuring platelets, and the flow cytometry has not been tested for the application. As such, there is no standard of functionality against which to compare the flow cytometry results. Attempts to use manual counting of stained platelets under fluorescent microscopy (hemocytometry) were unsuccessful, and required more refinement in process to be a viable counting method.

The Bioanalyzer counts individual events, but records no image of the event. It was not possible, using the Bioanalyzer alone, to determine whether the event consisted of a single cell or clump of cells. Agilent recommended using a vortexer to break apart cell clumps before putting the solutions into the test wells, but vortexing could not ensure that clumps would not remain.

Without an effective, objective method of establishing a true platelet count from each blood draw, an uncontrolled variable remains during all platelet adhesion tests – the platelet concentration in each day's d-PRP solutions. The current methodology provides, at best, a qualitative description of platelet concentration from day to day.

5.2.4 New Questions Raised

There were a few new questions raised by the flow cytometry results. Why was there a 10:1 ratio between the expected and the measured platelet events? It is possible

that the PRP process we employed actually generated PPP, and that the flow cytometry demonstrated the actual platelet counts. A reliable, proven method of counting platelets could provide validation of these results. This may involve sending the collected blood to a hospital with complete blood count (CBC) assay capabilities, or finding an improved microscopy approach that would allow manual cell counts using a hemocytometer slide.

Are the high counts of events from blue fluorescence excitation representative of damaged platelets? Was the platelet count more accurately described by combining the events from each fluorescence response, or by describing them separately? Once reliable platelet counts are established, the significance of the red/blue fluorescence events from Bioanalyzer flow cytometry can be elucidated. If the total event counts (red/blue together) were representative of actual platelet counts, then the differences in response become more significant. An alternative assay using a live-dead stain such a calcium stain could be used to identify the live/dead fraction of platelets, and then compared against a Bioanalyzer run from the same PRP batch. If the live/dead assays do not match, it is possible that the differences were due more to young platelets rather than damaged or otherwise non-viable platelets. Verification of this would again probably require CBC equipment or microscopy capable of characterizing individual platelet morphologies.

5.3 s-LbL Results

5.3.1 Overview

The functionality of s-LbL was tested for two primary reasons. First, suspicions had arisen that the methods used in the work of Eshaq [12] and Frilot [11], overestimated platelet surface coverage. Secondly, a baseline for adhesion on s-LbL was needed as a

negative control to determine whether the anomalous AO signal was reduced when d-LbL was used, as proposed by Hypothesis 1 (§1.5.1).

Although the percent surface coverages shown in Figure 52 for s-LbL appear to support the hypothesis that platelet adhesion increases with increased shear (Hypothesis 2, §1.5.2), decreases with added L-a under shear conditions (Hypothesis 3, §1.5.3), but was not strongly affected by added L-a under static conditions (Hypothesis 4, §1.5.4), as suggested by Frilot's work, the validity of these results depended on the specificity of the AO staining to platelets. Slides layered with s-LbL exposed to PBS without d-PRP, stained with AO and imaged with the TRITC filter indicated that the surface itself retained anomalous AO (Figure 56). The calculated percent surface coverage for PBS dynamic 0/20 μM Low/Mid/High and PBS-Static 0 μM were even larger than the results for the standard s-LbL platelet adhesion tests summarized in Figure 52. Both with and without chemical additive, shear increased fluorescence. The addition of L-a, through an unknown mechanism, reduced the amount of AO retained by the s-LbL surface.

The FITC-fibrinogen stain was used to assess the fibrinogen coverage after LbL, and to correlate platelet adhesion to fibrinogen accumulation along the final surfaces. AO can fluoresce under both FITC and TRITC conditions, depending on the way the molecule binds to surfaces or cells [52], and Figure 56 indicates that AO stained regions can be misidentified as FITC-tagged fibrinogen.

FITC and TRITC images taken of an s-LbL surface exposed to d-PRP, stained with both AO for platelets and FITC-fibrinogen for the fibrinogen coating, show a high degree of correlation between red and green fluorescence results (Figure 59 through Figure 62). The images suggest that platelets accumulate in areas of highest fibrinogen

accumulation. However, the anomalous staining from the PBS-only experiments prevents this conclusion from being made.

FE-SEM images (Figure 69 through Figure 71) suggest that AO stain was retained by the s-LbL surfaces because they were rough and porous at the nano-scale. These features may retain AO stain even after surface was rinsed in the standard AO staining protocol. The nano-scale features do not explain why stain retention was reduced when L-a was added to the fluid exposed to the surface, however.

5.3.2 Comparison of Results to Frilot, Eshaq, and the Literature

While the trends in the s-LbL summary figures (Figure 52 and Figure 56) match those from the later d-LbL experiments, the summary figure from the Red-Green experiments (Figure 56) showed fluorescence retained by the s-LbL surface in the absence of platelets. This anomalous retention indicates that these results were suspect, leaving the exact mechanism under which the stain results were occurring in s-LbL still somewhat unclear. The image of platelet adhesion on a plain glass slide results (Figure 57) was qualitatively similar to the d-LbL image of Figure 58. This agreement further supports Hypothesis 1 by indicating that under fluorescence microscopy, the results collected via d-LbL more closely resemble platelet accumulations. This statement holds true for at least platelet accumulations on a plain glass slide with no LbL substrate, relying on the thrombogenic properties of glass [72].

The summary of surface coverage in Figure 52 agrees with the work previously presented by Eshaq [12] and Frilot [11]. Namely, that L-a is a platelet chemical additive, increasing the production of pd-NO to inhibit platelet adhesion, but only in the dynamic regime, in the presence of sufficient shear stresses. This result supports the work of Eshaq

for fibrinogen surfaces. For the low and mid-shear conditions, there was little distinction between the presence of L-a. At the same time, the presence of chemical additive appears to have no effect in the static exposure to PRP condition, as indicated by Frilot for collagen surfaces. While the use of AO staining on s-LbL slides was subject to artifacts, it was important here to show, as a baseline, that results identical to those obtained by previous researchers could be obtained when the same methods were used.

There is a growing body of work in LbL technology expanding the use of different forms of dynamic LbL to improve upon the potential surfaces. As discussed in the background (§2.2), other researchers have moved away from static LbL processes to dynamic processes when highly homogeneous surfaces, particles, or structures are sought or required [39] [40] [73] [41].

5.3.3 Limitations and Sources of Error

As highlighted via the Red-Green tests, fluorescent microscopy was limited by the assay method for quantifying platelet coverage on s-LbL surface. It is still possible that s-LbL surfaces are more effective than d-LbL surfaces at retaining platelets from d-PRP experiments. It was therefore important to have a method to assess the amount of adhesion on s-LbL and d-LbL that was independent of the fluorescent method.

A modality was needed that could analyze micro- and nano-scale 3D surface morphologies, of slide areas, comparable to those that can be analyzed via fluorescence microscopy. Of the equipment available at Louisiana Tech, the only device that would have performed this function was the interferometer in the Metrology lab at the IfM. However, the machine has been inoperable for a while, and budget limitations may keep it inoperable for a while longer. The only other alternatives available for characterizing

the surfaces were limited in either function or scale. FE-SEM was able to provide qualitative images of the surface topologies, but a true 3D representation would be difficult to achieve. At the largest scale, it would be possible to take images under FE-SEM and manually count regions that may be presumed to be platelets or platelet accumulations. However, zoomed-in images would have to be taken of each presumed platelet or thrombus to be able to confirm the presence of a biological structure rather than a surface artifact. This would be time-consuming and impractical, and was therefore not considered as a useful substitution or complement to fluorescence microscopy. Atomic Force Microscopy (AFM) can readily identify large-scale accumulations, but does so on small regions ($\sim 40 \times 40 \mu\text{m}$ areas), and does so slowly. To take sufficient images to form a quantitative analysis of total surface adhesion would be impractical. These limitations in equipment proved a further incentive to the development of a surface that would work well with a simple method that has a long and well-established history of use in our laboratory, fluorescence microscopy.

5.3.4 New Questions Raised and Unresolved Questions

The discussions in the previous sections leave questions unresolved. What is the true surface adhesion comparison between s-LbL and d-LbL? Which of these surfaces is more effective at retaining platelets or thrombi? These questions remain unresolved because no 3D imaging mode was used. Without establishing actual platelet counts from direct measurements of cellular presence, rather than indirect indicators such as fluorescent stains, these questions cannot be answered with confidence. Once a direct evaluation of cellular presence can be made, the effectiveness of the two types of surfaces

can be more firmly established, and the reliability of fluorescence tagging as a platelet identifier in d-LbL surfaces can be confirmed.

On which of these surfaces is the effect of shear on platelet adhesion strongest?

On which of these surfaces is the effect of chemical additives strongest? These two questions allow for the possibility that s-LbL remains a viable surface on which to perform adhesion studies. A 3D imaging process or other methods could be used to compare the surface differences in platelet coverage in regions of different shear rates and in experiments with different chemical additives. It is possible that one surface will more effectively generate larger percent differences in a given condition than the other generates, or that one surface is preferred in all cases. Identifying the best surface to magnify differences in the various test conditions will provide tests of greater sensitivity to the effect being studied. If the surfaces prove to be individually more effective in different experiment modes, the selection of surfaces for an experiment could provide greater specificity to the effect being studied.

How was L-a affecting the background retention of AO on the s-LbL surface? Is this mechanism widespread, and can the fluorescence results of L-a conditions, even on d-LbL surfaces, be trusted when staining with AO? At the moment there is no good explanation for how the addition of L-a changes the fluorescence response in the absence of platelets. It is possible that the L-a acts as some sort of surfactant or fills the nano-scale pores and holes where AO would accumulate. FE-SEM microscopy or other nano-scale imaging techniques could be used to identify morphological changes, while a chemical analysis such as mass spectrometry or spectrography could be used to identify chemical changes to the surface.

5.4 d-LbL Results

5.4.1 Overview

In response to the functionality questions raised for s-LbL in our standard platelet adhesion experiments, discussed in §5.3, a new approach to developing nano-scale biointerfaces was developed. This improved method, d-LbL, was used to test all four hypotheses.

In conjunction with the s-LbL Red-Green tests (§4.4.2), the results of platelet adhesion experiments on d-LbL surfaces were used to test Hypothesis 1, discussed in §5.3.1. The s-LbL standard platelet adhesion tests were repeated on collagen and fibrinogen d-LbL surfaces once d-LbL functionality was established from Hypothesis 1 (§1.5.1). Figure 67 summarizes the d-LbL results used to test Hypotheses 2, 3, and 4. The results for all four hypotheses were tested for statistical significance using the comparison pairs listed in Table 4, Table 5, and Table 6, with the results for these tests shown in Table 7, Table 8, and Table 9, respectively.

The surface coverage data in Figure 67 suggest that platelet adhesion depends on shear stress (Hypothesis 2, §1.5.2). Statistical test pair 18 indicates that for the low and mid shear stress regions in the no chemical additive test condition, there was no statistically significant difference in the mean value of apparent adhesion. Figure 39 summarizes the calculated localized shear stress as a function of radial position, averaged for time and angular position around the Petri dish. The mean shear stress over the first third (“low”) of the radii and the second third (“mid”) were closer to each other than between low and high or mid and high. However, after the low shear region, the variances increase, and correlate well with the variance test results in statistical pair 18.

The rest of the relevant statistical tests, pairs 19-20, demonstrate a statistically significant dependence of both means and variances on shear stress region in platelet adhesion. The results suggest that platelet adhesion increases with increasing shear stress.

The reduction of apparent adhesion on d-LbL with the addition of L-a, as seen in Figure 67 was statistically significant for all dynamic cases and for the static case with collagen biointerface (Hypothesis 3, §1.5.3). Figure 68 indicates that the reduction became stronger as shear rate increased. The percent difference between the no chemical additive and chemical additive condition increases more than twofold, from ~17% in the low shear region to ~37% in the high shear region. The shear rate increase was ~400% (Figure 39), and the NO transport was only ~75% (Figure 41), suggesting that the effect of L-a was dependent on the dynamic flow conditions.

This strong dependence on the dynamic flow conditions was further tested by Hypothesis 4 (§1.5.4), comparing the effect of L-a in a static exposure to PRP and the dynamic flow condition. Statistical pairs 24 and 31 indicated an interesting result that involved the difference between fibrinogen and collagen biointerfaces. Figure 67 summarizes the d-LbL platelet adhesion tests, broken apart into the tests performed on fibrinogen and collagen biointerfaces. The collagen biointerface was used as a positive control of functionality, and for the most part showed the expected similarity to the fibrinogen results. Statistical test pairs 9-17 from Table 8 tested these similarities, and the results show the strong degree of correlation between the means of d-LbL collagen and fibrinogen biointerface platelet adhesion, and a large degree of correspondence in the degree of variance. However, a difference arises when comparing the differences between fibrinogen and collagen results in the static exposure to PRP condition, test pairs

13 and 17 and pairs 24 and 31. L-a had a statistically significant effect on fluorescent surface coverage in static conditions on the collagen surface, but not on the fibrinogen surface. The collagen biointerface test was a single positive control experiment, and this anomaly would have to be tested with further collagen tests. Test pair 32 showed that while the mean difference in fluorescent surface coverage appears to be different, the difference is not statistically significant.

5.4.2 Comparison of Results to s-LbL and Previous Studies

The results for d-LbL compare well with the s-LbL trends with respect to adhesion dependence on shear stress and chemical additive, and compare well against the expected results from Eshaq [11] and Frilot [11]. Both types of LbL showed an increase in apparent adhesion with respect to shear stress. Both also showed a decrease in apparent adhesion with respect to adding L-a under a dynamic flow condition. Table 7 has the statistical tests comparing s-LbL to d-LbL platelet adhesion results. For the no chemical additive condition, the mid-shear region results show no statistically significant difference, while the chemical additive (L-a) condition extends that similarity to the low-shear region. Figure 72 shows these differences in the percent area comparisons between d-LbL and s-LbL. At the high shear regions, and in the static exposure to PRP condition, the percent area differences were significant. However, as discussed for s-LbL (§5.3), the s-LbL results were considered unreliable, at least using fluorescence microscopy evaluation. The adhesion results for s-LbL shown in Figure 72 were even lower than those for the plain PBS s-LbL tests from the Red-Green tests (Figure 56).

The FE-SEM images of the s-LbL (Figure 69), d-LbL fibrinogen (Figure 70), and d-LbL collagen (Figure 71) surfaces indicate some morphological differences that should

be further explored. The s-LbL surface appears to have many more pockets or regions on the surface that may retain AO stain. The d-LbL surfaces have regions of smooth surfaces and regions that resemble some of the morphology seen widespread on the s-LbL slide tested.

There were no direct examples of other researchers generating d-LbL surfaces for use in platelet adhesion. However, the theory behind moving from an s-LbL process to a d-LbL process is well supported by other researchers. Kim et al. [15] and Everett and Higgins [74] reported successful generation of nano structures self-assembled under flow conditions. Their experiments took place in a continuous flow under microfluidic conditions. Zhang et al. [42] demonstrated that a dynamic technique with pressure and temperature controls could reduce the number of layers required for membrane generation from ~60 to ~4, while retaining the desired membrane characteristics when compared to standard dipping techniques. Jiang et al. [75] reported an exceptionally high level of uniformity and integrity in LbL films using a spin-assisted dynamic LbL process. Lu and Salac [76] discussed the use of electric fields to guide the self-assembly of multilayer films. Finally, Yin et al. [16] deposited PDDA and PSS under a vibration condition, resulting in dense, smooth films that had film grown comparable to standard techniques when generating multilayer films.

In all of these examples, the unifying concept was the addition of a dynamic component such as convective flow, pressure-driven porous flow through a membrane, or vibration, to homogenize the individual layers in multilayer films. Groups like Zhang et al. demonstrated that a dynamic LbL process led to a dramatic increase in function with less work and less layers. Yin et al. used the same substrate materials (PDDA, PSS) and

reported smooth films from a multilayer d-LbL process. This result compares well with the apparent morphology from the FE-SEM results, with smooth areas in both fibrinogen and collagen d-LbL surfaces.

5.4.3 Limitations and Sources of Error in d-LbL Experiments

As with the limitations reported for s-LbL (§5.3.3), one of the principal limitations in evaluating d-LbL as laid out in the four hypotheses for this work was that fluorescence microscopy does not provide a completely unambiguous way to identify platelet adhesion.

A unique source of potential error in the d-LbL process was confusing which was the “top” surface during layering. Even though the slide handling process helps keep the side of the slide manipulated by the forceps clearly identified throughout the process, an opportunity remained for the slides to be turned around about their long axis in the centrifuge tubes. This confusion could result in the slide being placed on the wax paper and dried with the “wrong” side up. Care was taken not to mark the slides with anything that could wash off into the LbL solutions until after the final AO rinse to prevent contamination in the liquids.

Early in the experiments to design the d-LbL process, fibril-like contamination of the various d-LbL liquids was encountered in the individual centrifuge tubes. This contamination was not a surprise, as the s-LbL process often resulted in the liquids growing milky in color and becoming filled with fibrils. Because of the smaller individual volumes involved in the d-LbL centrifuge tubes, it was easier to completely replace the liquid in a tube if it became milky or had fibrils. Care was taken to avoid

contaminated tubes from being used in the d-LbL process, but there was still the possibility that individual layers were generated with cross-contamination or fibrils.

Finally, though an objective standard was established in the exclusion of imaging zones during fluorescence microscopy, there was still room for subjectivity in the application of this standard. A truly objective standard for image inclusion or exclusion may be difficult to establish for fluorescence microscopy, leaving the possibility of unintentional selection bias when collecting data.

5.4.4 New Questions Raised

In addition to the LbL functionality questions raised in §5.3.4, several questions arise from the d-LbL discussion. Are any of the dynamic methods proposed by other researchers more effective in providing a biointerface for platelet studies? The three most relevant being, microfluidic flows for generating d-LbL inside microchannels under constant, laminar, alternating flows of the polyions and biointerfaces [74], vibration [16], and spinning [75]. While the current experiments indicated an improvement in surface performance and even morphology with the dynamic method, it is possible that one of these methods already reported in the literature will prove to be simpler, more effective at generating a homogeneous surface, or both.

Are the L-a effects on platelet adhesion due primarily to convective transport, shear stress, or both? Because the focus of this work was to validate an improved manufacturing technique, the study of flow conditions and chemical additive effects was limited to surface functionality tests. However, the particle tracking results indicated that the differences between shear stresses and NO transport could be studied by changing flow environments (§5.1).

Can the objective standard used for image exclusion be improved? The objective standard used to exclude images from imaging remains somewhat subjective – the researcher must compare a suspected image to the objective standard, and decide whether the exclusion criteria were met. If a computational standard could be generated to allow for automatic exclusion, the rules could be applied consistently, though it is likely that the standard would be somewhat inefficient at classification. Adaptive algorithms like artificial neural networks could be trained on researcher-selected excluded images to perform this function. A 3D imaging process could eliminate this need by counting areas that exceed a vertical threshold rather than depend on fluorescent accumulation.

How do the surface morphologies compare among d-LbL fibrinogen and collagen? Does d-LbL collagen provide a different adhesion response to L-a in static conditions than fibrinogen? These questions are related, as surface morphology has not yet been excluded as a factor in platelet adhesion and accumulation, as discussed in both this section and the s-LbL discussion (§5.3). These questions were not answered by the current work because the collagen test was limited to one positive control experiment. Surface morphology characterizations linked to platelet adhesion could help determine the extent to which the individual surface morphologies contribute to platelet activation, adhesion, and accumulation. Further testing could identify the extent to which the morphology effects are due to the LbL process or the biointerface material. Any L-a differences between fibrinogen/collagen adhesion results, if they continue to be evidenced in further tests, could then be attributed to either morphology or biointerface.

CHAPTER 6

CONCLUSIONS AND FUTURE WORK

6.1 Evaluation of Hypotheses

The discussions in the previous sections have provided a general overview of how the experiments performed in fulfillment of this dissertation answered the relative hypotheses questions. The conclusions that can be drawn from these discussions are discussed here.

6.1.1 Hypothesis 1

When s-LbL and d-LbL fibrinogen surfaces are exposed to either PBS or PRP and then stained with AO, the percent surface area that fluoresces will be smaller for the d-LbL surface than for the s-LbL surface (Hypothesis 1, §1.5.1).

The Red-Green tests, specifically the plain PBS on s-LbL, d-PRP on glass slides, and d-LbL with d-PRP indicated that s-LbL retained an anomalous quantity of AO, even without platelets present, while the d-LbL surfaces retained platelets with a morphology that resembled that of platelets on plain glass slides. From the experimental results, we conclude that d-LbL does retain less stain than the s-LbL condition. Furthermore, given the morphology of likely adhesion, it is more likely that the fluorescence results obtained from d-LbL were more representative of platelet adhesion or cellular material than background fluorescence.

6.1.2 Hypothesis 2

The shear stress on a glass slide that is placed in a Petri dish, covered with fluid, and agitated to generate a swirl flow will increase as the location on the slide changes from the center of the Petri dish to the edge, and the AO fluorescence percent surface coverage of d-LbL fibrinogen-coated slides that are exposed to PRP, with and without added L-arginine (L-a) will be significantly different on regions of the slide corresponding to different shear stresses (Hypothesis 2, §1.5.2).

Both the s-LbL and d-LbL results showed strong evidence of shear-dependent likely adhesion results, estimated by fluorescence, under both a control (no chemical additive) and an experimental (chemical additive) condition. The particle tracking program showed a somewhat linear shear gradient from the mid to the high shear region in the slide, though the low shear region remained nearly flat. Although the shear stresses were not nearly as high as physiological stresses, the flow condition described here was simple to set up and simple to process. Therefore, we can conclude that the d-LbL experiments showed shear-dependent conditions under different conditions with the generation of a simple shear gradient on a single slide.

6.1.3 Hypothesis 3

The addition of L-a to platelets in plasma will decrease observed fluorescent percent surface coverage of d-LbL surfaces under shear conditions (Hypothesis 3, §1.5.3).

Both the s-LbL and d-LbL experiments showed a significant reduction in fluorescence results – presumed platelet adhesion – with the addition of L-a under shear conditions. For the experimental case, d-LbL, the effect of L-a increased with increasing

shear and transport of pd-NO. We conclude that adding L-a to d-PRP decreases the observed fluorescence response. If this fluorescence response is proven to be a reliable indicator of platelet adhesion, this reduction under shear conditions is likely from the enhanced production of pd-NO from the addition of the pd-NO precursor L-a.

6.1.4 Hypothesis 4

When d-LbL surfaces are exposed to PRP, without flow, the fluorescence percent surface coverage will be smaller when L-a is added to the PRP, but the reduction of surface coverage will be significantly less than observed under shear flow of PRP (Hypothesis 4, §1.5.4).

While this hypothesis was partially validated on results from the single collagen control test, platelet adhesion experiments on fibrinogen d-LbL surfaces across multiple experiments did not demonstrate an effect of L-a on percent surface coverage. While the data support the work shown by Frilot on fibrinogen, the single collagen experiment did not replicate Frilot's results. The experiments provided no evidence to support the hypothesis that adhesion on fibrinogen was different with and without L-a, or that the reduction in coverage was significantly different between the static condition and dynamic flow condition. If there was a difference, it was not sufficiently strong to be verified with the methods used here.

6.2 Future Work

Though all four hypotheses have been tested within the experimental sets performed here, more work remains. These areas of future work can be broken down into several categories: 1) Platelet adhesion verification, 2) Fluid Dynamics, and 3) Surface design.

6.2.1 Platelet Adhesion

Experiments should be performed to clarify whether s-LbL or d-LbL is most effective at thrombogenesis or platelet adhesion. This clarification will require a large-scale 3D evaluation of the adhered surfaces, probably some form of interferometry. The evaluation of platelet size and morphology, as well as the confirmation of platelet accumulations (thrombi) will be the final piece in confirming the functionality of one surface preparation type over the other, or at least validate that fluorescence microscopy results available for d-LbL were an adequate representation of true platelet adhesion.

To explain the results in platelet adhesion further, a functional protocol for counting platelets from each PRP centrifuge run needs to be established. At a minimum, experiments need to be designed to correlate the results from the Bioanalyzer flow cytometry to the true platelet count and the potential functional/non-functional fraction these results could represent.

Alternate fluorescent tags should be explored to eliminate the AO tagging ambiguity. Because the surface coverage of activated, adhered platelets are the principal measurand sought in our experiments, a tag specific to activated platelets may be a way to both confirm the presence of platelets via fluorescence microscopy alone and remove the AO ambiguity. One possible alternative is the monoclonal antibody approach, with FITC-labeled antibodies specific to the platelet glycoprotein complex IIb/IIIa as described by Michelson [77] and van Werkum et al. [78]. One drawback to this alternative is the high cost of monoclonal antibody tags, and the very small volumes of these tags per batch.

Finally, the orders of magnitude differences in shear stress and convective transport between microchannel flows and swirl flows should be tested to exploit these differences and determine the relative roles of the principal amplifiers to chemical additive responses by platelets – shear stress and transport phenomena.

6.2.2 Fluid Dynamics

A CFD model that more adequately models the swirl flow should be designed and validated to provide 1) a better estimate of the shear stresses and transport phenomena on the slide surfaces, and 2) a test bed to test new conditions and make testable predictions on effects of shear stress, transport phenomena, or both.

6.2.3 Surface Design

The d-LbL and s-LbL surfaces need to be evaluated in three dimensions to explain the surface morphologies suggested by the FE-SEM results presented in this dissertation. Further experiments need to be performed with collagen in a d-LbL manufacturing process to determine whether collagen or fibrinogen serves as a better biointerface in platelet adhesion studies, or if the surfaces can be prioritized to target studies of specific aspects of platelet thrombogenesis and adhesion. Finally, the different forms of dynamic processes in d-LbL manufacture reported by other researchers could be evaluated for improved performance in generating better biointerfaces in platelet adhesion studies.

APPENDIX A

MATLAB PROGRAMS

In the attached optical media, the following copies of MATLAB® code used in this dissertation can be found, in the appropriate directories:

For Image Processing – percent surface area:

Directory: *\Matlab\Image Processing*

File Name: *improcess_FINAL.m*

Program description: Principal image processing program used to process the microscopy images, generate black and white thresholded images from the data to identify regions of thrombus accumulation from AO, calculate the percent surface area coverage by these threshold regions, and generate graphs and spreadsheets to document these calculations. Program developed for this dissertation, expanded from the image processing methods described by Eshaq [12]. Distributed under the GNU General Public License.

For Centroids particle size estimation

Directory: *\Matlab\Image Processing*

File Name: *Centroids_FINAL.m*

Program description: Secondary image processing program applied to the black and white images generated in *improcess_FINAL.m*. The program takes advantage of the third party code (see below) used in particle tracking by processing each individual image

through a sweep of estimated centroid sizes, calculating the number of centroids found in an image, and their attendant statistics, given a presumed centroid size and generate graphs and spreadsheets to document these calculations. These results provided a quantitative comparison of particle size distributions based on the different conditions, both flow and chemical. Distributed under the GNU General Public License.

For Particle tracking

Programs developed for this dissertation and provided by third parties were used to track the particles.

Directory: *\Matlab\Particle Tracking*

File Name for program developed for this dissertation: *ParticleTrack_FINAL.m*

Program description: Program takes video of moving particles, separates the video into individual frames, and processes the frames. The processing takes several stages. First, the frames are thresholded to provide black and white images. Then, information is collected to determine the center of the Petri dish for the polar coordinate calculations, and a zone of exclusion to ignore data that were extraneous or too noisy to be of use. A third-party set of programs is then used to evaluate each of these images and identify the particles in each of the images. These particles are kept track of during movement in subsequent frames, to allow for the following steps. The individual locations of the particles in sequential images are used to calculate velocities in Cartesian coordinates. The positions and velocities are translated to polar coordinates. Finally, shear stresses and NO diffusion constants are estimated. The data were plotted and saved to spreadsheets. Distributed under the GNU General Public License.

Third party software:

Program by The Math Works, provided as an added program to extend MATLAB®

functionality:

File Name: *dsxy2figxy.m*

Program description: translates data space coordinates into figure space coordinates.

Additional library of files from code provided by

Daniel Blair, blair@hysics.georgetown.edu

Eric Dufresne, eric.dufresne@yale.edu

Code home: <http://www.physics.georgetown.edu/matlab/>

Statement on the site as to the code provided:

"All of the code found here is free for use and distribution and should be considered covered under the terms of the GNU GPL <<http://www.gnu.org/copyleft/gpl.html>>."

Filenames for code provided by Dufresne and Blair [56]:

bpass.m

cntrd.m

lentrck.m

parse_noran.m

pkfnd.m

read_gdf.m

read_noran.m

track.m

Programs description: This library of code provides a means in MATLAB of tracking particles from images. The images need not be thresholded prior to using the program, but can operate more efficiently if done so. Because thresholding already worked well in *improcess_FINAL.m*, it was incorporated in the *ParticleTrack_FINAL.m* program, and used to feed thresholded images to this software suite. The software programs interact with each other to perform the following steps: 1) Identify the locations of local maxima in pixel color intensities, 2) Use these local maxima to estimate centroid size and statistics as well as location in individual images, and number these particles. 3) Use the centroids and statistics data to track the location of particles from one frame to the next. 4) Generate data arrays containing all of this information to be used by the rest of the program, *ParticleTrack_FINAL.m*.

APPENDIX B

COMPLETE DIGITAL ARCHIVE RECORD

This appendix contains a directory listing for the digital files that comprise the results for this dissertation. These files are included in the supplemental digital material provided on an optical disk. If the disk is missing, please contact the author at JuanMLopez.BME@gmail.com. The images include the full-size versions of the images included in the body of the dissertation.

From the root directory for the supplemental digital material:

File directories, listing each of the files contained in the data directories:

- 1) Flow Cytometry Directory Listing.txt
- 2) Imaging Data Directory Listing.txt
- 3) Matlab Directory Listing.txt
- 4) Particle Tracking Directory Listing.txt

File folders, containing the data listed in each of the directory listings enumerated above:

- 1) Flow Cytometry
- 2) Imaging Data
- 3) Matlab Directory
- 4) Particle Tracking

APPENDIX C
TECH DAIRY COW RECORD

130 - Cow Page DHI-203

72310101

LOUISIANA TECH DAIRY

Date of Test 5/4/2010

DRMG PCIDART

Printed 5/15/2010 1:36:09 PM

Barn Name 41

Index No. 41

Cow	Index No.	41	Breed	JE	DHI ID	111103085	PTA Milk	+610
	Barn Name	41			Name or number	7JE605	PTA % Fat	+58
	DHI ID	114960638					PTA Prot	+6
	Farm ID	114960638					PTA \$	+152
Date of Birth	11/15/2005						Rel.	0
PTA Milk	-245	PTA \$	+64					
PTA % Fat	+14	Rel.						
PTA Prot	-5	Pdlike(NM)						
Sire	DHI ID	112461127	PTA Milk	-824				
	Name or number	775	PTA % Fat	-19				
			PTA Prot	-13				
			PTA \$	-18				
Dam	Breed	JE	Rel.					
			Pdlike(NM)					

Lactation Production Summary

Calving Date	Age at Calving Yr - Mo	Days Dry Before Calving	Friesian	Days 3X Cond. Alt. Record	305 Day Lactation					Complete Lactation				Type of Record
					Milk	% Fat	Fat	% Prot	Prot	Days in Milk	Milk	Fat	Prot	
11/3/2007	1 - 11	0	B	0	14216	4.0	568	3.2	458	405	17560	716	581	DNR-AP
2/3/2009	3 - 2	53	B	0	17765	4.1	728	3.4	607	310	18015	737	816	DNR-AP
2/19/2010	4 - 3	71	C	0						75	4826	205	141	DNR-AP

Status Change	Last Test			Lifetime Production			Milk per Day Since 24 Mths of Age	Yield Deviation			Estimated Relative Producing Ability		
	Milk	% Fat	% Prot	Milk	Fat	Protein		Milk	Fat	Protein	Milk	Fat	Protein
Calved	58.0	4.3	3.2	40201	1858	1338	45	-1006	+7	-18	-25	+33	-6

Calf and Breeding Record

Calving Date	Body Wt (CWT)	Days Open	# Br	Successful Breeding Date	Sire		Dam		Persist of Lact Curve	Avg SCCS for Lact	ME Lactation			Heritability Deviation		
					Identity	Br	Sex Disp	Identity			Milk	Fat	Prot	Milk	Fat	Prot
11/3/2007	10	182	1	1/27/2007	1JE970		M7		106	4.6	18380	719	674	-579	+21	-36
2/3/2009	10	93	3	5/3/2008	7JE583		F	00160	113	3.2	18666	749	625	+1263	+86	+48
2/19/2010	10	75	2	5/7/2009	7JE778		F	00204	0	3.6	14820	622	454	-788	+23	-37

Test Day Data

Lact No	Calving Date	1st Test Day		2nd Test Day		3rd Test Day		4th Test Day		5th Test Day		6th Test Day		7th Test Day		8th Test Day		9th Test Day		10th Test		11th Test	
		SCCS	%Prot	SCCS	%Prot	SCCS	%Prot																
		Milk	%Fat	Milk	%Fat	Milk	%Fat																
1	11/3/2007	36	4.6	54	4.7	65	3.3	60	3.7	54	3.8	40	4.7	45	4.2	40	3.9	39	4.0	41	3.7	46	4.0
2	2/3/2009	52	3.6	78	4.0	81	3.4	82	3.6	52	4.4	60	4.2	40	4.2	60	4.3	47	4.3	42	4.8	47	4.0
3	2/19/2010	53		7	3.1	0	3.2																

Figure C-1 Tech Dairy Cow Record for Cow #41, scanned image of datasheet

APPENDIX D

STATISTICAL SAMPLES: T-TEST

Shown below is the test case to verify the Excel® t-test functionality. Data 1 and Data 3 are linearly changing identical vectors. Data 2 is randomly generated, between 0 and 1. Data 4 is Data 3 plus a random number between 0 and 1. Data 1 and 2 are clearly different from each other, whereas Data 3 and 4 are similar. For P-values ≥ 0.05 (when the significance is set at 0.05), the compared data are presumed to have the same means. For P-values ≤ 0.05 , the means are presumed to be different.

APPENDIX E

STATISTICAL SAMPLES: F-TEST

Table E-1 and Table E-2 show the validation tests for the Excel® F-tests. Table E-1 shows data that have the same means, with one pair of data showing similar variances, and the second pair of data showing a high difference in variances. An F-test with an alpha of 0.05 was performed on each pair, and shown to the right of the data. For P-values ≥ 0.05 , the compared data are presumed to have the same variances. For P-values ≤ 0.05 , the variances are presumed to be different.

Table E-1 Sample F-test to validate statistical process comparing data that are similar in variance/means and data that are significantly different in variance, with an α of 0.05

Similar Variance		Different variance		
Data 1	Data 2	Data 3	Data 4	
-9.00	-9.10	-9.00	-99.00	F-Test Two-Sample for Variances Similar Variance
-8.00	-8.09	-8.00	-89.00	
-7.00	-7.08	-7.00	-79.00	
-6.00	-6.07	-6.00	-69.00	
-5.00	-5.06	-5.00	-59.00	
-4.00	-4.05	-4.00	-49.00	
-3.00	-3.04	-3.00	-39.00	
-2.00	-2.03	-2.00	-29.00	
-1.00	-1.02	-1.00	-19.00	
0.00	-0.01	0.00	-9.00	
1.00	1.00	1.00	1.00	
2.00	2.01	2.00	11.00	F-Test Two-Sample for Variances Different Variance
3.00	3.02	3.00	21.00	
4.00	4.03	4.00	31.00	
5.00	5.04	5.00	41.00	
6.00	6.05	6.00	51.00	
7.00	7.06	7.00	61.00	
8.00	8.07	8.00	71.00	
9.00	9.08	9.00	81.00	
10.00	10.09	10.00	91.00	
11.00	11.10	11.00	101.00	
1.00	1.00	1.00	1.00	
1.00	1.01	1.00	10.00	

The second comparison, shown in Table E-2, verifies that the same conclusions as described in the first comparison hold valid, even if the means in the data are different.

Table E-2 Sample F-test to validate statistical process comparing data that are similar in variance with different means and data that are significantly different in variance, with an α of 0.05

Similar Variance		Different variance																										
Data1	Data2	Data1	Data2																									
-9.00	0.00	-9.00	0.00	F-Test Two-Sample for Variances Similar Variance <table border="1"> <thead> <tr> <th></th> <th><i>Data 1</i></th> <th><i>Data 2</i></th> </tr> </thead> <tbody> <tr> <td>Mean</td> <td>1</td> <td>10</td> </tr> <tr> <td>Variance</td> <td>38.5</td> <td>38.5</td> </tr> <tr> <td>Observations</td> <td>21</td> <td>21</td> </tr> <tr> <td>df</td> <td>20</td> <td>20</td> </tr> <tr> <td>F</td> <td>1</td> <td></td> </tr> <tr> <td>P(F<=f) one-tail</td> <td>0.5</td> <td></td> </tr> <tr> <td>F Critical one-tail</td> <td>0.470775</td> <td></td> </tr> </tbody> </table>		<i>Data 1</i>	<i>Data 2</i>	Mean	1	10	Variance	38.5	38.5	Observations	21	21	df	20	20	F	1		P(F<=f) one-tail	0.5		F Critical one-tail	0.470775	
	<i>Data 1</i>	<i>Data 2</i>																										
Mean	1	10																										
Variance	38.5	38.5																										
Observations	21	21																										
df	20	20																										
F	1																											
P(F<=f) one-tail	0.5																											
F Critical one-tail	0.470775																											
-8.00	1.00	-8.00	1.00																									
-7.00	2.00	-7.00	2.00																									
-6.00	3.00	-6.00	3.00																									
-5.00	4.00	-5.00	4.00																									
-4.00	5.00	-4.00	5.00																									
-3.00	6.00	-3.00	6.00																									
-2.00	7.00	-2.00	7.00																									
-1.00	8.00	-1.00	8.00																									
0.00	9.00	0.00	9.00																									
1.00	10.00	1.00	10.00																									
2.00	11.00	2.00	11.00																									
3.00	12.00	3.00	12.00																									
4.00	13.00	4.00	13.00																									
5.00	14.00	5.00	14.00																									
6.00	15.00	6.00	15.00																									
7.00	16.00	7.00	16.00																									
8.00	17.00	8.00	17.00																									
9.00	18.00	9.00	18.00																									
10.00	19.00	10.00	19.00																									
11.00	20.00	11.00	20.00																									
1.00	10.00	1.00	10.00	F-Test Two-Sample for Variances Different Variance <table border="1"> <thead> <tr> <th></th> <th><i>Data 3</i></th> <th><i>Data4</i></th> </tr> </thead> <tbody> <tr> <td>Mean</td> <td>1</td> <td>10</td> </tr> <tr> <td>Variance</td> <td>38.5</td> <td>3850</td> </tr> <tr> <td>Observations</td> <td>21</td> <td>21</td> </tr> <tr> <td>df</td> <td>20</td> <td>20</td> </tr> <tr> <td>F</td> <td>0.01</td> <td></td> </tr> <tr> <td>P(F<=f) one-tail</td> <td>7.77E-16</td> <td></td> </tr> <tr> <td>F Critical one-tail</td> <td>0.470775</td> <td></td> </tr> </tbody> </table>		<i>Data 3</i>	<i>Data4</i>	Mean	1	10	Variance	38.5	3850	Observations	21	21	df	20	20	F	0.01		P(F<=f) one-tail	7.77E-16		F Critical one-tail	0.470775	
	<i>Data 3</i>	<i>Data4</i>																										
Mean	1	10																										
Variance	38.5	3850																										
Observations	21	21																										
df	20	20																										
F	0.01																											
P(F<=f) one-tail	7.77E-16																											
F Critical one-tail	0.470775																											
1.00	1.00	1.00	1.00	MEAN SCALING																								

APPENDIX F
PARTICLE TRACKING TEMPLATE

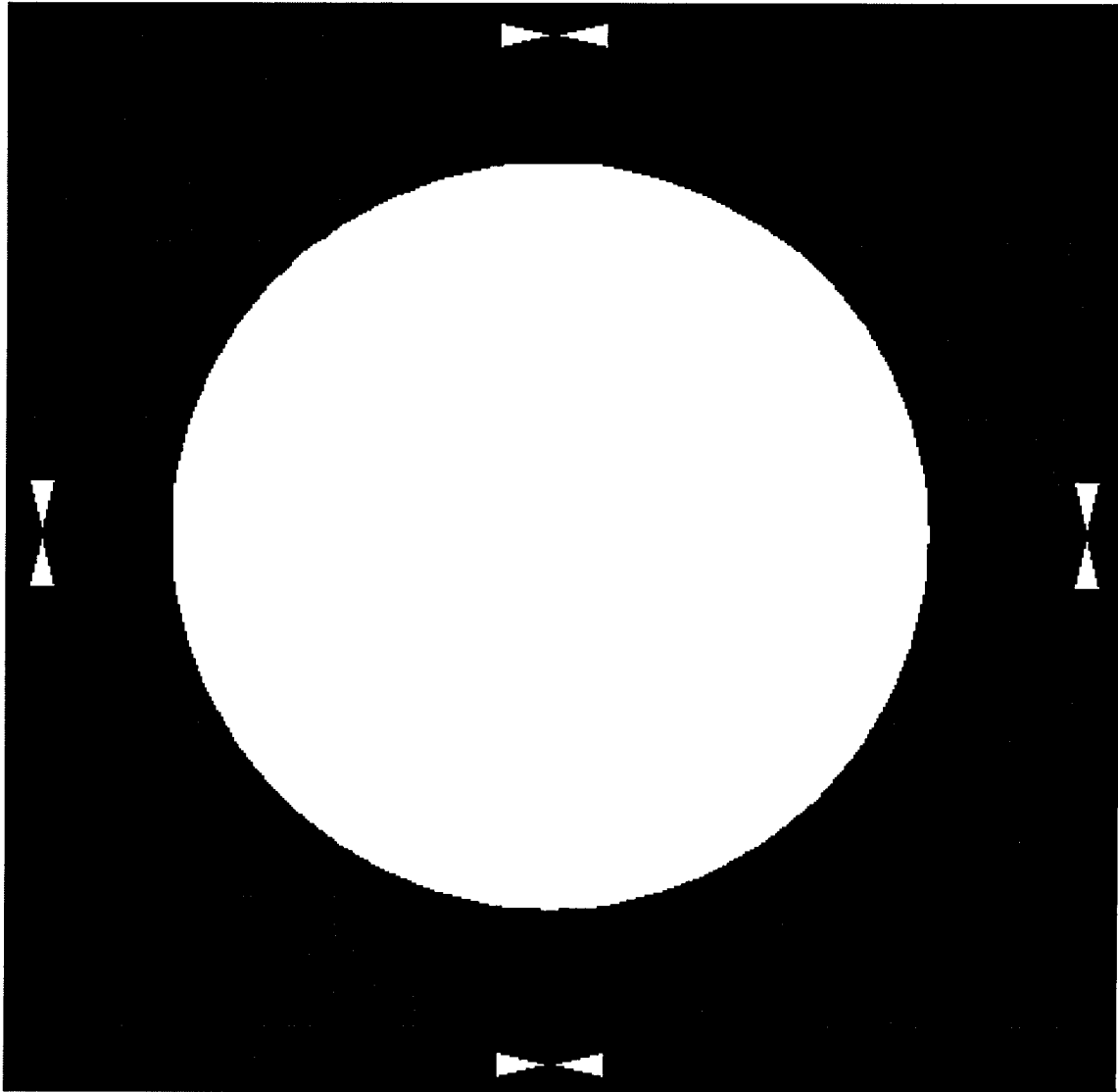


Figure F-1 Template used as a background for filming particle tracking videos.

APPENDIX G

MICROSCOPE SETTINGS FILE DETAILS

The microscope settings saved into the “Dr. Jones Platelets Acridine Orange 10-10-2009” settings file:

Tab: Capture

Image Size: 1316x1024

Shift Times: 1

Objective: 10x or 40x

Exposure: 666.67 ms

ISO sensitivity: ISO 200

Accumulation: Average

Count: 1

Exposure mode: Manual

Tab: Preview

Binning: off

Frame Average: off

Quality: normal

Tab: Color

White balance/black balance: off

Tab: Level

Channel RGB input: 0 1.0 255 output 0 255

Tab: Scale

Display: Show scale, imprint in image

Bar: solid line

Width: 1

Style: "μm"

Tab: Timelapse

N/A

Tab: Microscope:

Excitation light shutter: open

Adapter lens magnification: 0.5

Image quality: N/A

REFERENCES

- [1] D.M. Lloyd-Jones et al., "Defining and Setting National Goals for Cardiovascular Health Promotion and Disease Reduction: The American Heart Association's Strategic Impact Goal Through 2020 and Beyond," *Circulation*, vol. 121, pp. 586-613, January 2010, Published online before print.
- [2] U.S. National Center for Health Statistics, "Vital Statistics of the United States and National Vital Statistics Reports (NVSR)," <http://www.census.gov/compendia/statab/2010/tables/10s0078.pdf>; <http://www.cdc.gov/nchs/deaths.htm>, 2010.
- [3] K.S. Sakariassen and R.M. Barstad, "Mechanisms of thromboembolism at arterial plaques," *Blood Coagulation Fibrinolysis*, vol. 4, no. 4, pp. 615-625, August 1993.
- [4] R. Pifarre, "Thrombosis and cardiovascular disease," *Med Clin North Am.*, vol. 82, no. 3, pp. 511-522, May 1998.
- [5] N. Isaka, T. Tanigawa, M. Nishikawa, and T. Nakano, "High shear stress induced platelet aggregation (h-SIPA) and effects of antiplatelet therapy," *Nippon Rinsho*, vol. 56, no. 10, pp. 2624-2629, October 1998.
- [6] Z.M. Ruggeri, "Mechanisms initiating platelet thrombus formation," *Thromb Haemost*, vol. 78, no. 1, pp. 611-616, July 1997, Erratum in: *Thromb Haemost* 1997 Oct, 78(4):1304.
- [7] S.R. Steinhubl and D.J. Moliterno, "The role of the platelet in the pathogenesis of arterothrombosis," *American Journal of Cardiovascular Drugs*, vol. 5, no. 6, pp. 399-408, 2005.
- [8] J. Rivera, M.L. Lozano, L. Navarro-Nuñez, and V. Vicente, "Platelet receptors and signaling in the dynamics of thrombus formation," *Haematologica*, vol. 94, no. 5, pp. 700-711, May 2009.

- [9] J.F. Mustard, M.A. Packham, and R.L. Kinlough-Rathbone, "Platelets, blood flow, and the vessel wall," *Circulation*, vol. 81, no. 1 Suppl, pp. I24-7; discussion I40-1, Jan 1990.
- [10] R.K. Andrews and M.C. Berndt, "Platelet physiology and thrombosis," *Thromb Res*, vol. 114, no. 5-6, pp. 447-453, 2004.
- [11] C. Frilot, *Role of Nitric Oxide as a Modulator of Platelet Dense Granule Release*, 2001, Doctor of Philosophy Dissertation. Louisiana Tech University, Ruston, LA.
- [12] R. Eshaq, *The Effect of the Local Concentrations of Nitric Oxide and ADP on Platelet Adhesion and Thrombus Formation*, 2006, Master of Science Engineering Thesis. Louisiana Tech University, Ruston, LA.
- [13] C.D. Chin, V. Linderb, and S.K. Sia, "Lab-on-a-chip devices for global health: Past studies and future opportunities," *Lab on a Chip*, vol. 7, pp. 41-57, 2007.
- [14] P.S. Dittrich and A. Manz, "Lab-on-a-chip: microfluidics in drug discovery," *Nature Reviews Drug Discovery*, vol. 5, pp. 210-218, March 2006.
- [15] H. Kim, K. Lee, S. Kumar, and J. Kim, "Dynamic Sequential Layer-by-Layer Deposition Method for Fast and Region-Selective Multilayer Thin Film Fabrication," *Langmuir*, vol. 21, no. 18, pp. 8532-8538, 2005.
- [16] M. Yin et al., "Polyelectrolyte layer-by-layer self-assembly at vibration condition and the pervaporation performance of assembly multilayer films in dehydration of isopropanol," *Journal of Membrane Science*, vol. 358, no. 1-2, pp. 43-40, August 2010.
- [17] A. Veverka, J.M. Lopez, M.G. Watson, and S.A. Jones, "Behavior of Platelet in Dynamic and Static Conditions," in *BMES National Conference*, Pittsburgh, 2009, Poster.
- [18] A.C. Guyton and J.E. Hall, "Hemostasis and Blood Coagulation," in *Textbook of Medical Physiology*, 11th ed. Philadelphia, Pennsylvania, USA: Elsevier Saunders, 2006, ch. 36, pp. 457-468.
- [19] S. Goto, "Understanding the mechanism of platelet thrombus formation under blood flow conditions and the effect of new antiplatelet agents," *Curr Vasc Pharmacology*, vol. 2, no. 1, pp. 23-32, Jan 2004.

- [20] S. Goto, "Understanding the mechanism and prevention of arterial occlusive thrombus formation by anti-platelet agents," *Curr Med Chem Cardiovasc Hematol Agents*, vol. 2, no. 2, pp. 149-156, Apr 2004.
- [21] Y.P. Wu et al., "Platelet thrombus formation on collagen at high shear rates is mediated by von Willebrand factor-glycoprotein Ib interaction and inhibited by von Willebrand factor-glycoprotein IIb/IIIa interaction," *Atheroscler Thromb Vasc Biol*, vol. 20, no. 6, pp. 1661-1667, Jun 2000.
- [22] S. Tsuji et al., "A real-time analysis of mural thrombus formation in various platelet aggregation disorders: distinct shear-dependent roles of platelet receptors and adhesive proteins under flow," *Blood*, vol. 94, no. 3, pp. 968-975, August 1999.
- [23] Z.M. Ruggeri, "The role of von Willebrand factor in thrombus formation," *Thromb Res*, vol. 120, no. Suppl 1, pp. S5-9, 2007.
- [24] M. Sugimoto and S. Miyata, "Functional property of von Willebrand factor under flowing blood," *Int J Hematol*, vol. 75, no. 1, pp. 19-24, Jan 2002.
- [25] C. Thiemermann, "The Role of the L-Arginine: Nitric Oxide Pathway in Circulatory Shock," in *Advances in Pharmacology*, M.W. Anders, Ferid Murad and Joseph T. Coyle J. Thomas August, Ed., 1994, vol. 28, pp. 45-79.
- [26] S. Moncada et al., "The L-Arginine:Nitric Oxide Pathway," *Journal of Cardiovascular Pharmacology*, vol. 17, no. Suppl. 3, pp. S1-S9, 1991.
- [27] M.W. Radomski, R.M. Palmer, and S. Moncada, "An L-arginine/nitric oxide pathway present in human platelets regulates aggregation," *PNAS*, vol. 87, no. 13, pp. 5193-5197, 1990.
- [28] E. Gkaliagkousi, J. Ritter, and A. Ferro, "Platelet-Derived Nitric Oxide Signaling and Regulation," *Circulation Research*, vol. 101, pp. 654-662, 2007.
- [29] J.W.M. Heemskerk, W.M.J. Vuist, M.A.H. Feijge, C.P.M. Reutelingsperger, and T. Lindhout, "Collagen But Not Fibrinogen Surfaces Induce Bleb Formation, Exposure of Phosphatidylserine, and Procoagulant Activity of Adherent Platelets: Evidence for Regulation by Protein Tyrosine Kinase-Dependent Ca²⁺ Responses," *Blood*, vol. 90, no. 7, pp. 2615-2625, October 1997.
- [30] B. Savage, E. Saldívar, and Z.M Ruggeri, "Initiation of Platelet Adhesion by Arrest onto Fibrinogen or Translocation on von Willebrand Factor," *Cell*, vol. 84, no. 2, pp. 289-297, January 1996.

- [31] M. Hermann, Q.J. Lai, R.M. Albrecht, D.F. Mosher, and R.A. Proctor, "Adhesion of Staphylococcus aureus to Surface-Bound platelets: Role of Fibrinogen/Fibrin and Platelet Integrins," *The Journal of Infectious Diseases*, vol. 167, pp. 312-322, 1993.
- [32] G.A. Ozina et al., "Nanofabrication by self-assembly," *Materials Today*, vol. 12, no. 5, pp. 12-23, May 2009.
- [33] M.J. McShane and Y.M. Lvov, "Layer-by-Layer Electrostatic Self-Assembly," in *Dekker Encyclopedia of Nanoscience and Nanotechnology*, Second Edition ed., James A. Schwarz, Cristian I. Contescu, and Karol Putyera, Eds.: Taylor & Francis, 2009, pp. 1823-1840.
- [34] G.G.S. Grant, D.S. Koktysh, B. Yun, R.L. Matts, and N.A. Kotov, "Layer-By-Layer Assembly of Collagen Thin Films: Controlled Thickness and Biocompatibility," *Biomedical Microdevices*, vol. 3, no. 4, pp. 301-306, December 2001.
- [35] A. Hua, M. Feng, Y. Lvov, and S.A. Jones, "Coating Bio-Nanofilm on PDMS through Layer-by-Layer Self-Assembly," in *2nd Joint EMBS-BMES Conference*, Houston, TX, 2002, pp. 502-503.
- [36] A. Hua, M. Fang, S.A. Jones, and Y.M. Lvov, "Electrostatic Layer-by-Layer Nanoassembly on Biological Microtemplates: Platelets," *American Chemical Society*, pp. 1-5, December 2001, Published on Web.
- [37] A. Hua, S.A. Jones, and Y.M. Lvov, "Biomedical Applications of Electrostatic Layer-by-Layer Nano-Assembly of Polymers, Enzymes, and Nanoparticles," *Cell Biochemistry and Biophysics*, vol. 39, pp. 23-43, 2003.
- [38] A. B. Artyukhin, O. Bakajin, P. Stroeve, and A. Noy, "Layer-by-Layer Electrostatic Self-Assembly of Polyelectrolyte Nanoshells on Individual Carbon Nanotube Templates," *Langmuir*, vol. 20, no. 4, pp. 1442-1448, January 2004.
- [39] B.A. Grzybowski and C.J. Campbell, "Complexity and dynamic self-assembly," *Chemical Engineering Science*, vol. 59, pp. 1667-1676, 2004.
- [40] C. Jiang, S. Markutsya, and V.V. Tsukruk, "Compliant, Robust, and Truly Nanoscale Free-Standing Multilayer Films Fabricated Using Spin-Assisted Layer-by-Layer Assembly," *Advanced Materials*, vol. 16, no. 2, pp. 157-161, January 2004.

- [41] H. Denga et al., "Polyelectrolyte membranes prepared by dynamic self-assembly of poly (4-styrenesulfonic acid-co-maleic acid) sodium salt (PSSMA) for nanofiltration (I)," *Journal of Membrane Science*, vol. 323, no. 1, pp. 125-133, October 2008.
- [42] G. Zhang et al., "Preparation of polyelectrolyte multilayer membranes by dynamic layer-by-layer process for pervaporation separation of alcohol/water mixtures," *Journal of Membrane Science*, vol. 280, no. 1-2, pp. 727-733, September 2006, doi:10.1016/j.memsci.2006.02.031.
- [43] V. Srinivasan, V.K. Pamula, and R.B. Fair, "An integrated digital microfluidic lab-on-a-chip for clinical diagnostics on human physiological fluids," *Lab on a Chip*, vol. 4, pp. 310-315, May 2004.
- [44] S. Balslev et al., "Lab-on-a-chip with integrated optical transducers," *Lab on a Chip*, vol. 6, pp. 213-217, December 2005.
- [45] A. Tourovskaia, X. Figueroa-Masot, and A. Folch, "Differentiation-on-a-chip: A microfluidic platform for long-term cell culture studies," *Lab on a Chip*, vol. 5, pp. 14-19, 2005.
- [46] J. Gao, X. Yin, and Z. Fang, "Integration of single cell injection, cell lysis, separation and detection of intracellular constituents on a microfluidic chip," *Lab on a Chip*, vol. 4, pp. 47-52, October 2003.
- [47] T.A. Crowley and V. Pizziconi, "Isolation of plasma from whole blood using planar microfilters for lab-on-a-chip applications," *Lab on a Chip*, vol. 5, pp. 922-929, 2005.
- [48] E.T. Lagally, C.A. Emrichb, and R.A. Mathies, "Fully integrated PCR-capillary electrophoresis microsystem for DNA analysis," *Lab on a Chip*, vol. 1, pp. 102-107, November 2001.
- [49] J. Bäcka et al., "Distinctive regulation of contact activation by antithrombin and C1-inhibitor on activated platelets and material surfaces," *Biomaterials*, vol. 30, no. 34, pp. 6573-6580, December 2009.
- [50] M.G. Watson, Surface Morphology of Platelet Adhesion Influenced by Activators, Inhibitors and Shear Stress, 2010, Doctor of Philosophy Dissertation. Louisiana Tech University, Ruston, LA.
- [51] N.S. Nicholson et al., "Assessment of platelet function assays," *American Heart Journal*, vol. 135, no. 5, pp. S170-S178, May 1998.

- [52] E.G. Popov, Z.A. Gabbasov, I.Yu. Gavrilov, E.Ya. Pozin, and A.G. Mejlumian, "Accumulation and release of acridine derivatives by intact platelets," *Thrombosis Research*, vol. 47, no. 6, pp. 639-645, September 1987.
- [53] S.A. Krolenko, S.Y. Adamyan, T.N. Belyaeva, and T.P. Mozhenok, "Acridine orange accumulation in acid organelles of normal and vacuolated frog skeletal muscle fibres.," *Cell Biol Int.*, vol. 30, no. 11, pp. 933-939, November 2006.
- [54] G.J. Tangelder, D.W. Slaaf, and R.S. Reneman, "Fluorescent labeling of blood platelets in vivo," *Thrombosis Research*, vol. 28, no. 6, pp. 803-820, December 1982.
- [55] I. Skiljan, IrfanView, 2010, EULA, section 1a: IrfanView is free for educational use (schools, universities and libraries) and for use in charity of humanitarian organisations. Version 4.27: <http://www.irfanview.com>, <http://www.irfanview.net>.
- [56] D. Blair and E. Dufrense, Particle Tracking Software, Accessed: 05/2010.
- [57] J.A. Deiber and R.L. Cerro, "Viscous Flow with a Free Surface Inside a Horizontal Rotating Drum. I. Hydrodynamics," *Ind. Eng. Chem. Fundamen.*, vol. 15, no. 2, pp. 102-110, May 1976.
- [58] J. Yang, J.L. Welby, and M.E. Meyerhoff, "Generic Nitric Oxide (NO) Generating Surface by Immobilizing Organoselenium Species via Layer-by-Layer Assembly," *Langmuir*, vol. 24, no. 18, pp. 10265-10272, August 2008.
- [59] J.P. Lopes de Almeida, T. Freitas-Santos, and C. Saldanha, "Fibrinogen-Dependent Signaling in Microvascular Erythrocyte Function: Implications on Nitric Oxide Efflux," *Membrane Biology*, vol. 231, no. 1, pp. 47-53, October 2009.
- [60] X. Liu et al., "Diffusion-limited Reaction of Free Nitric Oxide with Erythrocytes," *The Journal of Biological Chemistry*, vol. 273, no. 30, pp. 18709-18713, July 1998.
- [61] X. Liu, Q. Yan, K.L. Baskerville, and J.L. Zweier, "Estimation of Nitric Oxide Concentration in Blood for Different Rates of Generation," *The Journal of Biological Chemistry*, vol. 282, no. 12, pp. 8831-8836, March 2007.
- [62] A.M. Plata, S.J. Sherwin, and R. Krams, "Endothelial Nitric Oxide Production and Transport in Flow Chambers: The Importance of Convection," *Annals of Biomedical Engineering*, vol. 38, no. 9, pp. 2805-2816, September 2010.

- [63] F.M. White, *Fluid Mechanics*, 5th ed. New York, NY, USA: McGraw-Hill Higher Education, 2003.
- [64] G.A. Truskey, F. Yuan, and D.F. Katz, *Transport Phenomena in Biological Systems*, 2nd ed. Upper Saddle River, New Jersey, USA: Pearson-Prentice Hall, 2009.
- [65] B.L. Welch, "The Generalization Of 'Student's' Problem When Several Different Population Variances Are Involved," *Biometrika*, vol. 34, no. 1-2, pp. 28-35, 1947.
- [66] C.A. Markowski and P. Edward, "Conditions for the Effectiveness of a Preliminary Test of Variance," *The American Statistician*, vol. 44, no. 4, pp. 322-326, Nov 1990.
- [67] P.A. Gentry, C.G. Jong, and P.K. Basrur, "Stability of bovine platelets stored at ambient temperature," *Comparative Hematology International*, vol. 2, no. 4, pp. 213-219, 1992.
- [68] F.K. Tsai, J.L. Lauer, and J.L. Shohet, "Aggregation of blood components on a surface in a microfluidic environment," *Journal of Applied Physics*, vol. 99, no. 2, pp. 1-7, January 2006.
- [69] J.B. McLeod, "Von Kármán's swirling flow problem," *Archive for Rotational Mechanics and Analysis*, vol. 33, no. 2, p. 91, Jan. 1969.
- [70] P.J. Zandbergen and D. Dijkstra, "Non-unique solutions of the Navier-Stokes equations for the Karman swirling flow," *Journal of Engineering Mathematics*, vol. 11, no. 2, p. 167, Apr. 1977.
- [71] M. La Rocca, G. Sciortino, and M.A. Boniforti, "A fully nonlinear model for sloshing in a rotating container," *Fluid Dynamics Research*, vol. 27, no. 1, pp. 23-52, July 2000.
- [72] Y. Imai and Y. Nose, "A new method for evaluation of antithrombogenicity of materials," *Journal of Biomedical Materials Research*, vol. 6, no. 3, pp. 165-172, September 2004.
- [73] H. Zhang, J. Duana, C. Wanga, and Z. Wang, "Cross-linked polyvinyl alcohol microspheres (PVA-MS) for modification of terylene microporous membranes self-assembled by a dynamic layer-by-layer technique," *Microporous and Mesoporous Materials*, vol. 132, no. 1-2, pp. 72-79, July 2010.

- [74] T.A. Everett and D.A. Higgins, "Electrostatic Self-Assembly of Ordered Perlyne-Diimide/Polyelectrolyte nanofibers in Fluidic Devices: from Nematic Domains to Macroscopic Alignment," *Langmuir*, vol. 25, no. 22, pp. 13045-13051, 2009, doi: 10.1021/la9019298.
- [75] D. Salac, W. Lu, C. Wang, and A.M. Sastry, "Pattern formation in a polymer thin film induced by an in-plane electric field," *Applied Physics Letters*, vol. 85, no. 7, p. 1161, June 2004.
- [76] W. Lu and D. Salac, "Electric Field Guided Self-Assembly of Molecules," in *Materials Research Society Symposium*, vol. 947, 2007.
- [77] A.D. Michelson, "Flow Cytometry: A Clinical Test of Platelet Function," *Blood*, vol. 87, no. 12, pp. 4925-4936, June 1996.
- [78] J.W. van Werkum, C.M. Hackeng, F.I. de Korte, F.W.A. Verheugt, and J.M. ten Berg, "Point-of-care platelet function testing in patients undergoing PCI: between a rock and a hard place," *Netherlands Heart Journal*, vol. 15, no. 9, pp. 229-305, September 2007.